A STUDY ON THE VERTICAL PROPAGATION OF PLANETARY WAVES AND THE EFFECTS OF THE UPPER BOUNDARY CONDITION

by

CARLOS ANTONIO CARDELINO

Computador Universitario
Universidad de la República Oriental del Uruguay
(1974)

SUBMITTED IN
PARTIAL FULFILLMENT
OF THE REQUIREMENTS FOR THE
DEGREE OF MASTER OF SCIENCE

at the

MASSACHUSETTS INSTITUTE OF TECHNOLOGY

September, 1978
(i.e. February 1979)

Signature of Author .....
Department of Meteorology
September 12, 1978

Certified by ....
.....
Thesis Supervisor

Accepted by .....
Chairman, Departmental Committee
on Graduate Students.

A STUDY ON THE VERTICAL PROPAGATION OF PLANETARY WAVES AND THE EFFECTS OF THE UPPER BOUNDARY CONDITION

by

CARLOS ANTONIO CARDELINO

Submitted to the Department of Meteorology on 12 September 1978 in Partial Fulfillment of the Requirements for the Degree of Master of Science

ABSTRACT

Linear mid-latitudes models on a beta-plane were formulated to study the simulation of the vertical propagation of forced planetary waves in numerical models. Computations were made applying the rigid top boundary condition $\omega=0$ at various finite heights with different vertical resolutions and compared with exact solutions. The influence of the zonal wind distribution and of Newtonian cooling was examined using vertical profiles of winds and temperature representatives of winter, fall, and summer.

The main conclusions are:

1) With constant values of the zonal wind and temperature, and without Newtonian cooling, no model is capable of representing the structure of a vertically propagating wave. This is due to the false reflection of planetary waves at the top. External modes, with no energy propagation, are well represented by the models.

2) With realistic distributions of temperature, zonal winds and Newtonian cooling, it is always possible to obtain a good simulation of planetary waves, provided there is enough vertical resolution. With good vertical resolution, the effect of the artificial top boundary condition is minimized during winter and summer because the mean zonal winds produce a natural reflective stratospheric layer. During fall, Newtonian cooling absorbs most of the upward energy before it reaches the top.

3) The absolute minimum number of levels necessary to obtain a relatively good wave structure simulation is ten.

4) The most important factor to obtain a good tropospheric representation is good resolution near the ground. For a fixed number of levels, the best results are obtained with high resolution at the extremes of the atmosphere.

5) For a fixed number of levels, the solutions are very sensitive to the position of the top. When the winds produce a reflective layer in the stratosphere, a relatively low top can improve the simulation. When Newtonian cooling is an important factor, a high top is better because more damping is allowed to occur. The optimum position of the top is therefore seasonally dependent.

Two "sponge layer" mechanisms to reduce the reflection of wave energy at the upper boundary were also tested. In one of them, a complex index of refraction modified by a coefficient of viscosity, was introduced in a layer below the upper boundary, in such a way that the waves could be damped before they reached the top. A complex index of refraction that increases smoothly with height was found to produce better results that a constant one. It was found that there is an optimum value of the viscosity coefficient, which is a function of the frequency of the waves and the depth of the sponge layer. Lower values produce insufficient damping, and higher values produce internal reflections due to the strong vertical gradient of viscosity. The second approach uses a single layer at the top to eliminate the reflected wave by producing destructive interference between the wave reflected at the top and the wave reflected at the bottom of the sponge layer. A generalization of this method when several frequencies are present is proposed.

Thesis Supervisor: Eugenia Kalnay-Rivas
Title: Associate Professor

TABLE OF CONTENTS

1. INTRODUCTION

The simulation of vertical propagating waves by numerical models depends strongly on the vertical resolution of the model and on the characteristics and position of the upper boundary. Poor vertical resolution is considered to be a possible cause of the inadequacy of the simulation of the stationary planetary waves (Manabe and Terpstra, 1974, and Kasahara et al., 1973). In the latter case, the use of a rigid top at 35 km also contributes to an unrealistic low simulation of the stratospheric temperature (Holton, 1975).

Lindzen et al. (1968) analyzed the effects of introducing $\frac{dp}{dt} = 0$ at some finite altitude as an upper boundary condition. Comparisons with results from an unbounded model showed that spurious reflections due to the upper boundary condition produced distortions in the wave structure.

More recently, in similar studies, Kirkwood and Derome (1977), and Nakamura (1976), using a quasi-geostrophic model made simulations of forced stationary waves. The results showed that insufficient resolution in the stratosphere can lead to a spurious energy reflection at the upper boundary and to an incorrect wave structure.

The dynamics of the planetary vertical propagating waves has been discussed by Charney and Drazin (1961), and Dickinson (1969), among others. Charney and Drazin showed that stationary quasi-geostrophic disturbances superimposed

on a uniform mean-zonal flow propagate energy vertically only when the zonal flow is westerly and less than a critical velocity. This critical velocity increases as the horizontal scale of the waves increases. Because of the observed mean winds, during the summer hemisphere when winds in the upper stratosphere are easterlies, there is no propagation of stationary waves. Under these conditions, the use of a rigid top as an upper boundary condition would not prevent a model from properly representing these waves. The westerly jet during the winter is sufficiently strong to prevent much propagation during the winter months. However, the propagation of ultra-long stationary waves are essential features in the dynamics of the stratosphere. In the equinoxes during the initial development of the westerly symmetric circulation, large upward propagation of planetary waves are predicted by the Charney-Drazin theory. There is no observational evidence of this prediction. Dickinson showed that there is a large attenuation of planetary waves propagating through sufficiently weak westerly winds due to the effect of Newtonian cooling.

In the present study we will be concerned with the simulation of vertically propagating waves by numerical models and with the determination of how the structure of forced waves is affected by the vertical resolution and by the type of boundary condition used at the top. We will

also be concerned with the development of an efficient mechanism to avoid or reduce the reflections generated at the top.

In a model with finite number of layers, there is no way to avoid the imposition of an upper boundary of the atmosphere which has no physical reality. The waves produced in the troposphere and propagated upward can reach the upper boundary and may be reflected by the artificial top of the model. The waves in the lower atmosphere may be affected by the spuriously reflected waves. In the real atmosphere, the waves can never reach the infinite height (p=0) within a finite time, so the condition $\frac{dp}{dt} = 0$ at p=0 has no influence on the waves. In a numerical model the waves can reach the top in a finite time, even if it is at p=0.

In the discussion of the upper boundary, two different problems arise. Firstly, the upper boundary can be placed anywhere. For example, someone interested in the simulation of the troposphere may want to put the upper boundary in the lower stratosphere. Because the reflection of vertical propagating waves is a natural phenomenon that occurs in the atmosphere, a boundary condition to avoid reflection can be very inaccurate. A proper top boundary condition should avoid both the spurious reflection of waves that propagate vertically, and the absorption of waves which in reality are

reflected. Secondly, although the top can be placed high enough to allow radiative damping and wave interactions, some waves can penetrate further and reach the top. In this case, a radiation condition or an equivalent mechanism must be used.

In this work, we discuss various alternatives to this problem, especially following the concept of "sponge layer" in the fashion introduced by Arakawa and Tokioka (1974).

In dealing with the vertical structure of the waves, two different lines of approach are possible. A steady-state approach where, given a basic state solution and suitable boundary conditions, we solve for the wave structure. Another way is to introduce the time dependence and look at the transient behavior of the flow. In this discussion we limit ourselves to the steady-state case, leaving the time dependence approach to a future study.

The ultimate goal is to study the effect of the vertical resolution and the characteristics of the boundary conditions used at the top in a general circulation model. However, a general circulation model involves many physical processes and simulates not only planetary waves of global scale, but also synoptic scale waves and other phenomena, and consequently, what we see is the coupled behavior of all of them. A general ciruclation model is too complicated to study the effects of vertical resolution and the upper boundary directly. For this reason, we are going to deal

with more simple numerical models as a prerequisite to a simular study with a general circulation model.

A description of the models used is given in Section 2. In Section 3 we examine how the upper boundary condition influences the vertical propagation of wave energy. The results of several simulations under different atmospheric conditions are presented in Section 4. Finally, in Section 5 we discuss alternative approaches to the upper boundary.

2. DESCRIPTION OF THE MODELS

In this section we will describe several simple models which share with the more complete ones some of the essential features to simulate vertical propagating waves. Two of these linear models are based on the primitive equations on a beta-plane, while the other two are based on the quasi-geostrophic equations.

The models are used to simulate the structure of forced quasi-stationary waves. The forcing is assumed to have small amplitudes so that the governing equations can be linearized. We shall consider small amplitude perturbations superimposed upon a basic state with zonal winds that are a function of pressure (or log-pressure) alone.

2.1 Basic Equations

The linear primitive equations on a beta-plane, in pressure coordinates are:

$$\frac{\partial \xi}{\partial t} + U \frac{\partial \xi}{\partial x} - \frac{\partial \omega}{\partial y} \frac{\partial U}{\partial p} = -f_0 \delta - \beta v \tag{1}$$

$$\frac{\partial \delta}{\partial t} + U \frac{\partial \delta}{\partial x} + \frac{\partial \omega}{\partial x} \frac{\partial U}{\partial p} = -\nabla^2 \phi + f_0 \xi - \beta u \tag{2}$$

$$\frac{\partial T}{\partial t} + U \frac{\partial T}{\partial x} + v \frac{\partial T_0}{\partial y} + \left(\frac{\partial T_0}{\partial p} - \frac{R T_0}{p c_p} \right) \omega = -\alpha T \tag{3}$$

$$\frac{\partial \omega}{\partial p} + \delta = 0 \tag{4}$$

$$\frac{\partial \phi}{\partial p} = -\frac{R}{p} T \tag{5}$$

in which the beta-plane approximation $f = f_o + \beta y$ was made, neglecting βy except when f is differentiated. In equations (1) to (5) δ is the horizontal divergence $\frac{\partial u}{\partial x} + \frac{\partial v}{\partial y}$, ξ is the vertical component of the vorticity vector $\frac{\partial v}{\partial x} - \frac{\partial u}{\partial y}$, and α is the pressure dependent Newtonian cooling coefficient. Other symbols used here are as follows:

- x eastward horizontal coordinate
- y northward horizontal coordinate
- p pressure
- u eastward perturbation velocity
- v northward perturbation velocity
- ω vertical p-velocity ($\frac{dp}{dt}$)
- ϕ perturbation geopotential
- T perturbation temperature
- U mean zonal wind
- T_o temperature of the basic state
- f_o Coriolis parameter
- β variation of Coriolis parameter with the latitude coordinate $\frac{df}{dy}$
- g acceleration of gravity

R gas constant

c_p specific heat at constant pressure

A second system of linear primitive equations on a beta-plane is derived using log-pressure coordinates defined by $z = -H \ln(\frac{p}{p_s})$ where $H = \frac{RT}{g}$ is a scale height, and p_s is a standard reference pressure. The equations are:

$$\frac{\partial \xi}{\partial t} + u \frac{\partial \xi}{\partial x} - \frac{\partial w}{\partial y} \frac{\partial u}{\partial z} = - f_0 \delta - \beta v \tag{6}$$

$$\frac{\partial \delta}{\partial t} + u \frac{\partial \delta}{\partial x} + \frac{\partial w}{\partial x} \frac{\partial u}{\partial z} = - \nabla^2 \phi + f_0 \xi - \beta u \tag{7}$$

$$\frac{\partial T}{\partial t} + u \frac{\partial T}{\partial x} + v \frac{\partial T_0}{\partial y} + \left(\frac{\partial T_0}{\partial z} + \frac{g}{c_p} \right) w = - \alpha T \tag{8}$$

$$\frac{\partial w}{\partial z} + \delta - \frac{w}{H} = 0 \tag{9}$$

$$\frac{\partial \phi}{\partial z} = \frac{R}{H} T \tag{10}$$

where w is the z-vertical velocity $\frac{dz}{dt}$.

For these two systems of equations (called models P and Z for reference) is easy to derive the quasi-geostrophic equations (called models PG and PZ).

The equations for model PG are:

$$\frac{\partial \xi_g}{\partial t} + U \frac{\partial \xi_g}{\partial x} = -\beta v_g + f_o \frac{\partial \omega}{\partial p} \tag{11}$$

$$\frac{\partial T}{\partial t} + U \frac{\partial T}{\partial x} + v_g \frac{\partial T_o}{\partial y} + \left(\frac{\partial T_o}{\partial p} - \frac{R T_o}{p c_p} \right) \omega = -\alpha T \tag{12}$$

$$\frac{\partial \phi}{\partial p} = -\frac{R}{p} T \tag{13}$$

in which the geostrophic vorticity $\xi_g = \frac{\partial v_g}{\partial x} - \frac{\partial u_g}{\partial y} = \frac{\nabla^2 \phi}{f_o}$

The equations for model ZG are:

$$\frac{\partial \xi_g}{\partial t} + U \frac{\partial \xi_g}{\partial x} = -\beta v_g + f_o \left(\frac{\partial W}{\partial z} - \frac{W}{H} \right) \tag{14}$$

$$\frac{\partial T}{\partial t} + U \frac{\partial T}{\partial x} + v_g \frac{\partial T_o}{\partial y} + \left(\frac{\partial T_o}{\partial z} + \frac{g}{c_p} \right) W = -\alpha T \tag{15}$$

$$\frac{\partial \phi}{\partial z} = \frac{R}{H} T \tag{16}$$

The use of two different systems of vertical coordinates will allow us to make comparisons and derive conclusions with respect to the simulation of vertical propagating waves on general circulation models, as most of these models use vertical pressure coordinates.

2.2 Formulation of the Models

The four systems have solutions of the form:

$$(\psi, \chi, \phi, \omega, T) = \text{Real} \left\{ (E, D, F, W, T) \; e^{i(kx + \ell y + \omega t)} \right\} \qquad (17)$$

in which k is the longitudinal wavenumber, ℓ is the meridional wavenumber, and ω is the frequency. The velocity potential χ defined by $\chi = \nabla^2 \delta$ and the streamfunction ψ defined by $\psi = \nabla^2 \xi$ are also introduced.

By substitution of expression (17) into the models, it is possible to solve for the variables E, D, F, W, and T.

As an example, we consider model ZG. First, we obtain:

$$\xi = -m^2 \; E \; \exp\left[i (kx + \ell y + \omega t) \right] \qquad (18)$$

$$\delta = -m^2 \; D \; \exp\left[i (kx + \ell y + \omega t) \right] \qquad (19)$$

$$\nabla^2 \phi = -m^2 \; F \; \exp\left[i (kx + \ell y + \omega t) \right] \qquad (20)$$

$$\sigma_g = ik \; E \; \exp\left[i (kx + \ell y + \omega t) \right] \qquad (21)$$

in which $m^2 = k^2 + \ell^2$.

Applying equations (18) to (21) to the system (14) to (16), we obtain:

$$-i\omega m^2 E - i m^2 K U E = -\beta i K E + f_o \frac{dW}{dz} - \frac{f_o}{H} W$$

$$i\omega T + iKUT + iKE \frac{\partial T_o}{\partial y} + \left(\frac{\partial T_o}{\partial z} + \frac{g}{c_p} \right) W = -\alpha T$$

$$\frac{dF}{dz} = \frac{R}{H} T$$

Using the thermal wind relation $\frac{\partial T_O}{\partial y} = - \frac{fH}{R} \frac{dU}{dz}$, and the fact that $F = f_O E$, we arrive to the system:

$$\frac{dW}{dz} = \frac{i}{f_o^2} \left(\beta K - \omega m^2 - K m^2 U \right) F + \frac{1}{H} W \qquad (22)$$

$$\frac{dF}{dz} = \frac{i R S}{(\omega + UK - i\alpha) H} W + \frac{K}{(\omega + UK - i\alpha) H} \frac{dU}{dz} F \qquad (23)$$

In order to simulate conditions similar to numerical weather prediction models, finite differences in the vertical were used. The atmosphere is divided from $p = p_{top}$ to $p = p_b$ into N layers with variable grid intervals, as shown in Figure 2.1.

By specifying F_1 at $p = p_b$ and W_N at $p = p_{top}$,

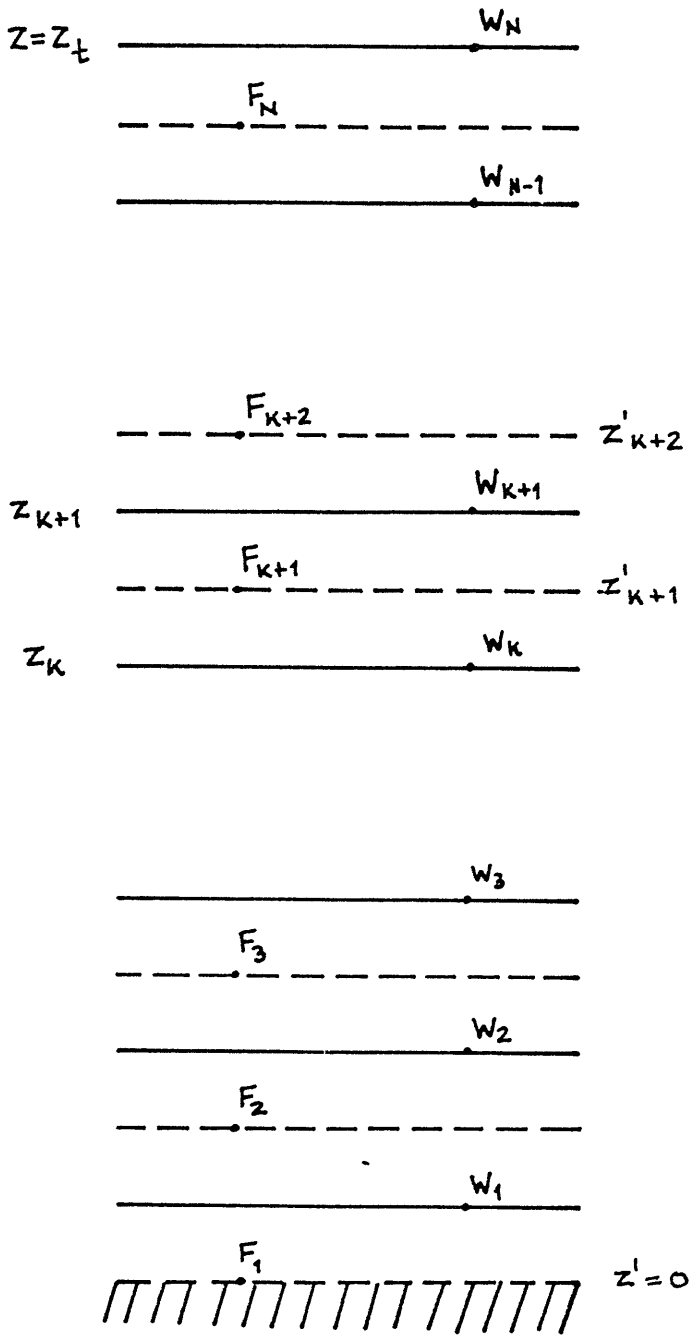

Figure 2.1 Vertical Distribution of Variables.

and using the finite difference form of system (22) to (23), a linear algebraic system of 2N-2 equations is obtained. By changing $\Delta z_k = z_{k+1} - z_k$, N and p_{top}, various models from low resolution to high resolution are obtained.

Similar descriptions can be made for models P, PG, and Z.

2.3 Basic State and Specification of Parameters

Since we are interested in the performance of numerical prediction models, it is desirable to choose the basic state and the different parameters in our models as close as possible to those of the real atmosphere. The mean temperature profile for mid-latitudes was taken from Houghton (1977) and is shown in Figure 2.2. The static stability $S = \frac{\partial T_o}{\partial p} - \frac{RT_o}{p\, c_p}$ for the P and PG models, and $S = \frac{\partial T_o}{\partial z} + \frac{g}{c_p}$ for the Z and ZG models is calculated using the temperature profile shown.

The basic zonal winds are plotted in Figure 2.3. These profiles are similar to those used by Nakamura (1976) and Charney and Drazin (1961). The winter profile presents a strong stratospheric jet. The fall presents weak westerlies, and the summer easterlies in the stratosphere. The profile of Newtonian cooling coefficient is based on Dickinson (1973) and is shown in Figure 2.4.

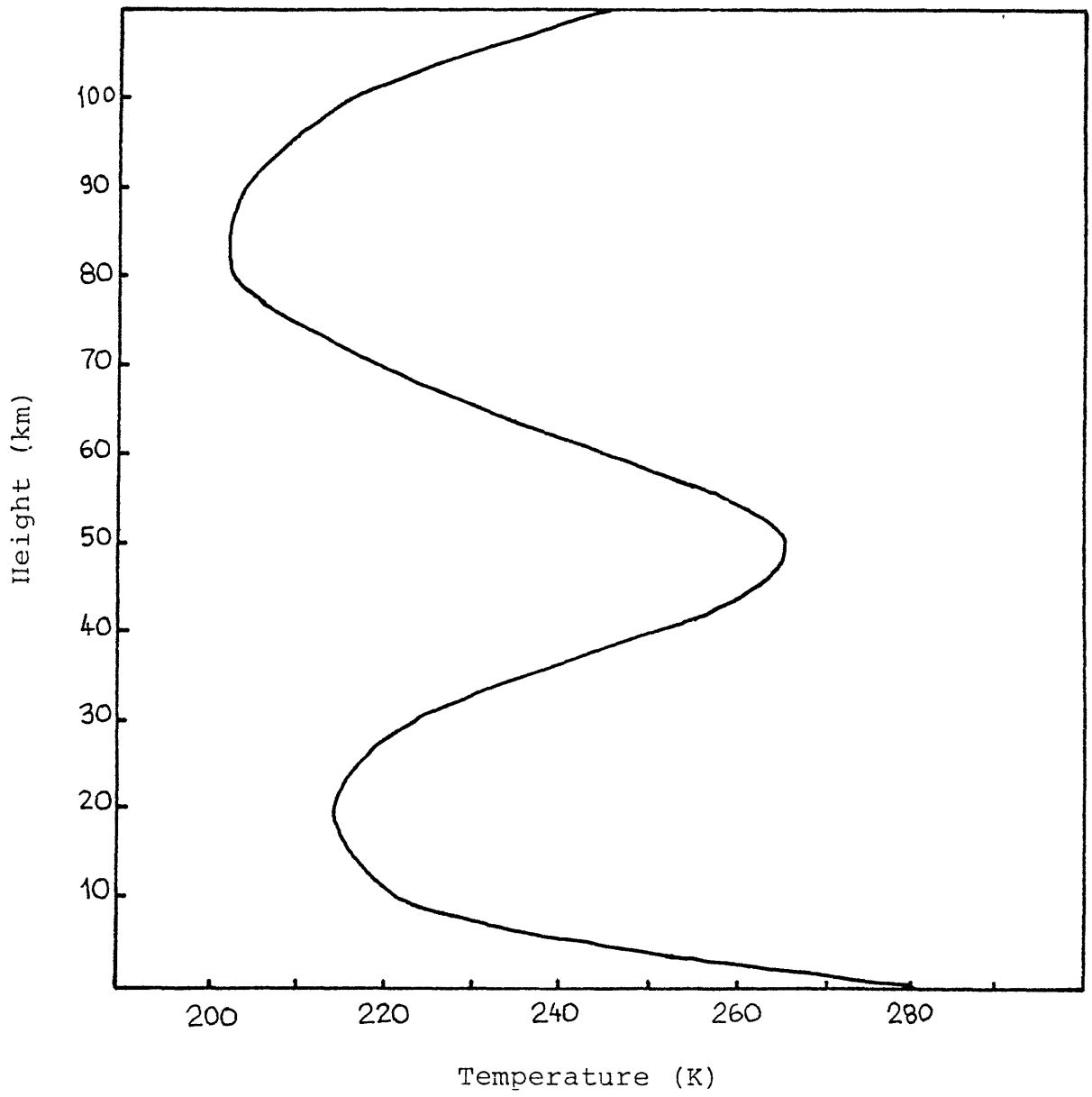

Figure 2.2 Vertical Profile of Mean Temperature

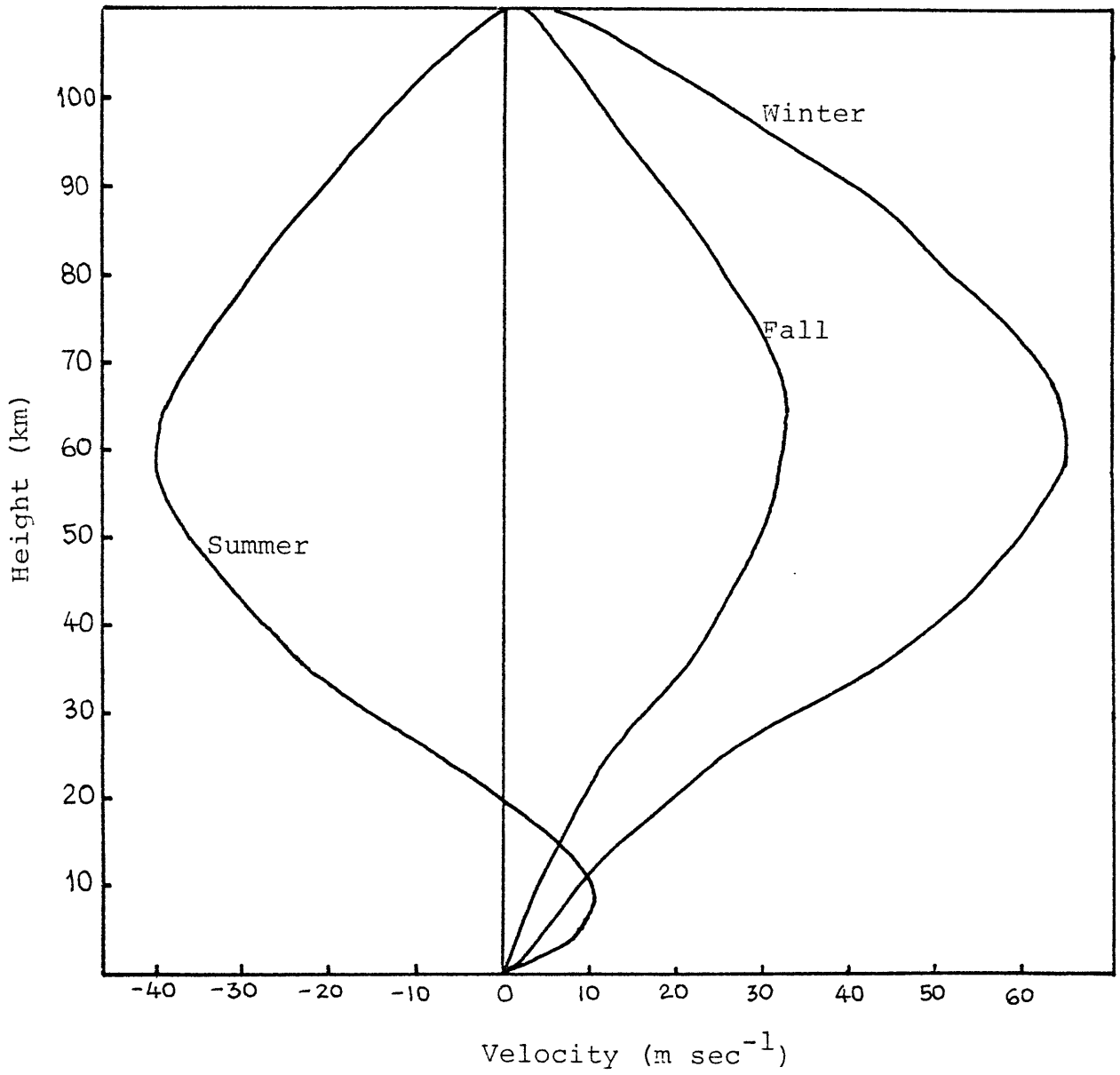

Figure 2.3 Vertical Profiles of the Mean Zonal Wind.

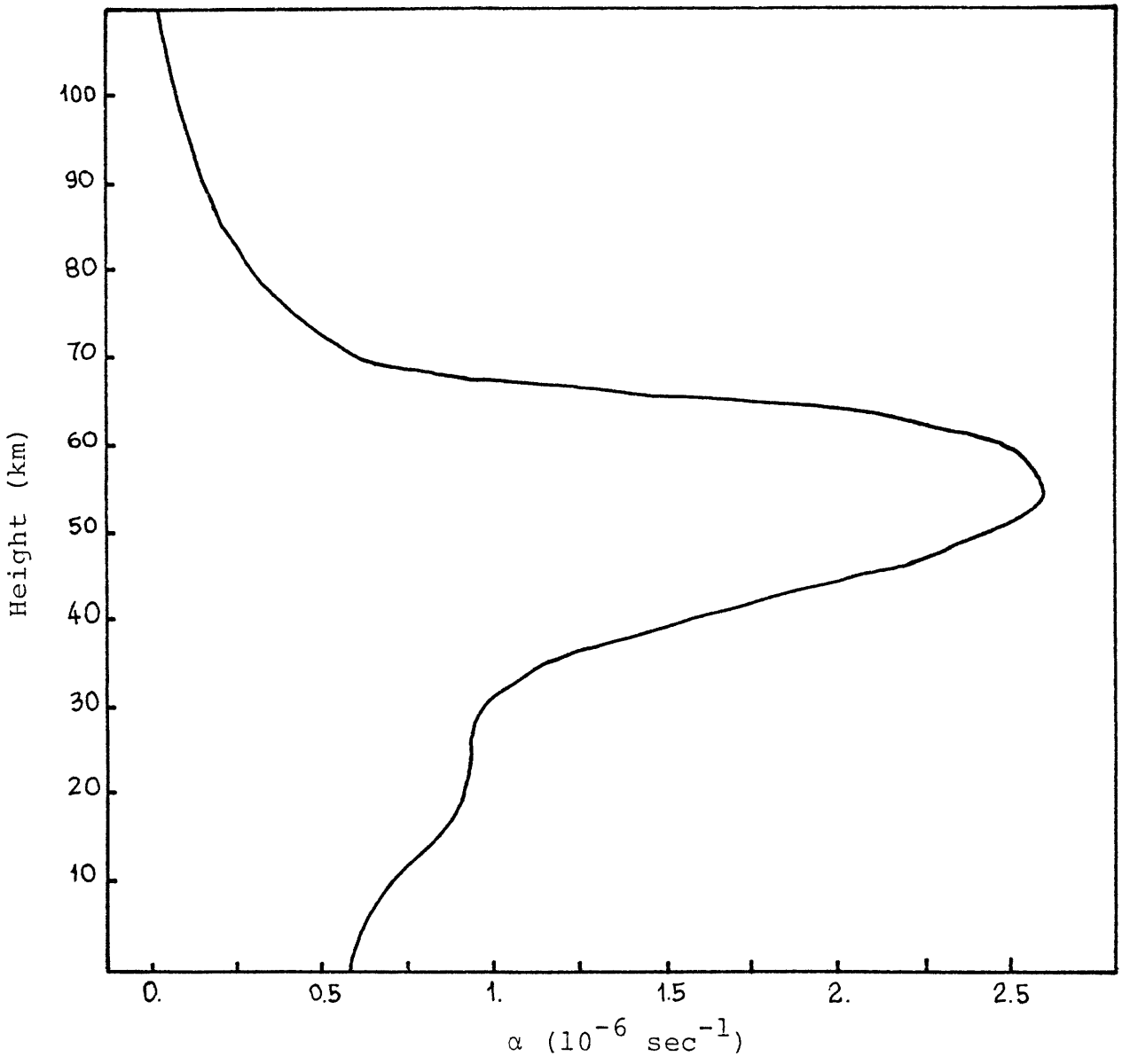

Figure 2.4 Vertical Profile of the Newtonian Cooling Coefficient

Our beta-plane is centered at 55° N because, according to observations presented by Matsuno (1970), the vertical propagating waves in winter with wavenumber 1 have a maximum amplitude at 55° N. Consequently $f_o = 1.194 \times 10^{-4}$ sec^{-1}, and the value of β is 1.313×10^{-11} m^{-1} sec^{-1}. We made experiments with wavenumbers 1 and 2. For $L_x = \frac{2\pi}{k}$, we used the length of the latitude circle at 55°, and half of that length, respectively. For $L_y = \frac{2\pi}{\ell}$, we used values similar to those presented by Charney and Drazin, 18 000 km and 9 000 km. The phase velocity $c = \frac{\omega}{k}$ was taken equal to zero for the simulation of stationary waves. Computations with $c = 5$ m sec^{-1} were also made.

In our models, the variables have been assumed to have the form:

$$X(x,y,p,t) = X(p)\ e^{i(kx+\ell y+\omega t)}$$

The real part of it,

$$X_R(p)\ \cos(kx+\ell y+\omega t) - X_i(p)\ \sin(kx+\ell y+\omega t)$$

can be written as

$$|X(p)|\ \cos(kx+\ell y+\omega t - \varepsilon(p))$$

in which the phase ε is a function of pressure.

In the results we will present the phase ε and the scaled amplitude $e^{-z/2H}\,|E(p)|$ as a function of pressure. The advantage of using the scaled amplitude is due to the fact that it is proportional to the square root of the wave-energy density.

At the surface $p = p_b$ (or $z=0$) the forcing is specified by

$$\phi(x, y, p=p_b, t) = F\, e^{i(kx+ly+\omega t)}$$

in which F is an arbitrary constant.

The upper boundary condition is different for the models in pressure coordinates than in the log-pressure coordinates. For all models, the upper boundary condition is specified by

$$\omega(x, y, p=p_{top}) = 0 \qquad \text{or} \qquad w(x, y, z=z_{top}) = 0$$

while for reference models (Z and ZG) a radiation condition at the top of the model is used.

As will be seen in the next section, a model with coefficients independent of the vertical coordinate is needed in order to apply a radiation condition. A model that uses log-pressure coordinate has coefficients independent of z, if U, H, and α are constant (see equations (22) to (23)). To show it, expression (17) is applied to the system (11) to (13), to obtain:

$$-i\omega m^2 E - i m^2 K U E = -i\beta K E + f_o \frac{dW}{dp}$$

$$i\omega T + i K U T + i K E \frac{dT_o}{dy} + \left(\frac{\partial T_o}{\partial p} - \frac{R T_o}{p c_p} \right) W = -\alpha T$$

$$\frac{dF}{dp} = -\frac{R}{p} T$$

Using the thermal wind relation $\frac{\partial T_o}{\partial y} = \frac{fp}{R} \frac{\partial U}{\partial p}$ and the relation $F = f_o E$, we obtain:

$$\frac{dW}{dp} = \frac{i}{f_o^2} \left(\beta K - \omega m^2 - K m^2 U \right) F$$

$$\frac{dF}{dp} = \frac{K}{\omega + UK - i\alpha} \frac{dU}{dp} F - \frac{i \frac{R}{p} \left(\frac{\partial T_o}{\partial p} - \frac{R T_o}{p c_p} \right)}{\omega + UK - i\alpha} W \qquad (24)$$

Then, assuming U, T_o, and α independent of pressure, is not enough to obtain constant coefficients because equation (24) becomes

$$\frac{dF}{dp} = \frac{i R^2 T_o}{c_p p^2 (\omega + UK - i\alpha)} W$$

in which pressure p appears explicitly.

The use of a radiation condition in the log-pressure models makes them appropriate as reference models. Models with a rigid top may be compared to them. The description

of the implementation of the radiation condition is done in the next section.

3. VERTICAL PROPAGATION OF WAVE ENERGY

In this section, we examine how the upper boundary condition and the wave mean-zonal-winds interaction influence the vertical propagation of wave energy.

We start with the system (22) to (23), assuming an isothermal basic state, so that the scale height H and the static stability S are constant. We also assume a constant basic-zonal wind U and no damping, $\alpha = 0$.

By elimination of W, we obtain

$$\frac{d^2F}{dz^2} - \frac{1}{H}\frac{dF}{dz} - \frac{RS(\beta K - \omega m^2 - K m^2 U)}{H f_0^2 (\omega + UK)} F = 0 \qquad (25)$$

Equation (25) has the analytic solution:

$$F(z) = A e^{n_1 z} + B e^{n_2 z}$$

where

$$(n_1, n_2) = \frac{1}{2H} \pm \left(\frac{1}{4H^2} - \frac{RS(\beta K - \omega m^2 - K m^2 U)}{H f_0^2 (\omega + UK)} \right)^{1/2}$$

If $A = 1 - \frac{4HRS(\beta - m^2(U-c))}{f_o^2 H(U-c)} < 0$, sinusoidal solutions are possible and waves propagate vertically, while if $A > 0$ only exponential solutions result. Consequently, the condition of vertical propagation is given as follows:

$$0 < U - c < U_{crit} = \frac{\beta}{m^2 + \frac{f_o^2}{4HRS}} \tag{26}$$

At the level $z = z_{crit}$, where $U - c = U_{crit}$, the waves are reflected, while at another critical level, where $U - c = 0$, the waves are absorbed.

The upward energy flux is given by $\overline{\omega\phi}$, where the overbar denotes zonal mean. From equation (17) we obtain

$$\overline{\omega\phi} = \frac{1}{2} \text{ Real } (W F^*)$$

where the asterisk denotes the complex conjugate. Using equations (22) and (23) we evaluate:

$$\overline{\omega\phi} = \frac{H(\omega + UK)}{2RS} \text{ Real } \left(\frac{1}{i} \frac{dF}{dz} F^* \right) \tag{27}$$

$$F(z) = A\, e^{(1/2H + E)z} + B\, e^{(1/2H - E)z}$$

with E_r = Real $E > 0$, and E_i = Imag $E > 0$ for definiteness.

With $B = 0$, and after some manipulations,

$$\overline{\omega\phi} = E_i \frac{H(\omega+UK)}{2RS} |A|^2 \, e^{(1/2H + 2E_r)z}$$

In a similar way, with $A = 0$,

$$\overline{\omega\phi} = -E_i \frac{H(\omega+UK)}{2RS} |B|^2 \, e^{(1/2H + 2E_r)z}$$

Consequently, the A term is responsible for the propagation of energy upward, while the B term represents the downward propagating mode.

Alternatively, by using the form

$$F(x,y,z,t) = |F(z)| \cos(Kx + \ell y + \omega t - \varepsilon(z))$$

in equation (27), the expression for the upward energy flux is given by

$$\overline{\phi\omega} = \frac{-H(\omega+UK)}{2RS} |F(z)|^2 \frac{d\varepsilon}{dz}$$

Consequently, the vertical flux of energy depends upon the tilt of the wave with height. A wave with the phase tilted windward transports energy upward, while waves with phase lines tilted downstreams transport wave energy downward. A vertical wave (phase constant with height) does not transport energy vertically. These results were first obtained by

Eliassen and Palm (1961).

In this study, the models Z and ZG will be used as control solutions to test the effect of a rigid boundary condition in the models P and PG. For that purpose, a radiation condition is used in the log-pressure coordinate models.

Above a certain level, we assume that the flow is adiabatic and that the vertical shear of the mean flow vanishes. Under these conditions, solving for W in equations (22) and (23) results in

$$\frac{d^2W}{dz^2} - \frac{1}{H}\frac{dW}{dz} - \frac{RS(\beta K - \omega m^2 - K m^2 U)}{H f_0^2 (\omega + UK)} W = 0 \qquad (28)$$

The upper-boundary condition is derived by requiring that the wave energy be propagated away from the source below the assumed top of the atmosphere. We already showed that vertical propagation of energy is only possible if expression (26) is satisfied. Under this condition, the solution which propagates energy upward is chosen by setting $B = 0$ in

$$W(z) = A e^{n_1 z} + B e^{n_2 z}$$

This implies the boundary condition:

$$\frac{dW}{dz} - n_1 W = 0 \qquad \text{at} \quad z = z_{top} \qquad (29)$$

If condition (26) is not satisfied, we will have external modes. $A = 0$ is required to have the energy bounded as z goes to infinity, which leads to the boundary condition:

$$\frac{dW}{dz} - n_z W = 0 \qquad \text{at} \quad z = z_{top} \tag{30}$$

The system to be solved consists of equations (22) and (23) together with the lower boundary condition (Section 1.3) and the upper boundary condition (29) or (30).

Next, we examine the effect of introducing $\frac{dp}{dt} = 0$ at some finite altitude as an upper boundary condition. Transformation of the dependent variable in the vertical structure equation (26) from W to $\Omega = e^{-z/2H} W$ gives,

$$\frac{d^2\Omega}{dz^2} + \gamma^2 \Omega = 0 \tag{31}$$

where γ is defined by $\gamma^2 = \frac{RS(\beta K - \omega m^2 - Km^2 U)}{Hf^2(\omega + UK)} - \frac{1}{4H^2}$ (32)

The solution of (31) is:

$$\Omega(z) = A e^{i\gamma z} + B e^{-i\gamma z}$$

We are going to consider the radiation condition case ($B=0$, only upward propagation of wave energy) to be the exact solution in the following discussion. Assuming for convenience that the amplitude of the forcing is equal to 1, the vertical structure is $\Omega(z) = e^{i\gamma z}$.

If the upper boundary is $\frac{dp}{dt} = 0$ (or $\frac{dz}{dt} = 0$) we obtain $\Omega = 1$ at $z = z_b$, and $\Omega = 0$ at $z = z_{top}$. Then,

$$A + B = 1$$

$$A\, e^{i\gamma z_t} + B\, e^{-i\gamma z_t} = 0$$

and

$$A = \frac{-e^{i\gamma z_t}}{e^{i\gamma z_t} - e^{-i\gamma z_t}} = \frac{1}{2} + \frac{i}{2} \cot \gamma z_t \qquad (33)$$

$$B = \frac{e^{i\gamma z_t}}{e^{i\gamma z_t} - e^{-i\gamma z_t}} = \frac{1}{2} - \frac{i}{2} \cot \gamma z_t \qquad (34)$$

A and B are complex numbers that become infinite when

$$e^{i\gamma z_t} - e^{-i\gamma z_t} = 0 \qquad (35)$$

or when $\gamma z_t = j\pi \qquad (j = 1, 2, \ldots)$

Comparing with the exact solution, we have that the real part of A is ½ instead of 1, while the real part of B is not zero, so that there is downward energy wave propagation.

For free oscillations in the atmosphere, $\Omega = 0$ at $z = z_b$ and at $z = z_{top}$. We obtain an homogeneous system of equations in A and B. To obtain non-trivial solutions:

$$\begin{vmatrix} 1 & 1 \\ e^{i\gamma z_t} & e^{-i\gamma z_t} \end{vmatrix} = 0$$

which is equation (35). The resonance in the forced case corresponds to the free oscillation resonance.

From this discussion it is clear that with the boundary condition $\frac{dz}{dt} = 0$ (or $\frac{dp}{dt} = 0$) at $z = z_{top}$ B cannot be zero, therefore, there will be spurious reflections. A discussion of various ways to avoid or reduce the reflections produced at the upper boundary will be done in a later section.

4. NUMERICAL RESULTS

In this section, numerical results obtained with the four linear models previously described are reported. In the analysis of the results obtained with models that use different vertical coordinates, the distribution of computational levels that each model has, must be taken into consideration. The top of the models were placed at .0001 mb, or about 110 km, and five different resolutions were used, N = 5, 10, 30, and 100, where N is the number of levels. The simulations thus obtained were compared to a reference simulation produced with the log-pressure model, with N = 200, and using a radiation condition. The different distribution

of levels are presented in the following table:

	Model P					Model Z				
Number of Levels	5	10	30	50	100	5	10	30	50	100
Troposphere (0-10 km)	3	7	22	37	74	-	1	3	5	10
Stratosphere (10-50 km)	1	2	7	12	25	1	3	9	15	31
Mesosphere (50-110 km)	-	-	-	-	-	3	5	17	28	58

The similarity in the representation of the stratosphere is only apparent. The pressure model that best represents the stratosphere has its uppermost computational level at 35.1 km. The position of the uppermost computational level is presented in the following table, in kilometers:

Number of Levels	5	10	30	50	100
Model Z	88.1	93.9	97.4	98.1	98.6
Model P	15.3	18.9	27.7	30.5	35.1

The quasi-geostrophic models were tested by reproducing some of the results that appear in the paper by Derome and Kirkwood (1977). Although the formulation of the models are different, they are formally equivalent. Results using the primitive equation models are described in the next subsection.

4.1 Comparison Between the Primitive Equation Models and the Quasi-Geostrophic Models

In general, primitive equation models represent an improvement with respect to quasi-geostrophic models because the assumption of small Rossby number, which is violated in regions of strong winds and in the tropics, is not made. Then, it was interesting to study the performance of our approximate primitive equation model in the simulation of vertical propagating waves. In Figures 4.1, 4.2, and 4.3 we present three cases in which models Z and ZG are solved under the same conditions. Figure 4.1 corresponds to constant conditions: $U = 20$ m sec^{-1}, $\alpha = 0$, and $T_o = 239^o$ K (or H=7 km), and Figures 4.2 and 4.3 correspond to winter conditions, with and without Newtonian cooling respectively.

In every case, the amplitudes calculated with the primitive equation model are smaller, although there is agreement in the vertical structure presented. For the constant case, both simulations are consistent with the case of upward propagation discussed by Charney and Drazin (1961), with the wave tilting westward with height. However, for the model Z, the energy density is no longer uniform, suggesting the presence of some mechanism of dissipation. Figures 4.2 and 4.3 support this idea. Comparing the ZG models with and

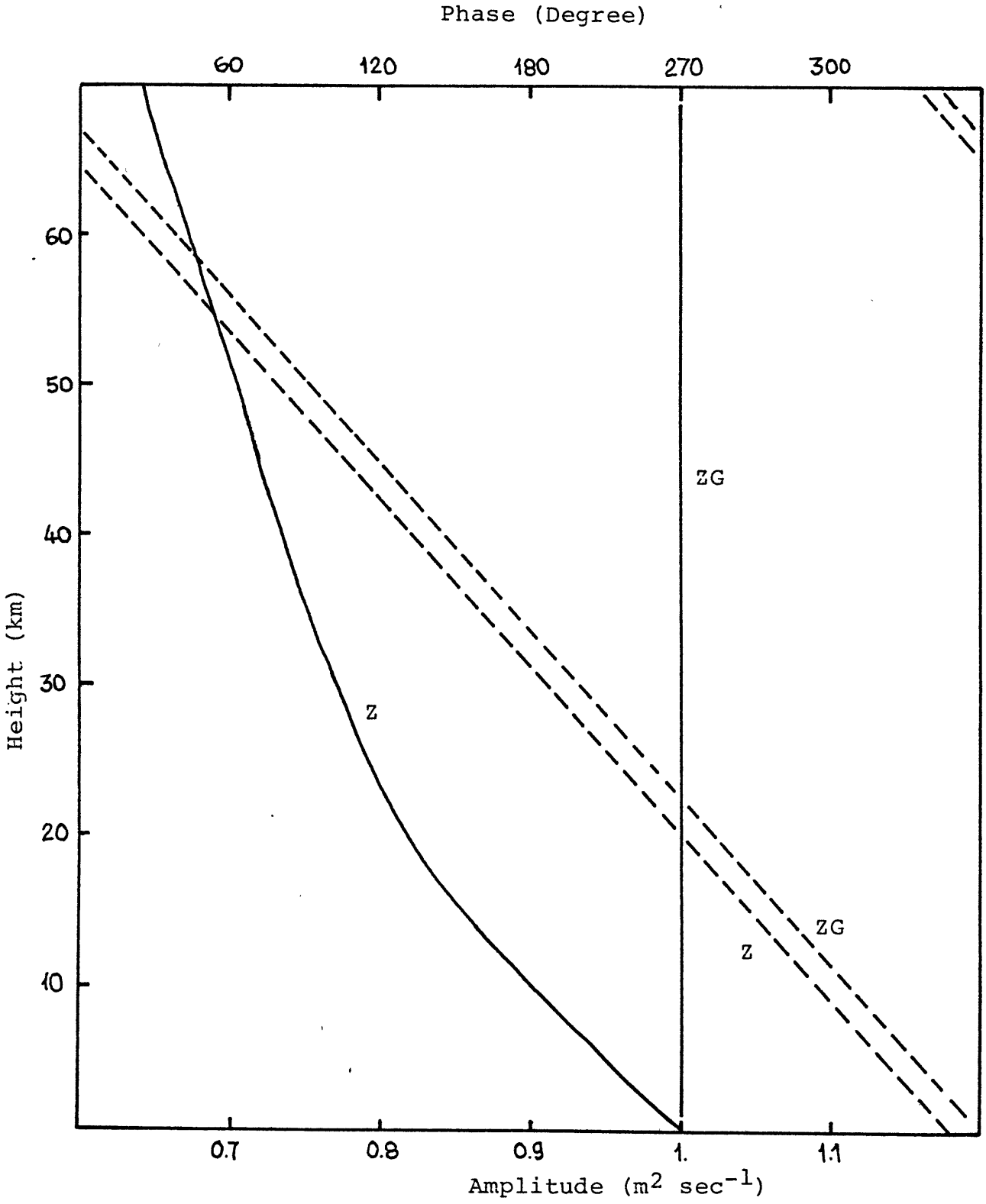

Figure 4.1 Scaled Amplitude (Solid Line) and Phase (Dashed Line) Computed Using the Z and ZG Reference Models (200 Levels), with $\bar{U}$ = 20 m sec^{-1}, α=0, and T_o=239°K

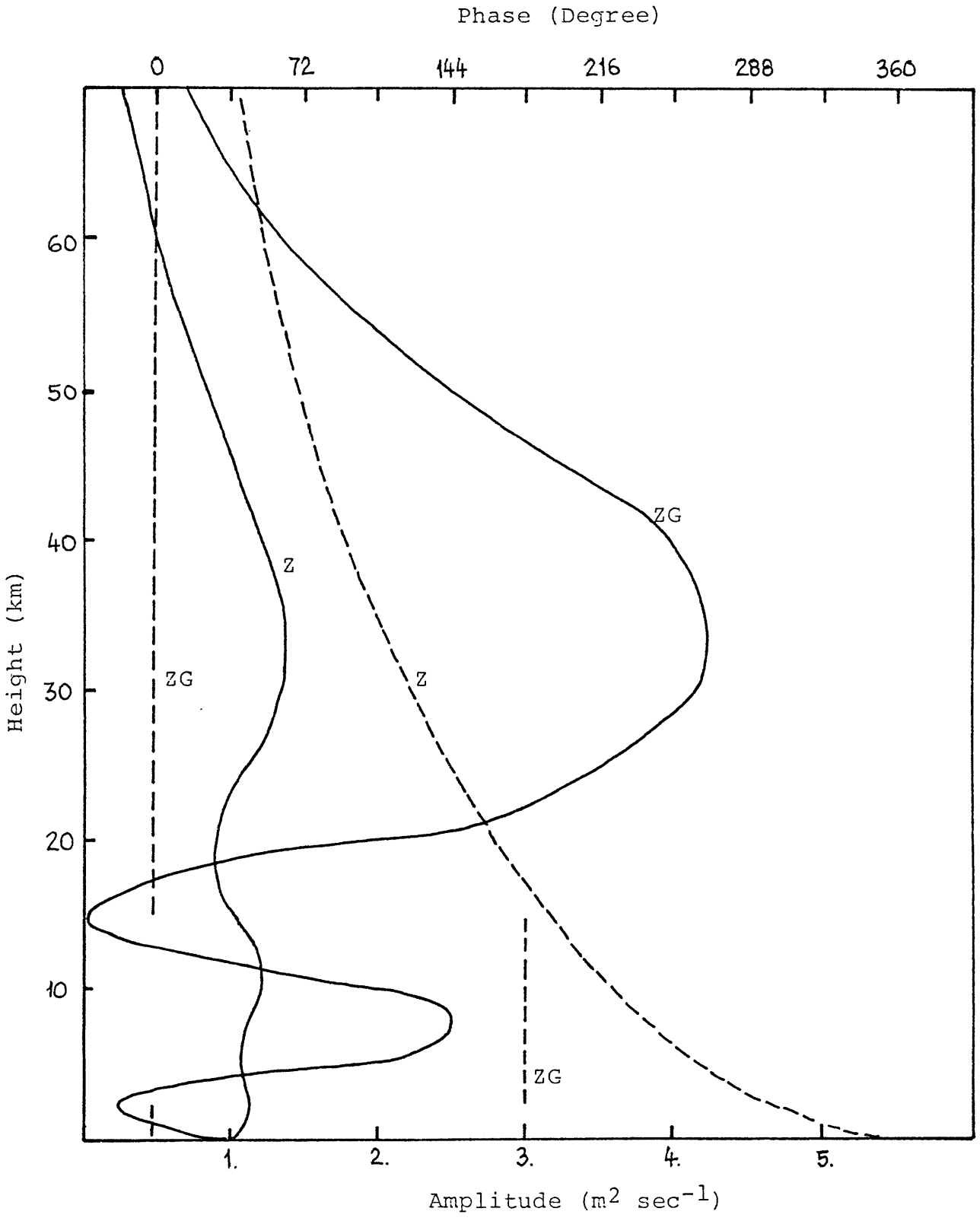

Figure 4.2 Scaled Amplitude (Solid Line) and Phase (Dashed Line) Computed Using the Z and ZG Reference Models (200 Levels), for Winter Winds and α=0.

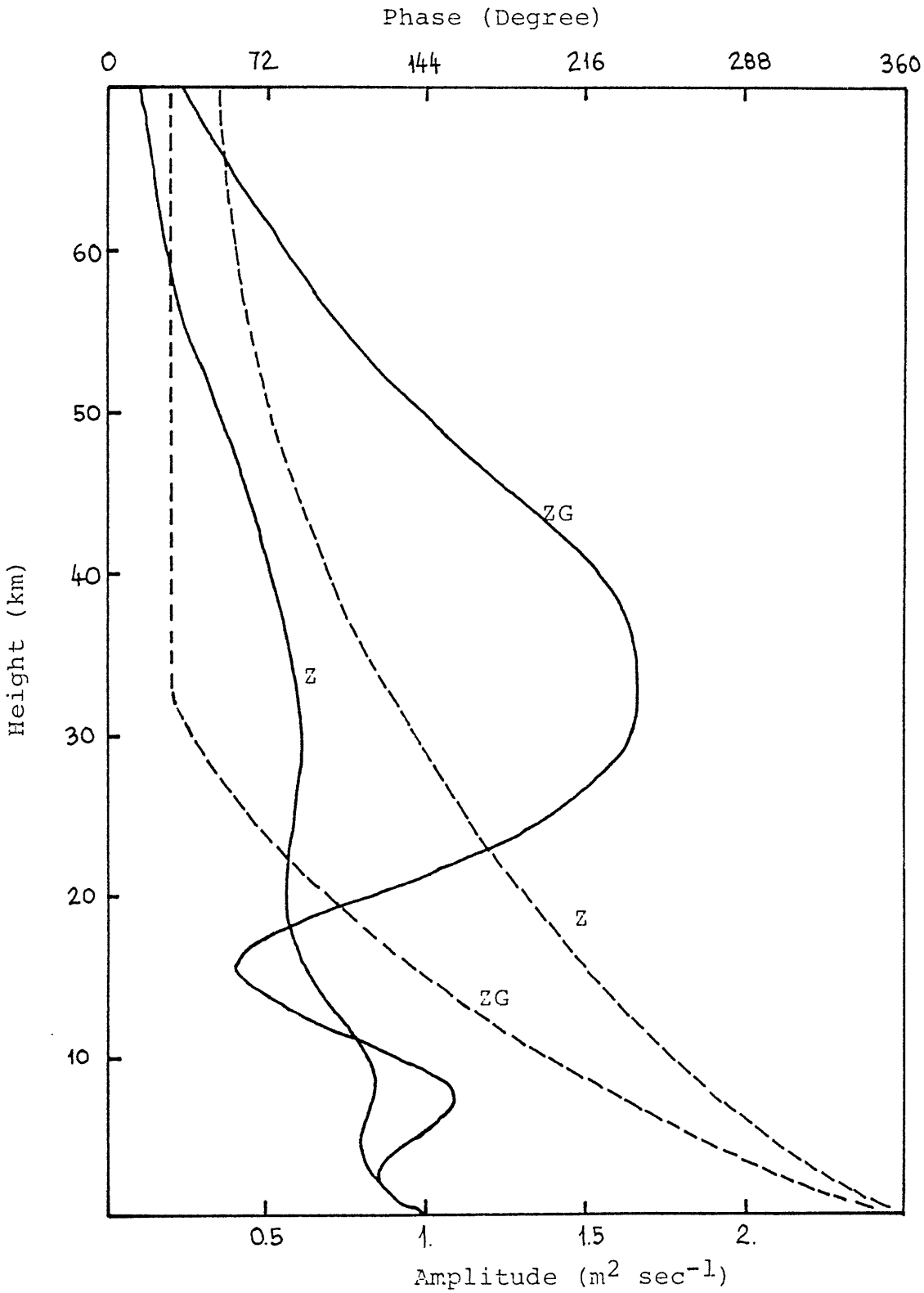

Figure 4.3 Scaled Amplitude (Solid Line) and Phase (Dashed Line) Computed Using the Z and ZG Reference Models (200 Levels), for Winter Winds with Newtonian Cooling.

without Newtonian cooling, it is clear that the inclusion of a damping mechanism modifies the vertical structure of the wave and reduces the upward flux of energy.

Since we have not included any explicit dissipation mechanism in our primitive equation model, this effect must be due to the model's approximations. This is confirmed by the following analysis of the model Z. By applying expressions (18) to (21) to model Z (equations (6) to (10)) we obtain:

$$(m^2\omega + m^2 KU - \beta K)\, E = (\beta l + i f_o m^2)\, D - l \frac{dU}{dz} W$$

$$(m^2\omega + m^2 KU - \beta K)\, D = -(\beta l + i f_o m^2)\, E + K \frac{dU}{dz} W + i m^2 F$$

$$(\omega + UK - i\alpha)\, T + l \frac{\partial T_o}{\partial y} D + K \frac{\partial T_o}{\partial y} E - i S W = 0$$

$$\frac{dF}{dz} = \frac{R}{H} T$$

$$\frac{dW}{dz} - \frac{W}{H} = m^2 D$$

in which $\frac{dT_o}{dy} = -\frac{fH}{R}\frac{dU}{dz}$ by the thermal wind relation and S is the stability parameter, $S = \frac{dT_o}{dz} + \frac{g}{c_p}$.

To keep the analysis simple, we assume constant conditions, that correspond to the situation presented in

Figure 4.1. Then, with U, H, T_o constant and $\alpha = 0$, we solve for W,

$$\frac{d^2W}{dz^2} - \frac{1}{H}\frac{dW}{dz} + \frac{SR\,m^4}{HU}\cdot\frac{m^2U-\beta}{(m^2KU-\beta K)^2+(\beta\ell+if_0m^2)^2}W = 0$$

The coefficient of W is a complex number that produces a complex index of refraction in this wave equation. The damping effect is due to this complex index of refraction. To confirm this interpretation, we repeat the simulations for constant and for winter conditions, but with $\ell = 0$. In this situation ($\ell=0$) the index of refraction is no longer a complex number. For constant conditions, both simulations are identical, with the energy density constant with height. For winter conditions the results are shown in Figure 4.4. The wave structure is the same in both simulations, with differences in the computed amplitudes.

For the general case, $\ell \neq 0$, the index of refraction is complex. This important limitation comes from the fact that we have assumed a constant Coriolis parameter except when it is explicitly differentiated. This "constant coefficient" assumption was made to allow solutions of the form described in (17). The undesirable complex index of refraction does not appear if we keep $f_o + \beta y$ in the equation and solve for the vertical structure equation, as shown by Lindzen (1967).

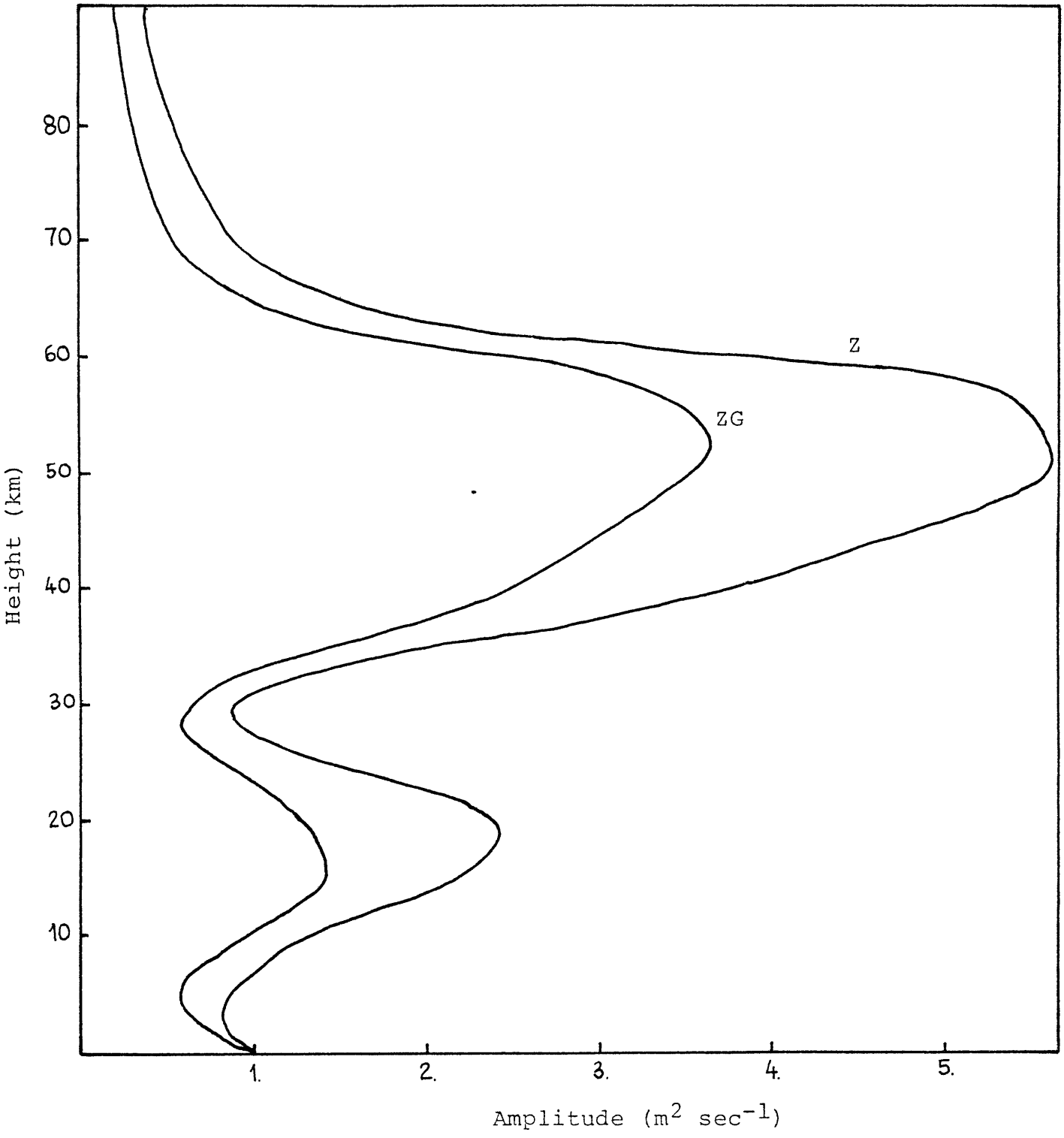

Figure 4.4 Scaled Amplitude Computed Using the Z and ZG Reference Models (200 Levels), for Winter Winds with Meridional Wavenumber $\ell=0$.

However, with this approach, solutions of the form described in (17), with the advantages of simplicity and the possibility of one-dimensional formulation, are no longer possible.

Therefore, in the remainder of this work we are going to limit the discussion to the quasi-geostrophic models ZG and PG.

4.2 Results Obtained with Constant Conditions

Before the study of the vertical propagating waves under general conditions is done, we are going to study the behavior of the models PG and ZG using constant zonal wind, and with $\alpha = 0$ in an isothermal atmosphere. The results obtained under such conditions will help in the interpretation of the results obtained under more general conditions.

In Figure 4.5, the results of the wave structure computed using both models are presented. The values used were $T_o = 239^o$ K (or H=7 km), $\alpha = 0$, and $U = 20$ m sec^{-1}. The reference solution (model ZG with number of levels N = 200) has the scale amplitude constant with height, with a vertical wavelength of about 70 km. The solutions obtained with the PG model clearly indicate that the condition $\frac{dp}{dt} = 0$ at some finite height, is capable of modifying the numerical solution. The scaled amplitudes are no longer constant with height but there is no net vertical propagation of energy since the phase is still constant with height. Figure 4.5 also shows that the

R = Reference

S = 100, 30, 10

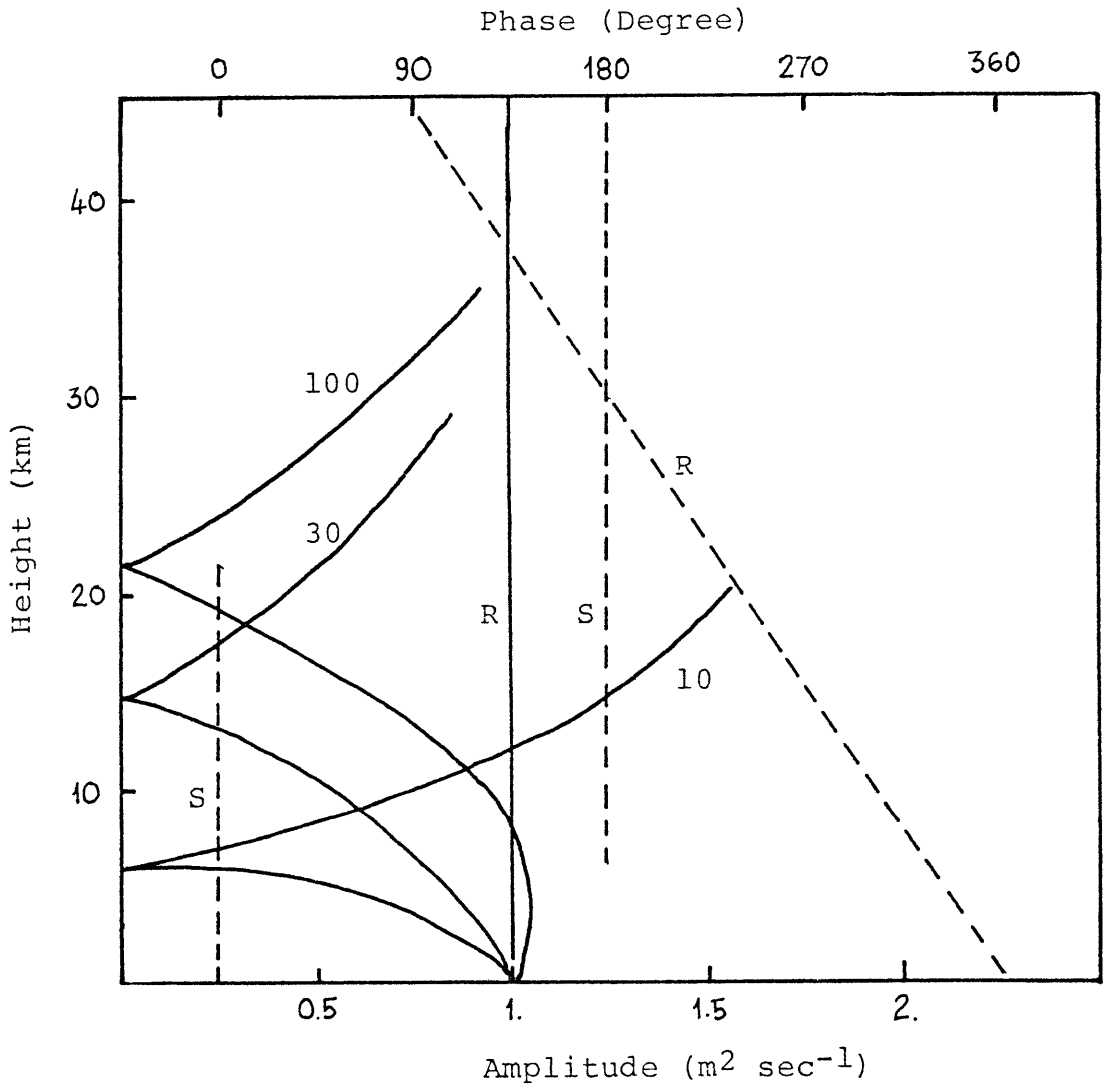

Figure 4.5 Scale Amplitude (Solid Line) and Phase (Dashed Line) Computed Using the Reference ZG Model and the PG Model, with 100, 30, and 10 Levels. $U = 20$ m sec^{-1}, $\alpha = 0$, and $T_o = 239^o$ K.

solution is sensitive to the vertical resolution of the model. As N (the number of levels) decreases, the uppermost computational level is lowered, and this produces the effect of a rigid top at some finite height (Lindzen et al., 1968). When the wave energy reaches this upper boundary, the wave is reflected and the energy propagates downward. The interference produced by the forced and the reflected waves modify the computed solution.

To test the effect of the rigid top and the vertical resolution of model ZG, we performed the same experiments using both the radiation condition and $\frac{dz}{dt} = 0$. The vertical resolution was tested using $N = 10$, 30, 50, 100, and 200. When the condition $\frac{dz}{dt} = 0$ is used (Figure 4.6), the solution is drastically altered. Because of the more uniform distribution of levels in the ZG model, the solutions for $N = 30$ to $N = 200$ are the same. The phase is no longer tilted westward with height and presents discontinuities at 18 and 52 km. The solution $N = 10$ is even worse with a discontinuity at 11 km. When the radiation condition is used (Figure 4.7), the $N = 10$ solution is completely erroneous. As the vertical resolution is increased, the numerical solution approaches the reference solution. From $N = 50$ to $N = 200$ there is practically no difference in the solution.

The results obtained by applying the boundary condition $\omega = 0$ (or W=0) at $p = p_{top}$ illustrate the conclusion already obtained by Lindzen et al. (1968). The application of that

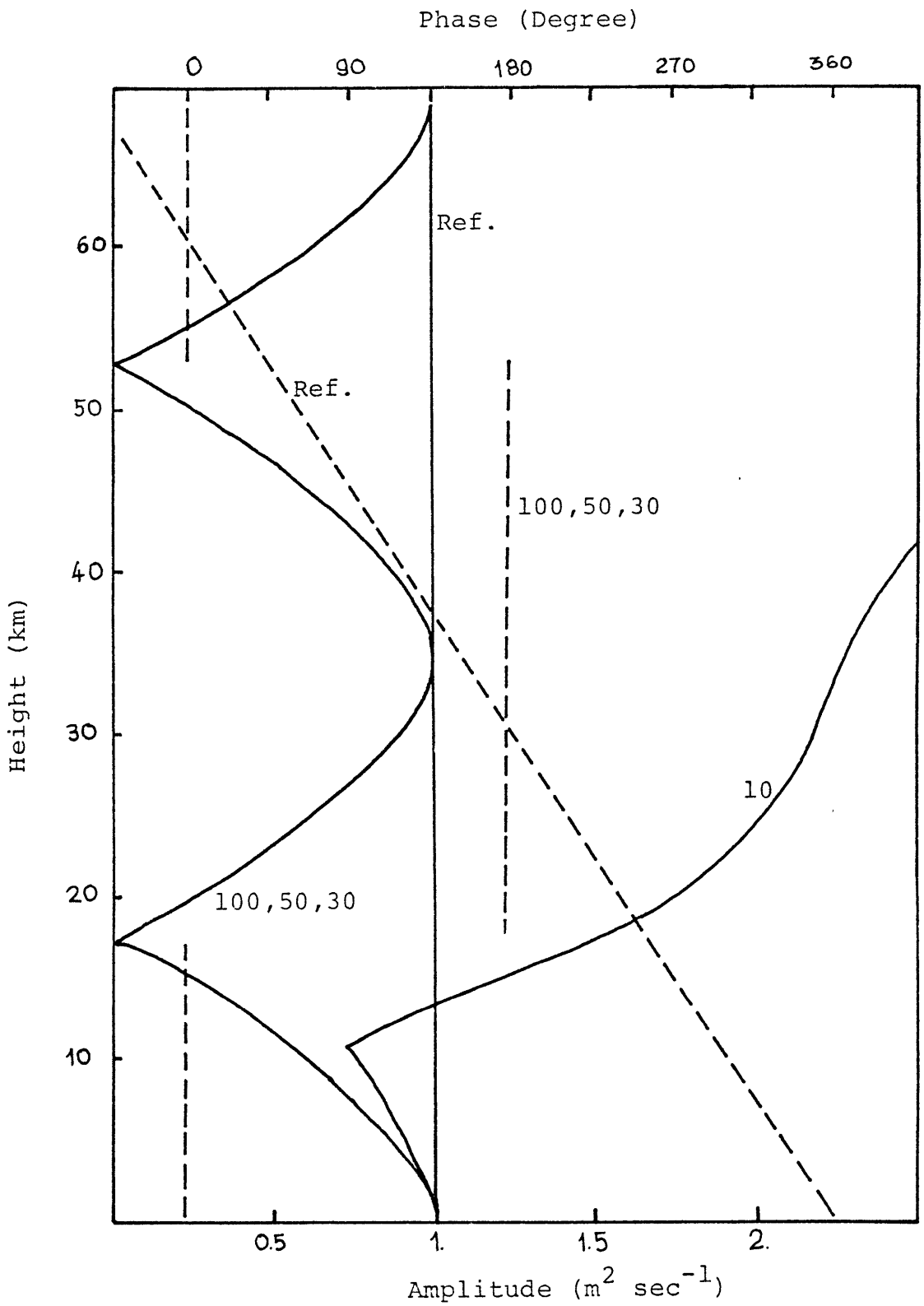

Figure 4.6 Scale Amplitude (Solid Line) and Phase (Dashed Line) Computed Using the Reference Model and the ZG Model, with Rigid Top and Levels 100, 50, 30, and 10. $U = 20$ m sec^{-1}, $\alpha = 0$, and $H = 7$ km.

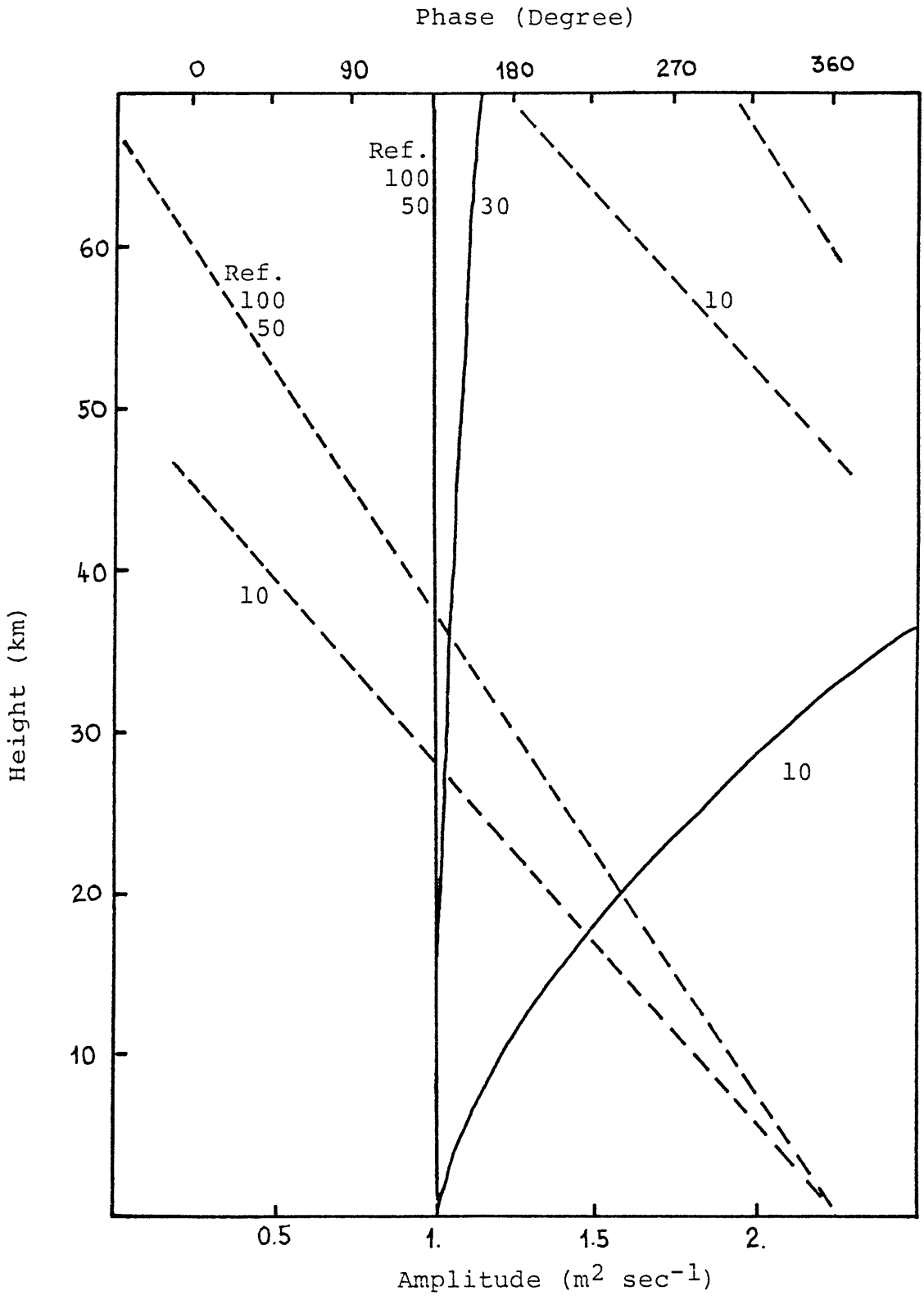

Figure 4.7 Scale Amplitude (Solid Line) and Phase (Dashed Line) Computed Using the Reference Model and the ZG Model, with Radiation Condition and Levels 100, 50, 30, 10. $U = 20$ m sec^{-1}, $\alpha = 0$, and $H = 7$ km.

boundary condition in a finite difference model, has the effect of a rigid top at some finite height producing spurious reflections which are dependent on the vertical resolution of the model. They also suggest that for a typical general circulation model with a number of vertical levels of the order of 10, the standing planetary waves are seriously misrepresented throughout the whole troposphere and stratosphere. This problem will be discussed in more detail in a later section.

For the numerical values used in this experiments we can calculate, using expression (25), the critical velocity at which the waves are reflected. In our case, the critical velocity is 34.8 m sec^{-1}. In order to study the solution corresponding to an external mode, we carried out the same experiment but increasing the mean zonal wind to a value higher than the critical velocity. In Figure 4.8 the results using $U = 60$ m $sec^{-1} > U_{crit}$ are presented. In contrast with the internal mode situation, the structure of the external wave can be properly simulated by both models, regardless of the use of a rigid top. The solution shows an external wave without any propagation of vertical energy. Only for the $N = 10$ case there is a small difference in the amplitude. The similarity of results in this case is due to the fact that the medium produces internal reflection, because of the large value of U. Consequently, much less energy can arrive to the upper boundary.

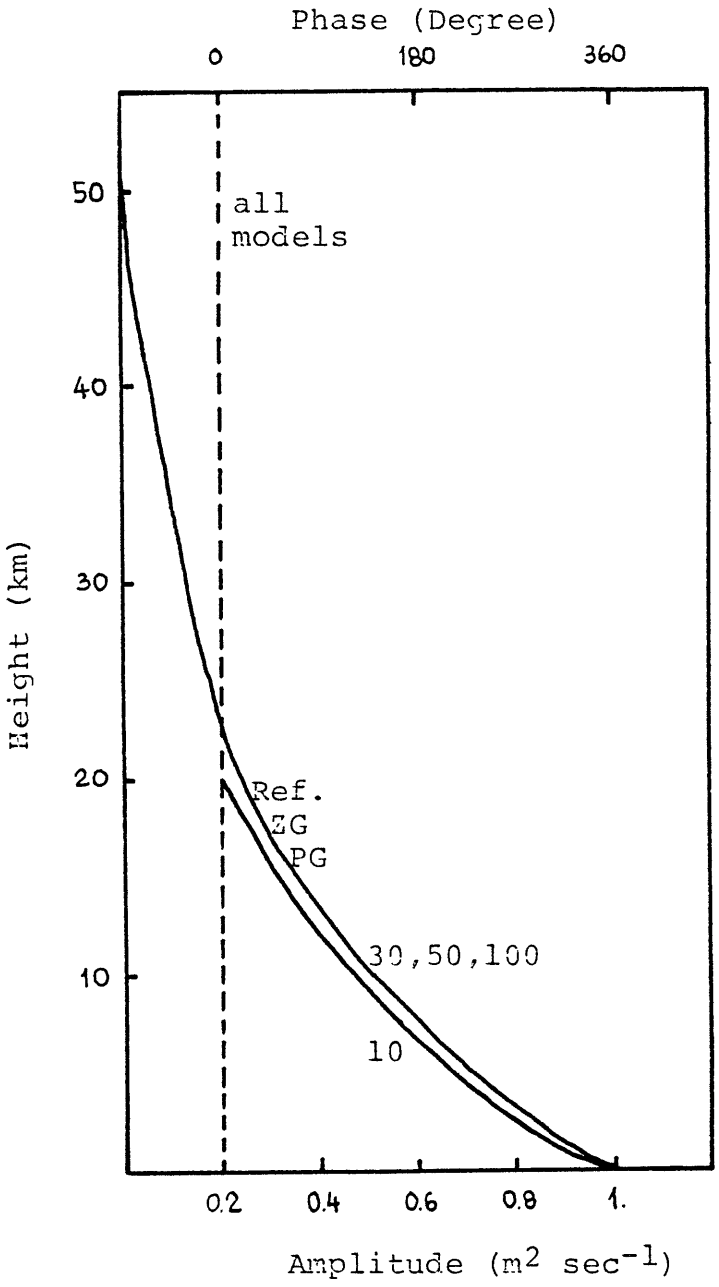

Figure 4.8 Scale Amplitude (Solid Line) and Phase (Dashed Line) Computed Using the Reference Model and the ZG and PG Models with a Rigid Top and Levels 100, 50, 30, and 10. $U = 60$ m sec^{-1}, $\alpha = 0$, and $H = 7$ km (or $T_o = 239^o$ K)

4.3 Simulations with Realistic Winds and Dissipation

In this section we discuss several experiments made with realistic winds and dissipation for Winter, Summer, and Fall conditions. The temperature, zonal winds, and Newtonian cooling profiles are those described in Section 1.3.

In order to be able to use an exact radiation condition in model ZG we modified the temperature, mean zonal wind, and Newtonian cooling coefficient profiles, above 75 km. In this region, the temperature is kept constant at 210^{o} K, the Newtonian cooling coefficient at 1.5×10^{-7} sec^{-1}, and the mean zonal winds are 55, 24, and -30 m sec^{-1} for Winter, Fall, and Summer respectively. Later we repeat the computations with a rigid top boundary condition.

4.3.1 Control Solutions with and without Newtonian Cooling

The results obtained with model ZG with $N = 200$ are taken as reference solutions with which other results are compared. In interpreting the results we have to have in mind the effects of the zonal winds and the dissipation due to Newtonian cooling. A critical velocity can be determined analytically for an isothermal adiabatic atmosphere with constant mean zonal winds (expression (26)). For stationary waves, with westerly winds less than the critical velocity,

the medium allows a vertical flux of energy. Otherwise, the medium behaves as a reflector and the wave energy density decays exponentially.

The results for Winter are presented in Figure 4.9. The scaled amplitude of the wave is oscillatory below 40 km and decays toward the top of the model. The upper region of strong westerly winds, in which the amplitude decays and the phase remains constant, represents a reflective medium. In the region of light westerly winds, the medium allows a wave of the internal type. The oscillatory nature of the waves in this region is a result of the interference between the forced waves and the reflected waves due to the presence of the upper winds. The results show how the medium allows an external mode above a certain level and an internal mode below that level.

To study the effect of the Newtonian cooling, the same simulation with $\alpha = 0$ was performed. The wave is now vertical (the phase is constant in the vertical) with discontinuities at 15 and 3 km produced by the interference between the upward and downward waves. The computations clearly indicate that the inclusion of the radiative damping modifies the vertical structure of the wave and substantially decreases the net upward flux of energy. It is interesting to notice that the damping has small influence on where the maximum of the amplitude occurs but strongly reduces it.

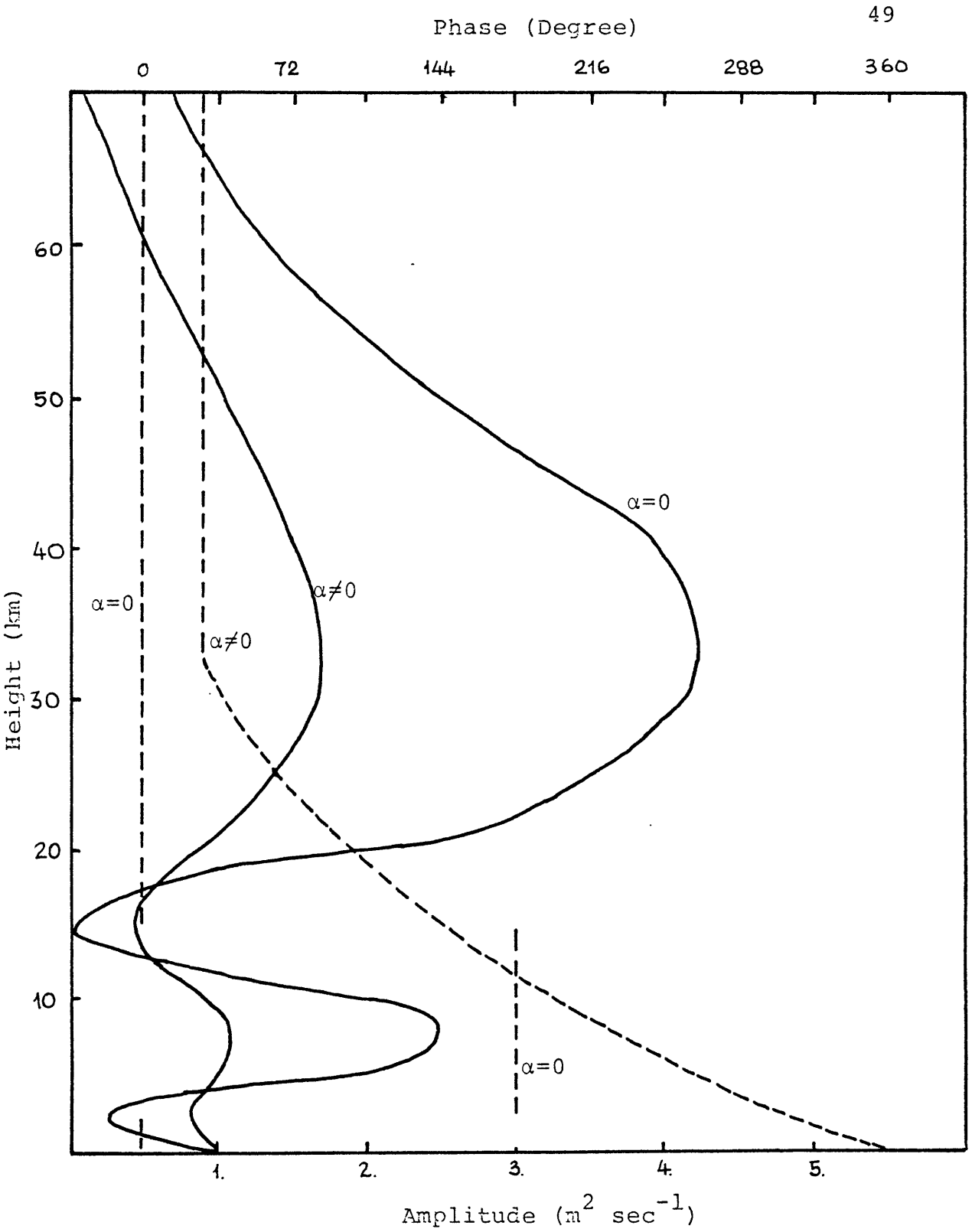

Figure 4.9 Scale Amplitude (Solid Line) and Phase (Dashed Line) Computed Using the Reference Model for Winter without Cooling ($\alpha=0$) and with Cooling (α from Figure 2.4).

For Fall conditions (Figure 4.10) the zonal winds are westerly and weak at all levels, so there is no restriction to the vertical propagation of wave energy. The phase tilted westward all the way up. The case $\alpha = 0$ shows the importance of the radiative damping in Fall, as was pointed out by Dickinson (1969). The results confirm the observational evidence that there is not a large upward propagation of planetary waves as predicted by the Charney-Drazin theory.

For Summer conditions (Figure 4.11) the results are qualitatively similar to those of Winter. The strong easterly stratospheric jet does not allow propagation of wave energy. Up to 20 km, with westerly winds, the wave is oscillatory. Above this level, the wave decays very rapidly. The phase becomes constant above 20 km, confirming the existence of the upper reflective medium. As in previous cases, when $\alpha = 0$, the amplitude of the wave is greater and, consequently, the intensity of the interference is also greater.

4.3.2 Different Horizontal Wavenumbers and Phase Velocity

In another set of experiments we study the behavior of the ZG model under different horizontal wavenumbers k and ℓ, and phase velocity c according to the following table:

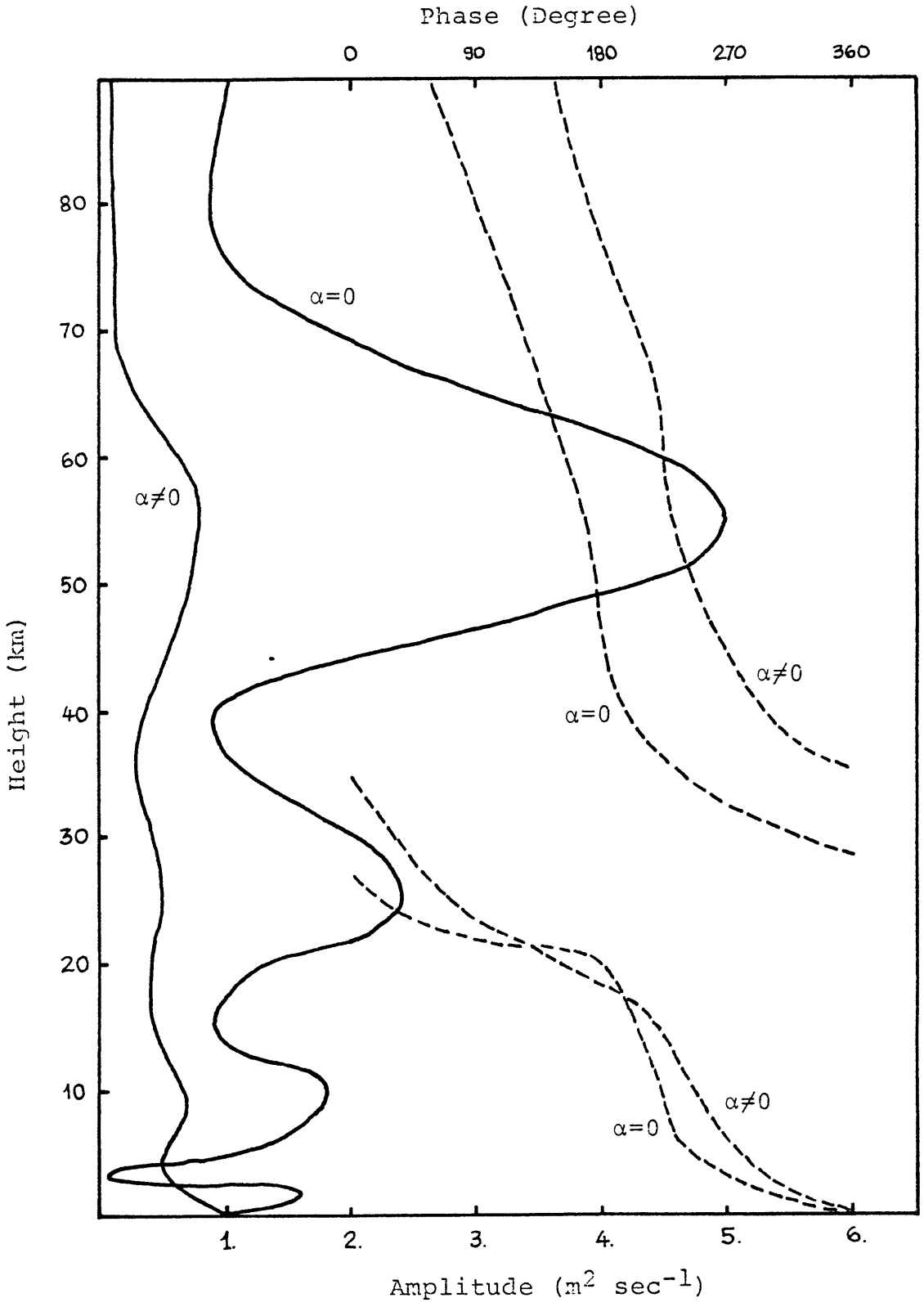

Figure 4.10 Scale Amplitude (Solid Line) and Phase (Dashed Line) Computed Using the Reference Model for Fall without Cooling ($\alpha=0$) and with Cooling (α from Figure 2.4).

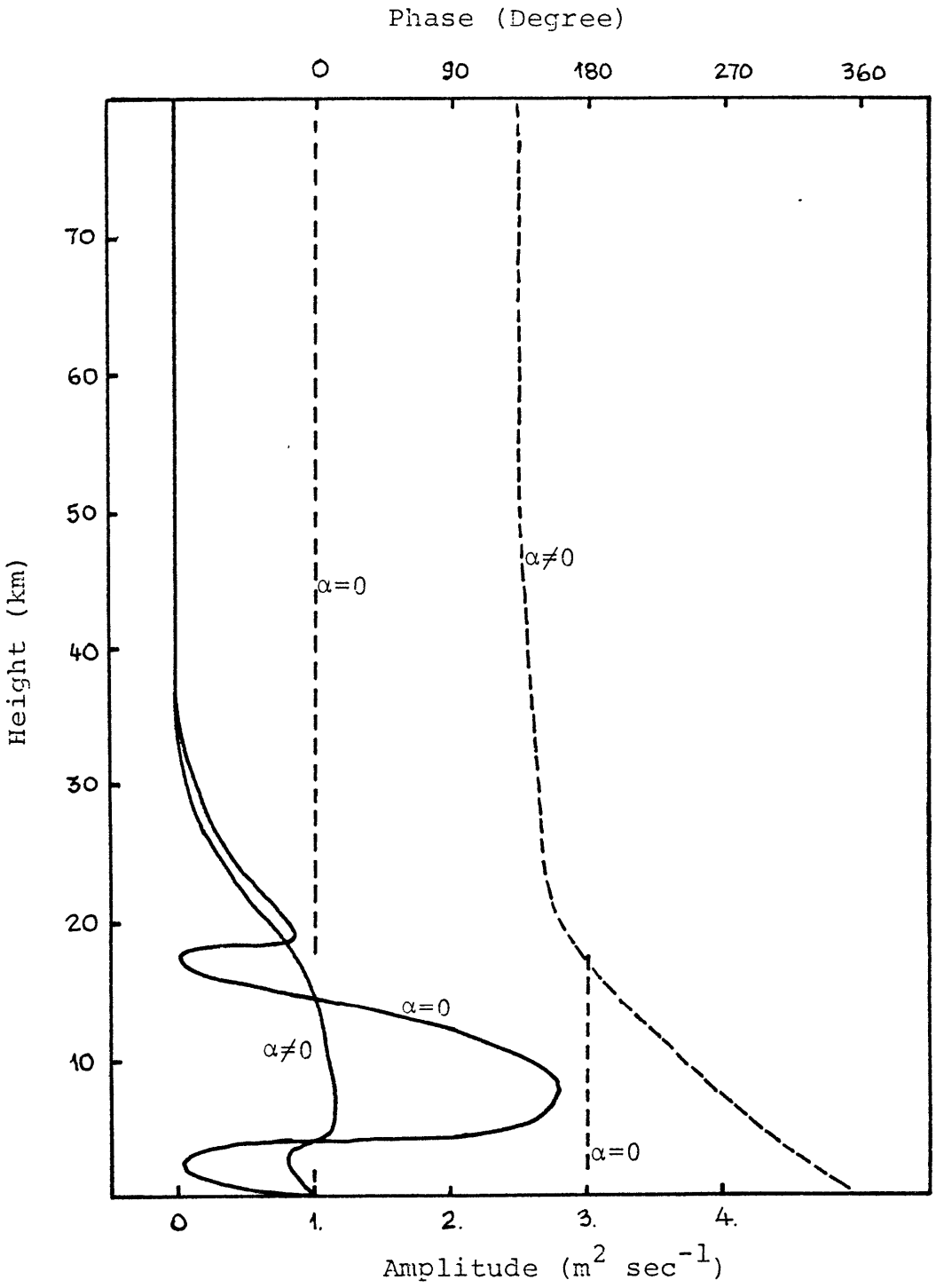

Figure 4.11 Scale Amplitude (Solid Line) and Phase (Dashed Line) Computed Using the Reference Model for Summer without Cooling ($\alpha=0$) and with Cooling (α from Figure 2.4).

Case	k	ℓ	c
I	2.7347×10^{-7}	3.4902×10^{-7}	0.
II	2.7347×10^{-7}	6.9804×10^{-7}	0.
III	5.4696×10^{-7}	3.4902×10^{-7}	0.
IV	5.4696×10^{-7}	6.9804×10^{-7}	0.
V	2.7347×10^{-7}	3.4902×10^{-7}	5.
VI	2.7347×10^{-7}	6.9804×10^{-7}	5.

Case I represents a stationary wave with zonal wavenumber 1, and a northward width of 18 000 km. Case II reduces the northward width to 9 000 km.

Cases III and IV are the same as I and II but for zonal wavenumber 2.

Cases V and VI are transient waves, with zonal wavenumber 1 and northward widths of 18 000 and 9 000 km respectively.

Simulations for Winter, Summer, and Fall were made for the six cases. The results are shown in Figures 4.12, 4.13, and 4.14. The general features for each season, discussed in the previous section, are present in these simulations.

In Winter (Figure 4.12) for cases II, III, and IV, the waves are reflected at a lower level -about 12, 13, and 7 km respectively. Using expression (26) we evaluate the critical velocity for the first four cases, assuming $\alpha = 0$ and $H = 7$ km. The critical velocities are 34.8, 17.7, 21.8, and 13.6 m sec^{-1} respectively. These values explain the reduction of vertical penetration and confirm the observational

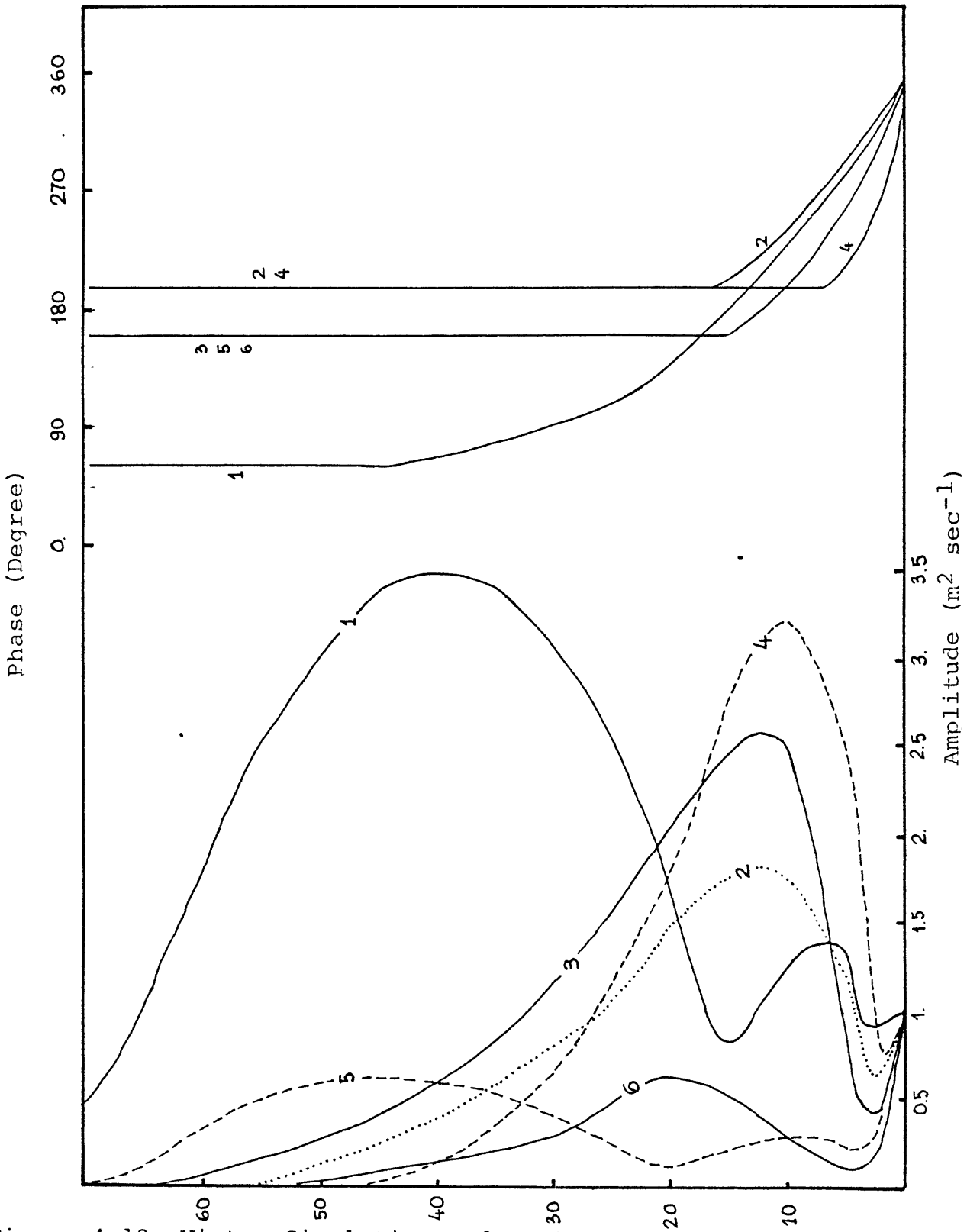

Figure 4.12 Winter Simulations of Scaled Amplitude (left) and Phase (right) Computed Using the Reference Model for Cases I to VI (1 to 6 in the Figure) Described in the Table of Page 53.

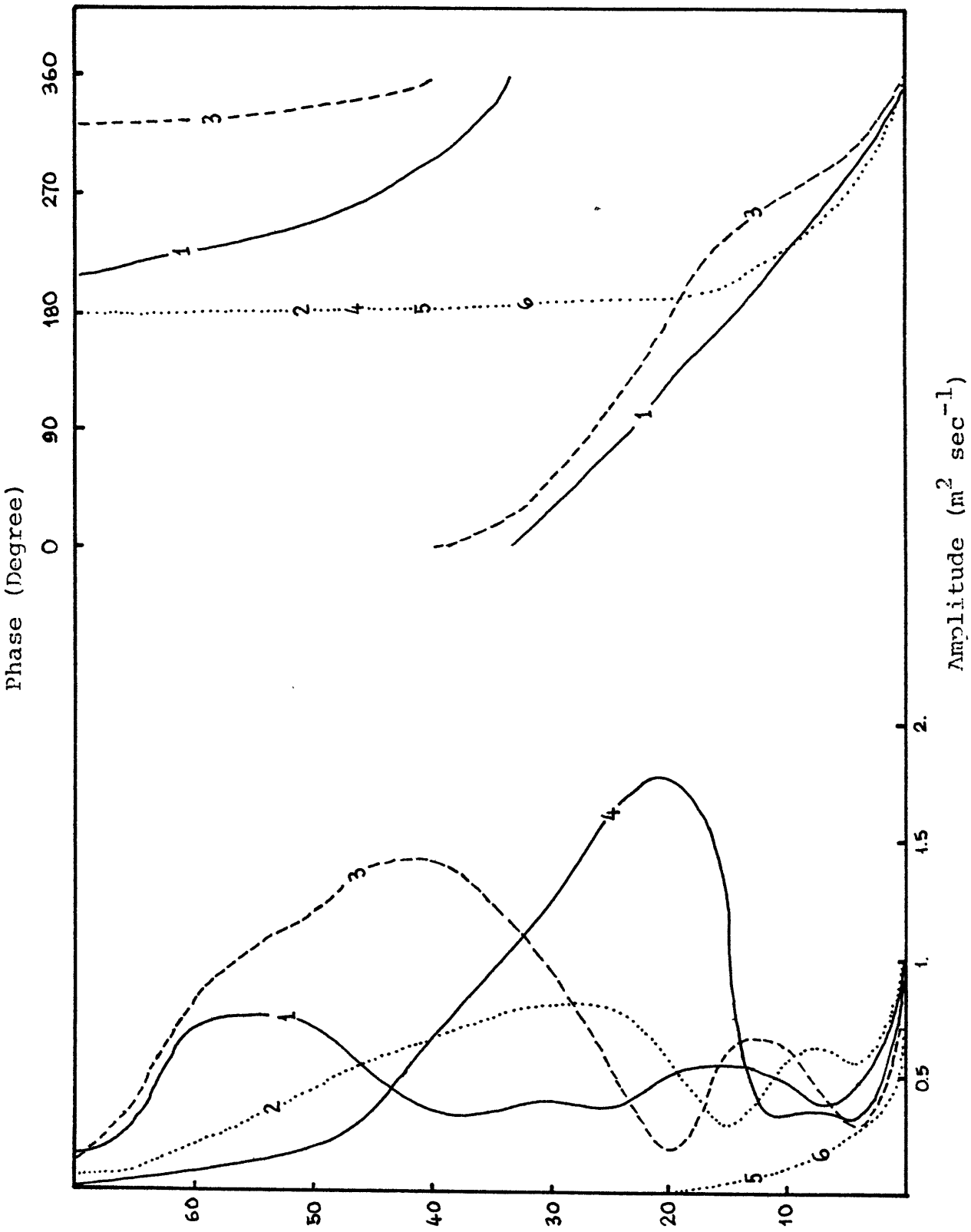

Figure 4.13 Fall Simulations of Scaled Amplitude (left) and Phase (right) Computed Using the Reference Model for Cases I to VI (1 to 6 in the Figure) Described in the Table of Page 53.

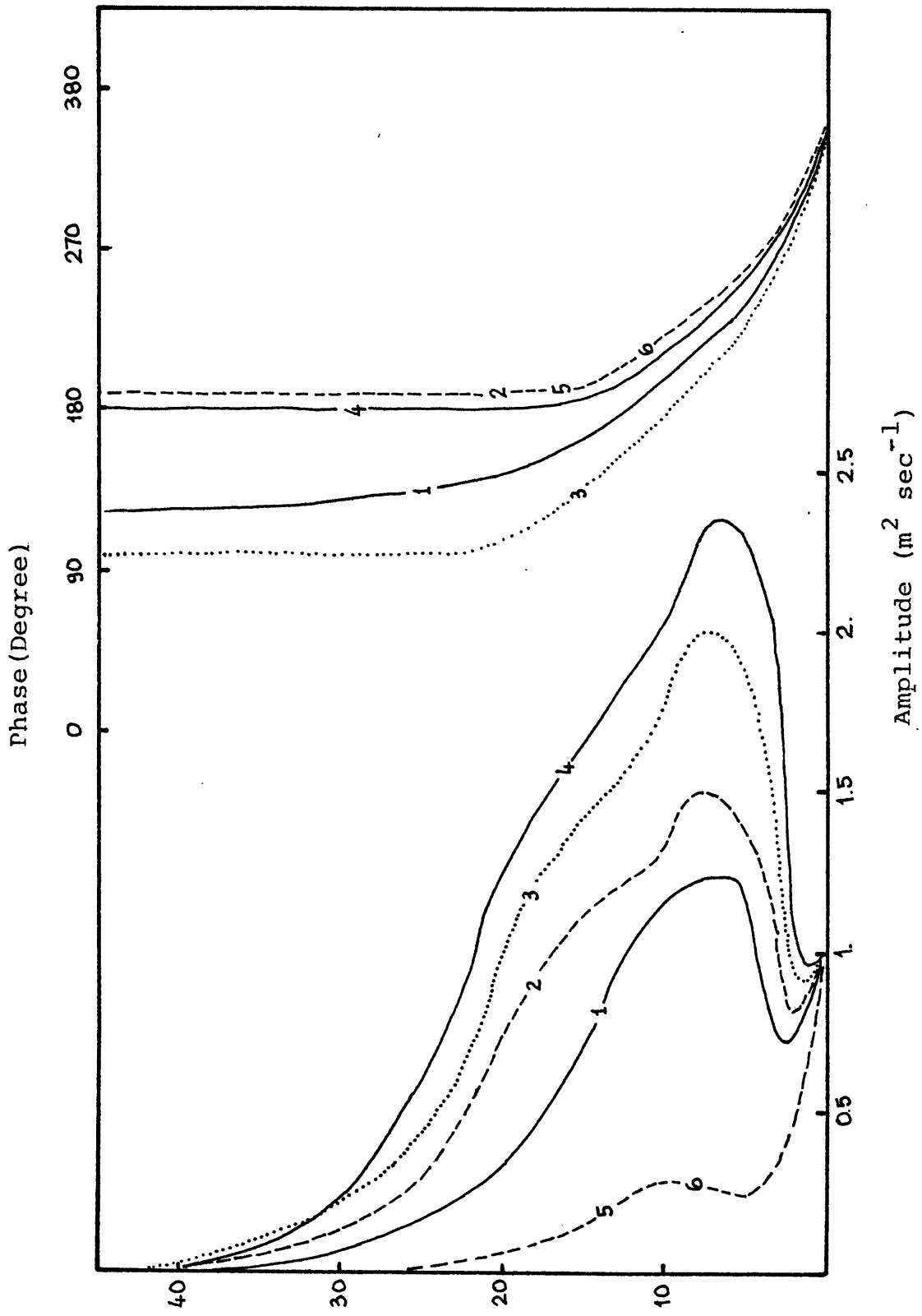

Figure 4.14 Summer Simulations of Scaled Amplitude (left) and Phase (right) Computed Using the Reference Model for Cases I to VI (1 to 6 in the Figure) Described in the Table of Page 53.

evidence that wavenumber 1 is one of the most freely propagating waves in the atmosphere. The inclusion of $c = 5$ m sec^{-1} (cases V and VI) results in more vertical penetration (see expression (26)), but reduces significantly the amplitude of the wave.

In Fall (Figure 4.13), with weak westerlies, there is no inhibition of the vertical propagation of wave energy. However, for cases II and IV, the medium allows a wave of the external type in the upper levels. We confirmed these results by calculating the index of refraction γ under constant conditions using expression (32). For cases I and III, γ is real, while for II and IV, γ is imaginary.

In Summer (Figure 4.14), the decreasing of the horizontal wavelengths results on an increasing in the amplitude at low levels, without changing the wavelike structure. At upper levels, the easterlies inhibit vertical propagation.

These results suggest that the effect of the artificial top boundary condition $\omega = 0$ will be much more serious for the longest stationary planetary wave than for waves which are either shorter or transient.

4.3.3 Winter Simulations

The performance of the model PG under Winter conditions is shown in Figure 4.15. The $N = 100$ model is in very good agreement with the control solution, so we may conclude that

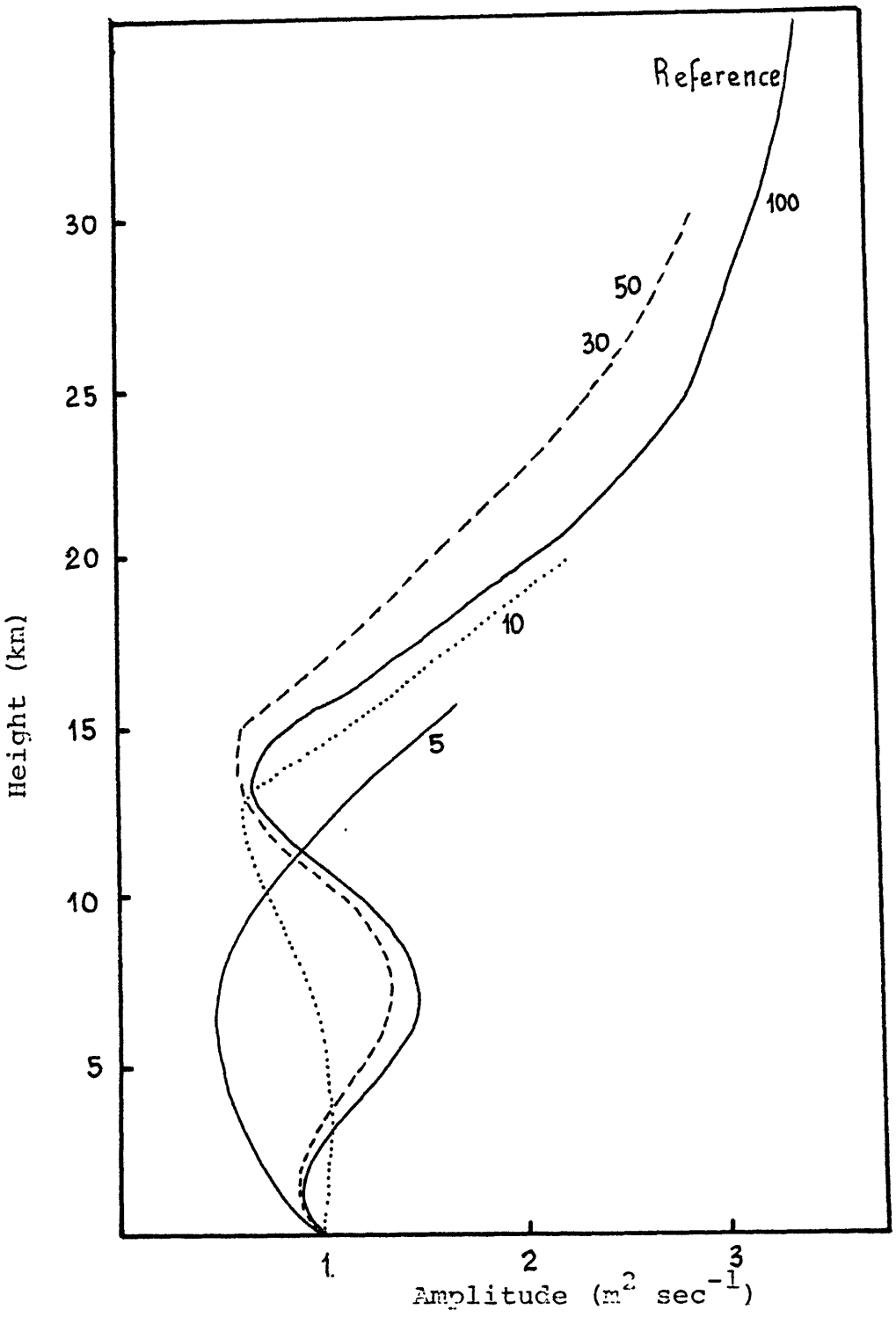

Figure 4.15 Winter Simulations of Scaled Amplitude Computed Using the Reference Model and the PG Model with a Rigid Top and Levels 100, 50, 30, 10, and 5.

the spurious reflection at the rigid top is insignificant. The amplitude and energy propagation of the forced wave are small in the vicinity of the upper boundary. The decrease in resolution produces systematic changes in the computed structure, until $N = 5$ model has little resemblance with the control solution.

We have already shown that the use of a rigid top produces undesirable reflections. By decreasing the resolution of the PG models, we decrease the height of the highest computational level. If the resolution is sufficiently poor, the model becomes completely unaware of the existence of the reflecting layer produced by the strong westerly winds. Consequently, the forced wave in a low resolution model is not subject to an internal reflection by the medium, and propagates energy to the upper boundary where it suffers reflection.

Figure 4.16 shows the performance of the model ZG with a rigid top boundary condition. The simulations with $N = 30$, 50, and 100 are identical to the reference solution. The wave structure is well represented because the models have many levels uniformally distributed throughout the atmosphere, and consequently, they can simulate accurately the atmospheric conditions. When the levels decreased to $N = 10$ and 5, the model could not resolve the wave structure properly due to the sparcity of layers in the lower atmosphere. With $N = 10$ there is only one level in the troposphere, while for $N = 5$, the first computational level

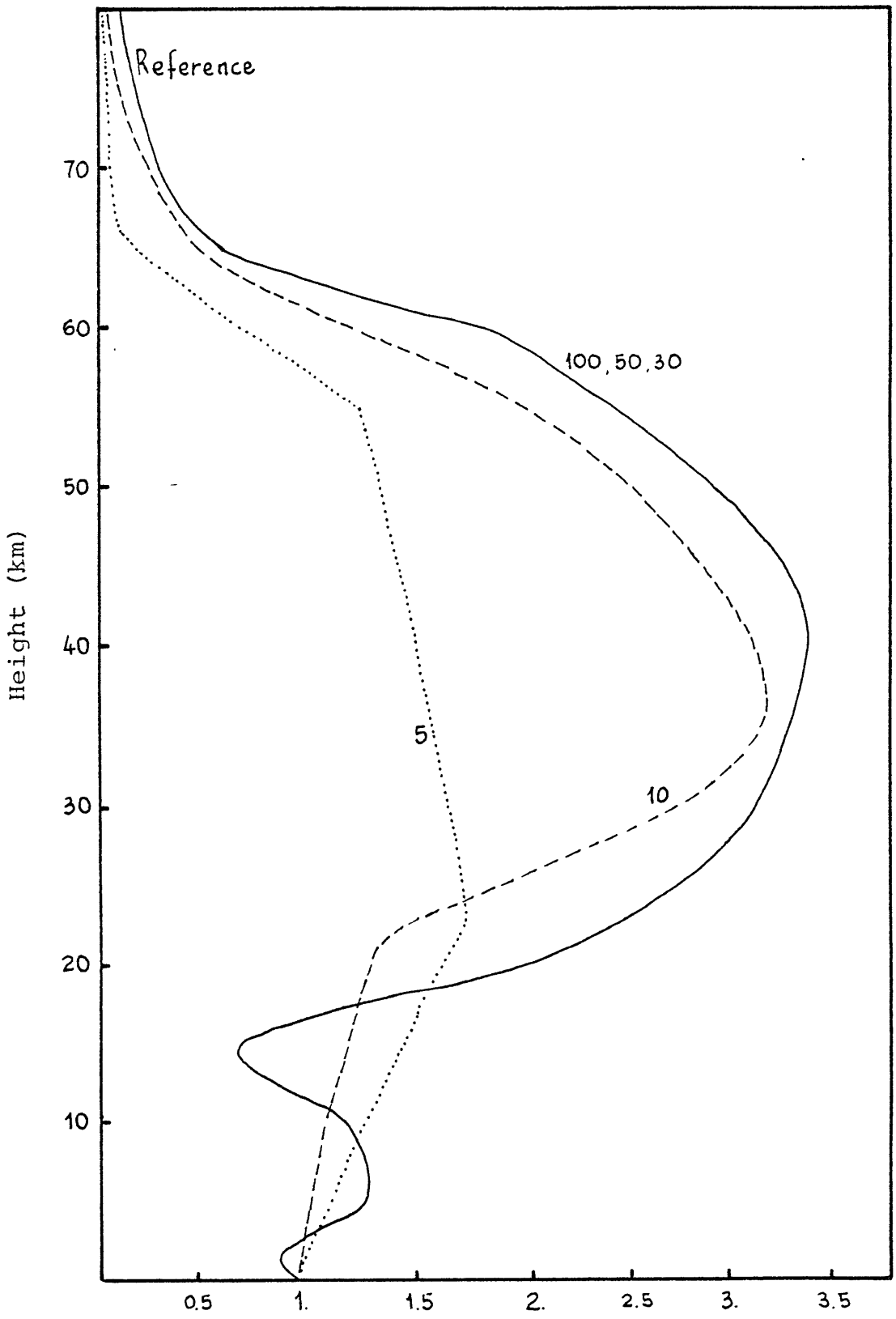

Figure 4.16 Winter Simulations of Scaled Amplitude Computed Using the Reference Model and the ZG Model with a Rigid Top and Levels 100, 50, 30, 10, and 5.

is in the mid-stratosphere.

4.3.4 Fall Simulations

Figure 4.17 shows the PG computations for Fall conditions. The results are in reasonable agreement with the control simulation, suggesting that the upper boundary condition is not that important. The Fall zonal winds, being westerly and weak at all levels, do not inhibit the vertical propagation of wave energy. Consequently, the explanation here must be different from the winter case. In the fall, Newtonian cooling must be the mechanism that absorbs most of the vertical propagating wave energy before it reaches the upper boundary. To test this interpretation, the same simulation with $\alpha = 0$ was performed. The results are shown in Figure 4.18. The PG simulations have little resemblance with the control solution. The oscillatory nature of the waves and the discontinuities in the phase are a consequence of the interference between the forced wave and the reflected wave. Then, with $\alpha = 0$, more wave energy reaches the upper boundary and is reflected down, increasing by interference the amplitude of the wave.

An important difference with the Winter simulations are the solutions obtained with low resolution models. The $N = 10$ and 5 models produce a reasonable simulation of the troposphere and low stratosphere. These results have an important significance for the simulation of planetary vertical waves by

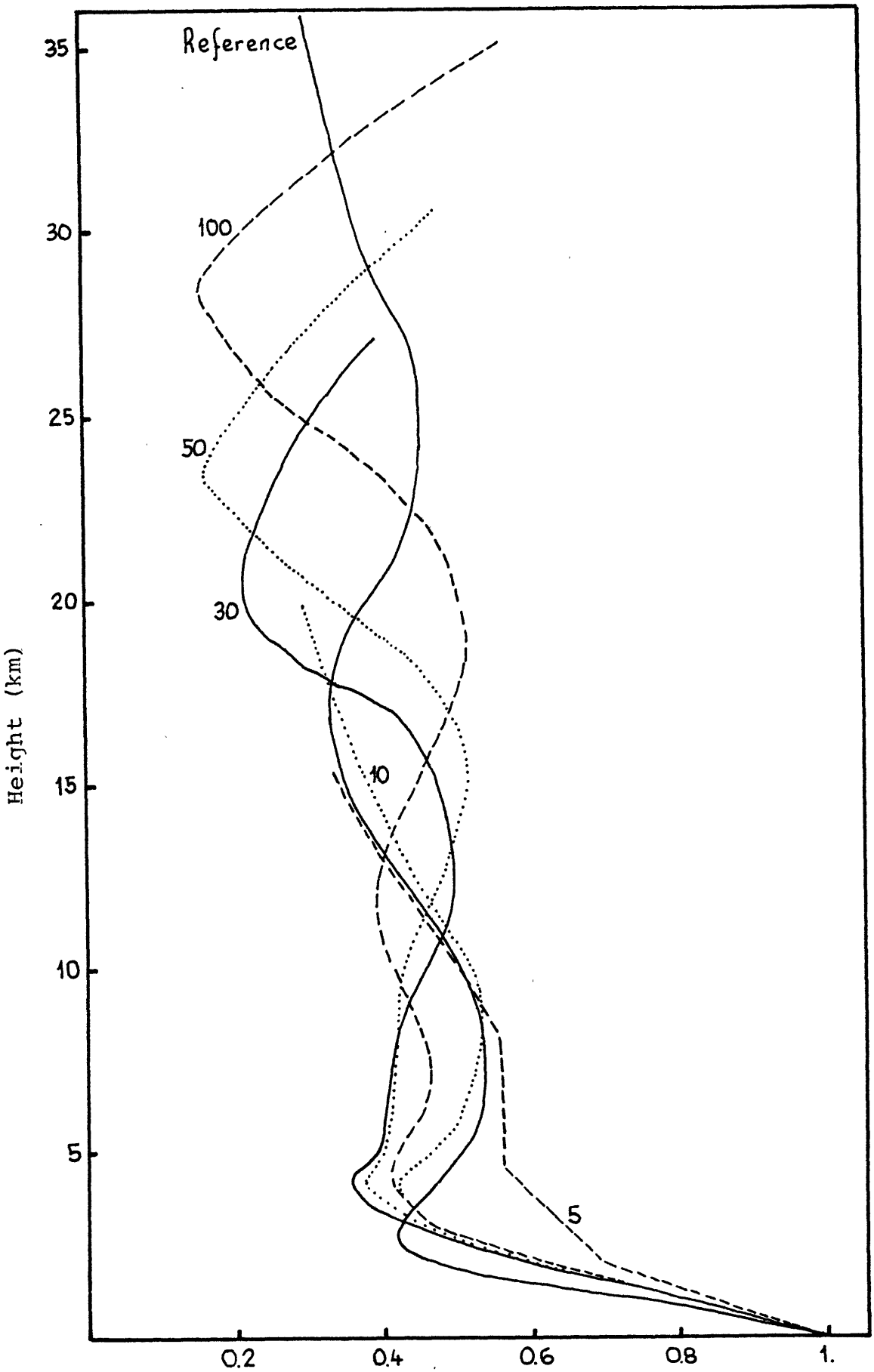

Figure 4.17 Fall Simulations of Scaled Amplitude Computed Using the Reference Model and the PG Model with a Rigid Top and Levels 100, 50, 30, 10, and 5.

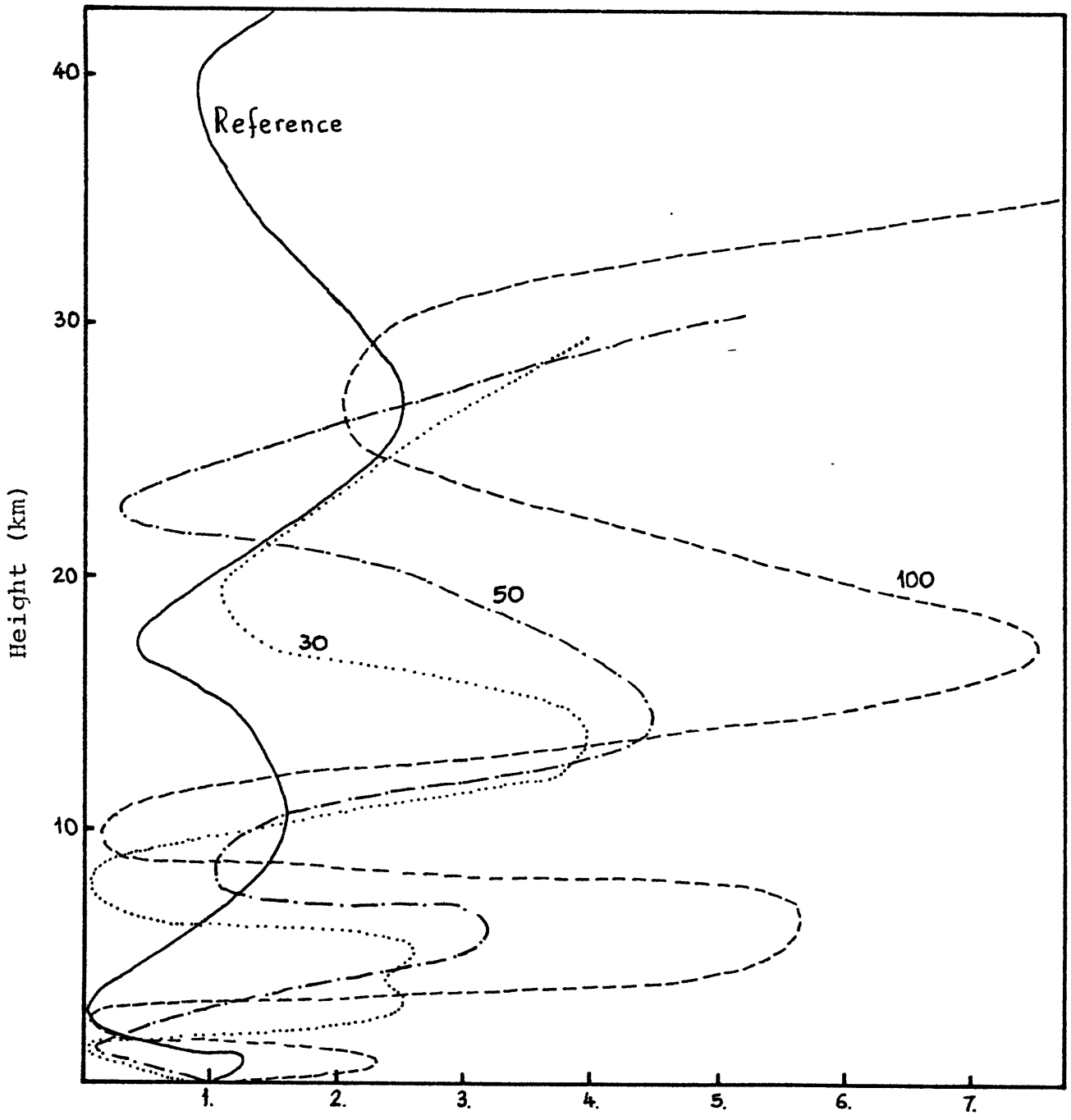

Figure 4.18 Fall Simulations without Newtonian Cooling (α=0) of Scaled Amplitude Computed Using the Reference Model and the PG Model with a Rigid Top and Levels 100, 50, and 30.

general circulation models. They suggest that with a proper lower boundary condition (orography and surface temperature), a good tropospheric resolution will produce adequate tropospheric results regardless the conditions of the upper atmosphere.

The Fall simulations using model ZG are shown in Figure 4.19. The N = 100, 50, and 30 models produce similar results. The mesosphere is not well represented due to the effects of the upper boundary conditions. Some of these effects also affect the stratospheric wave structure.

The simulations with low resolution (N = 5 and 10) are completely erroneous due to the scarcity of computational levels in the lower atmosphere.

4.3.5 Summer Simulations

For Summer conditions, we must expect results similar to those of Winter. During the Summer the stratospheric easterlies prevent the vertical propagation of wave energy, while during the Winter this is done by the high westerly winds.

The results using the pressure model are in Figure 4.20. For the low resolution simulations we obtained the expected departures from the control solution, due to the fact that the model is unaware of the easterly winds. The N = 100, 50, and 30 models present a good agreement with the reference case. The PG models have all the computational levels in the

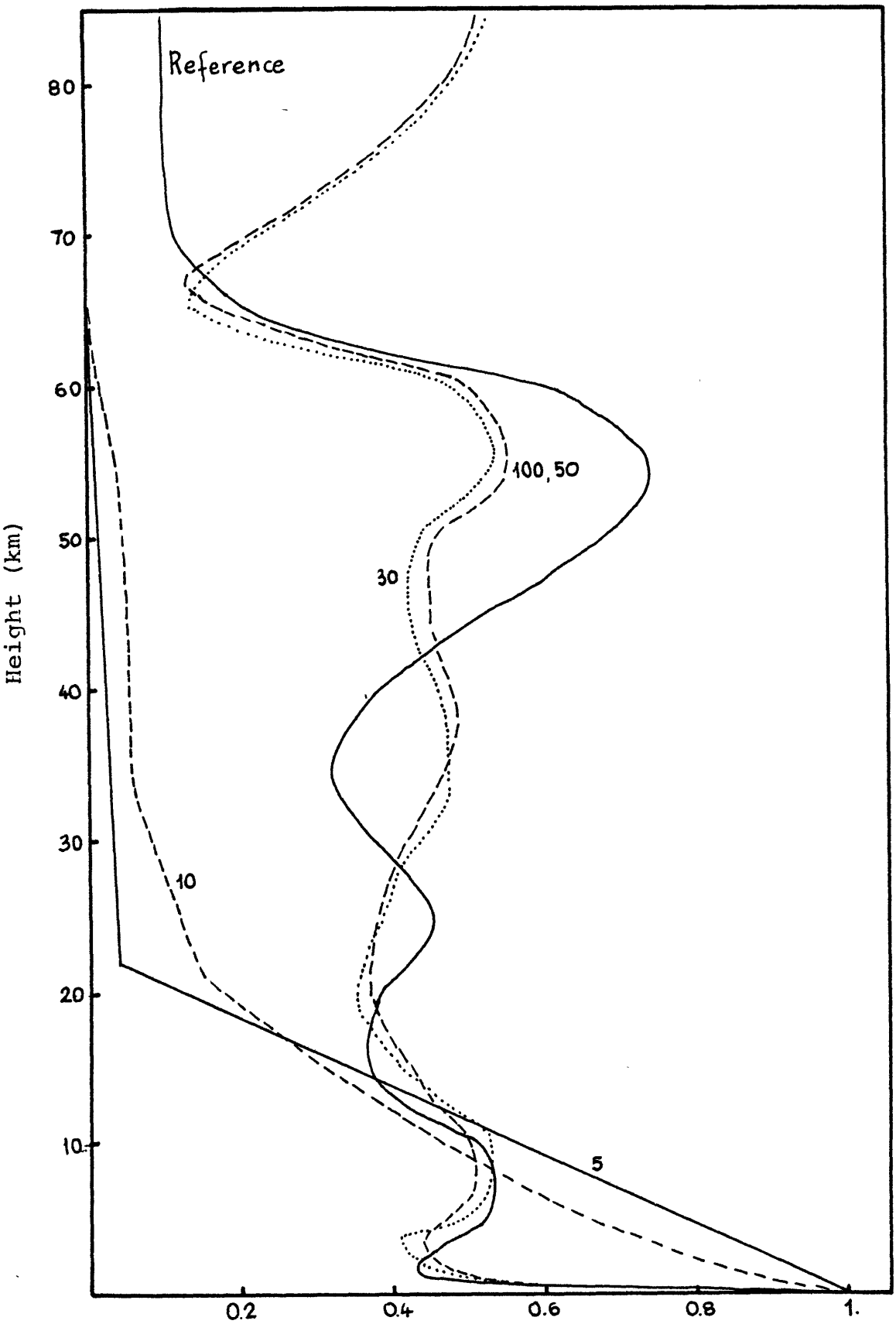

Figure 4.19 Tall Simulations of Scaled Amplitude Computed Using the Reference Model and the ZG Model with a Rigid Top and Levels 100, 50, 30, 10, and 5.

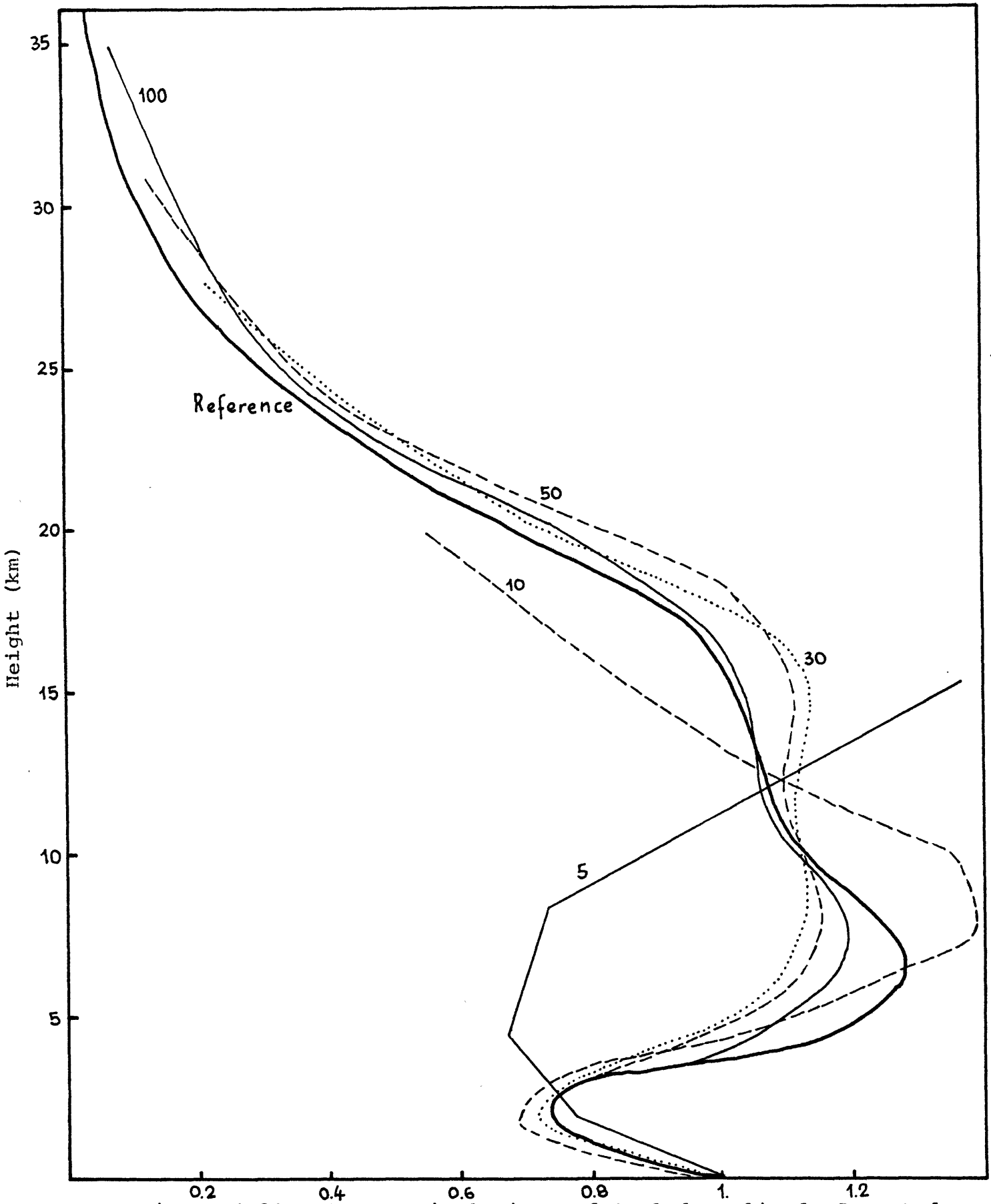

Figure 4.20 Summer Simulations of Scaled Amplitude Computed Using the Reference Model and the PS Model with a Rigid Top and Levels 100, 50, 30, 10, and 5.

troposphere and low stratosphere, where the main activity takes place during the Summer. Figure 4.21 shows the simulations with the log-pressure coordinate model. The N = 100 and 50 simulations are in good agreement with the reference case. As the resolution decreases, the wave structure becomes erroneous. The sparcity of levels in the troposphere and low stratosphere is responsible for this misrepresentation.

4.3.6 Rigid Top at 35, 20, and 12 km

We have seen that the vertical profiles of the zonal winds in the stratosphere for Summer and Winter were very important in the determination of the structure of the vertical propagating waves. For Fall, with weak westerly winds, the damping effect produced by Newtonian cooling is the main factor.

By decreasing the depth of the atmosphere in the model, we do not allow some of these factors to interact with the vertical propagating waves. Several experiments with a rigid top at 35, 20, and 12 km were made for Summer, Winter, and Fall conditions. The model ZG was used because, as we already saw, a numerical model which uses Δz increments provides a more uniform resolution for waves that propagate energy vertically than a model that uses constant Δp increments, since these waves have a sinusoidal dependence

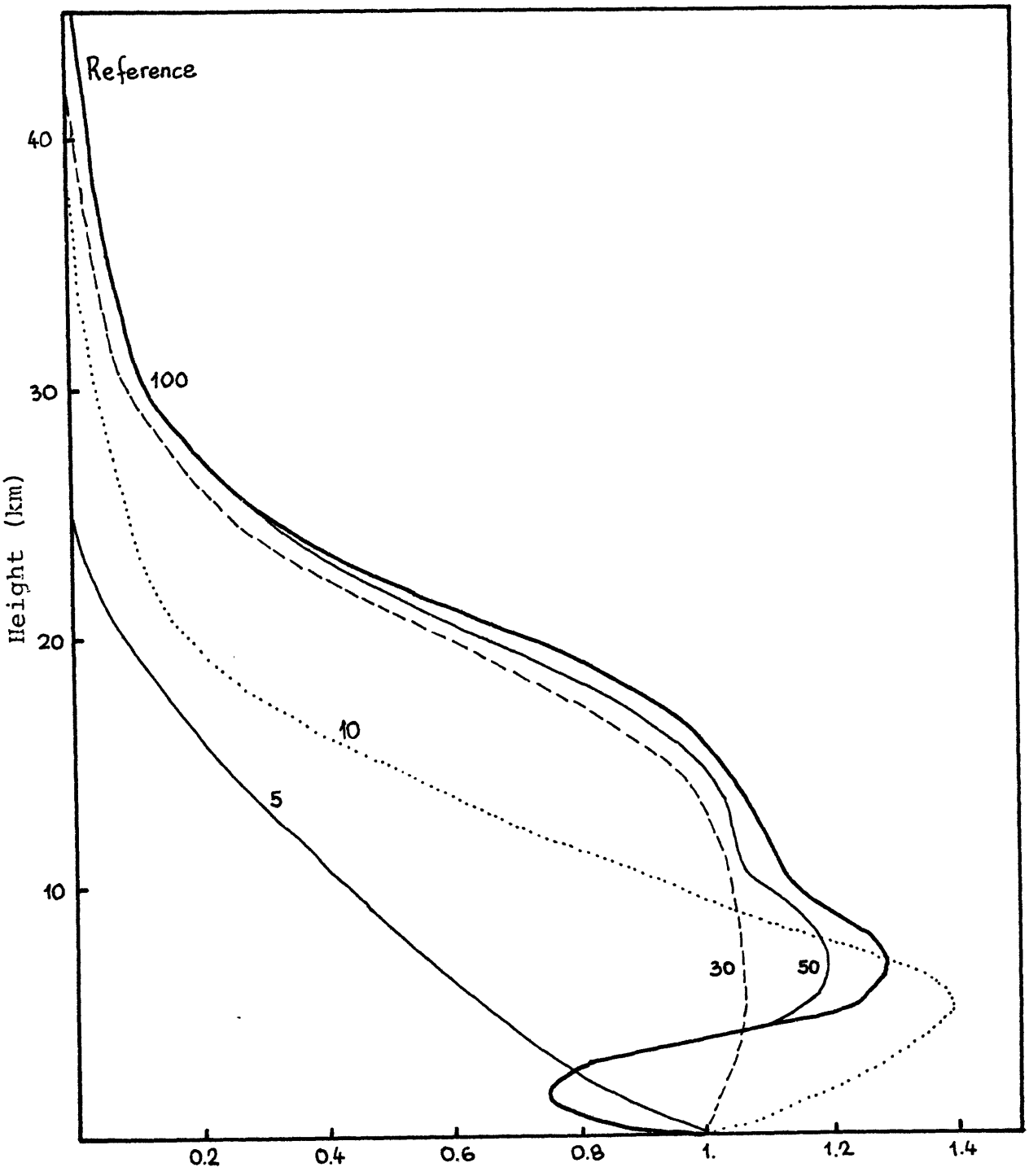

Figure 4.21 Summer Simulations of Scaled Amplitude Computed Using the Reference Model and the ZG Model with a Rigid Top and Levels 100, 50, 30, 10, and 5.

on z. The effect of decreasing the depth of the atmosphere, using a pressure model that simulates a currently used general circulation model, will be discussed in the next section.

Figure 4.22 shows the simulation of the reference case together with the simulation using a rigid top at 35 km for Summer, Winter, and Fall. For Summer there is no difference in the scale amplitude between both simulations. The model is well aware of the presence of the easterly winds above 20 km. The boundary condition specified at the top had no influence upon the solution. For Winter, the rigid top qualitatively simulates the presence of the reflective layer produced by the strong westerly winds, although there are small quantitative differences in the calculated amplitudes. The Fall simulations present more differences, because the rigid top interrupts the vertical propagation producing spurious reflections. The interaction between the upward and downward modes produces the wavelike profile. The decrease in resolution using the rigid top, produces little effect in model ZG, as shown in Figure 4.23.

The simulations for each season, with the top at 20 km (about 50 mb) and at 12 km (about 100 mb), are presented in Figures 4.24, 4.25, and 4.26. In all cases, the solution is strongly affected by the upper boundary condition, and gets worse when the top is lowered.

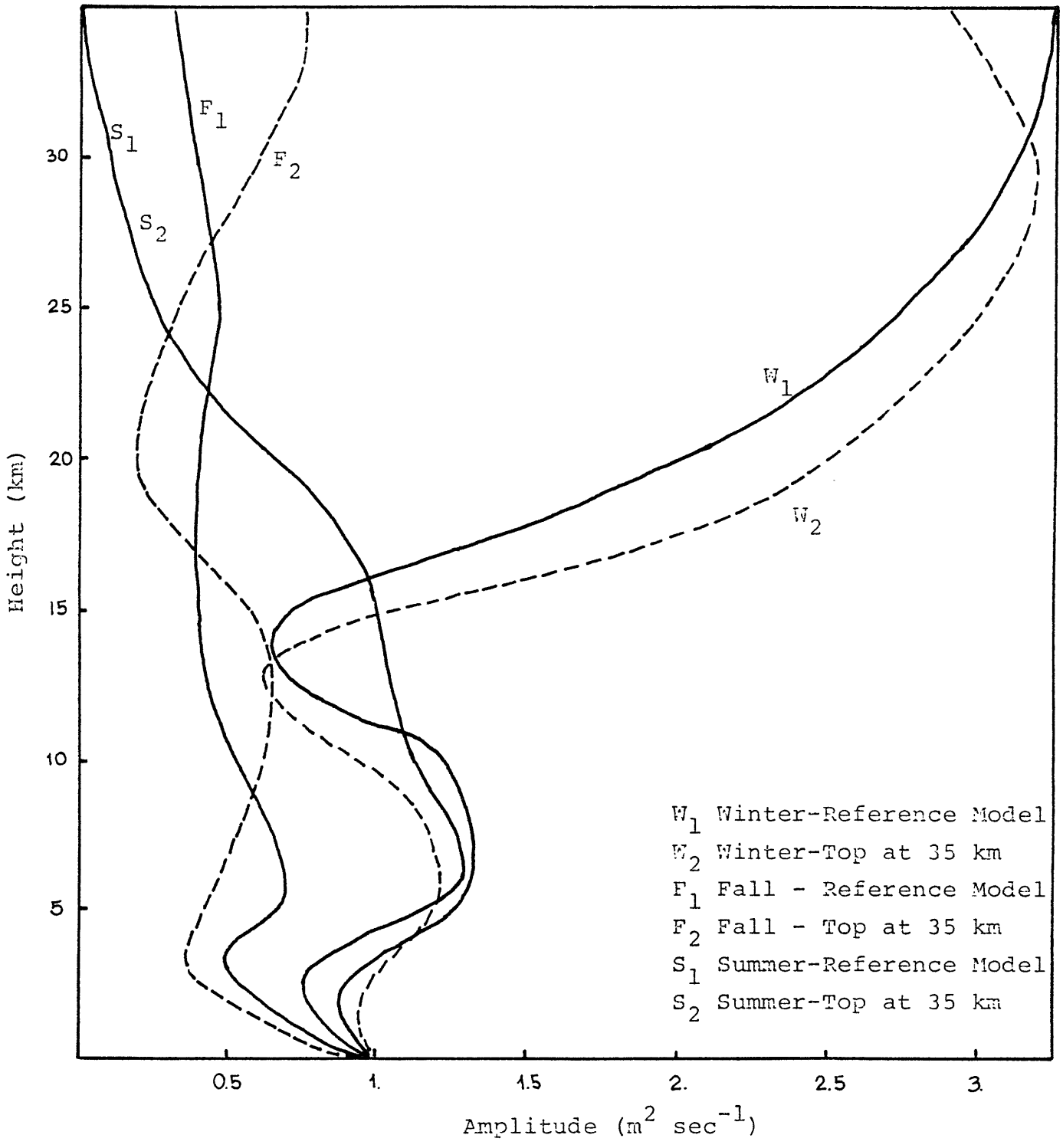

Figure 4.22 Scale Amplitudes Computed Using the Reference Model (Solid Line) and the ZG Model (N=50) with a Rigid Top at 35 km (Dashed Line), for Winter, Fall, and Summer.

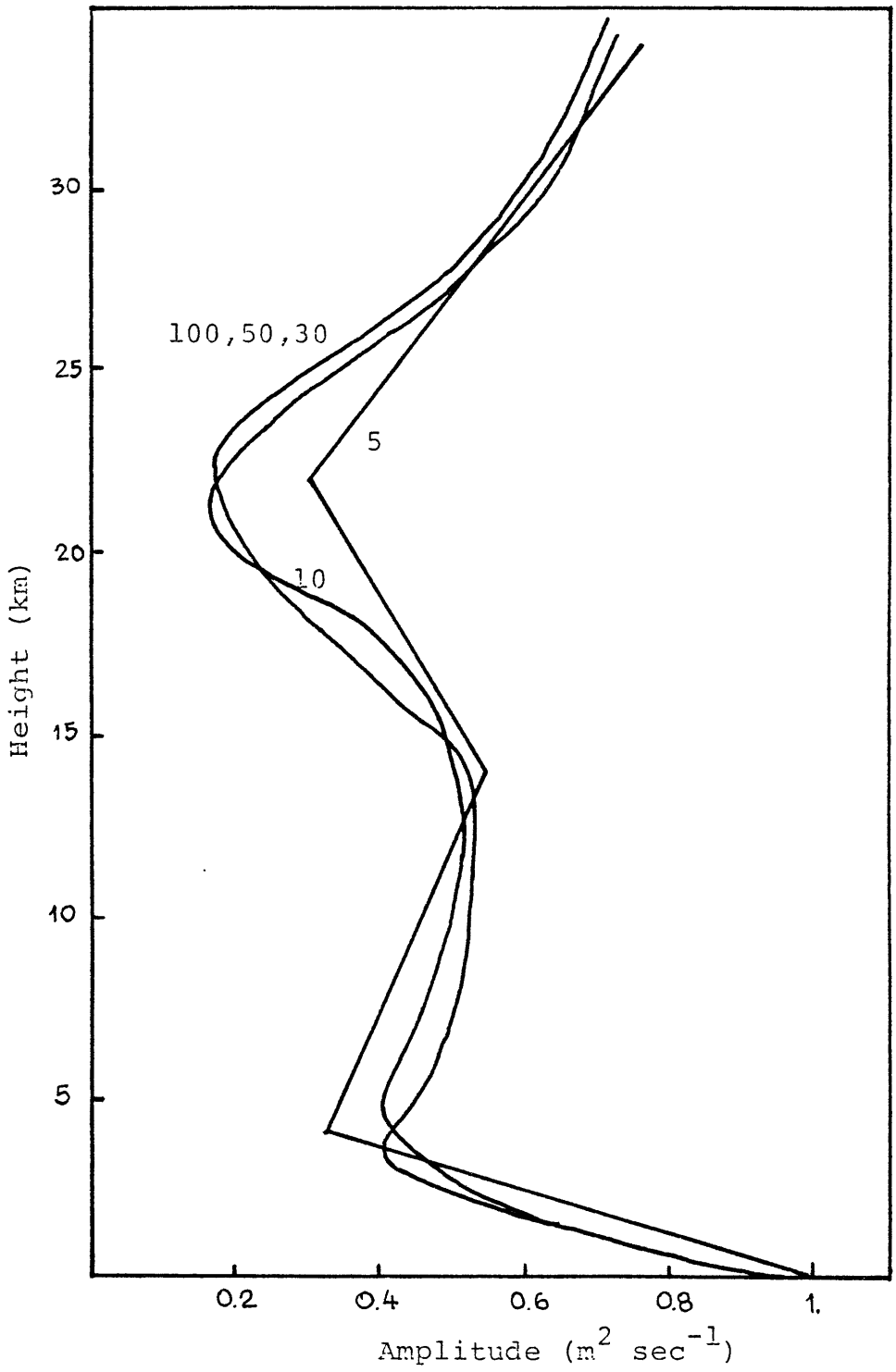

Figure 4.23 Fall Simulations of the Scale Amplitude Using the ZG Model with a Rigid Top at 35 km and Levels 100, 50, 30, 10, and 5.

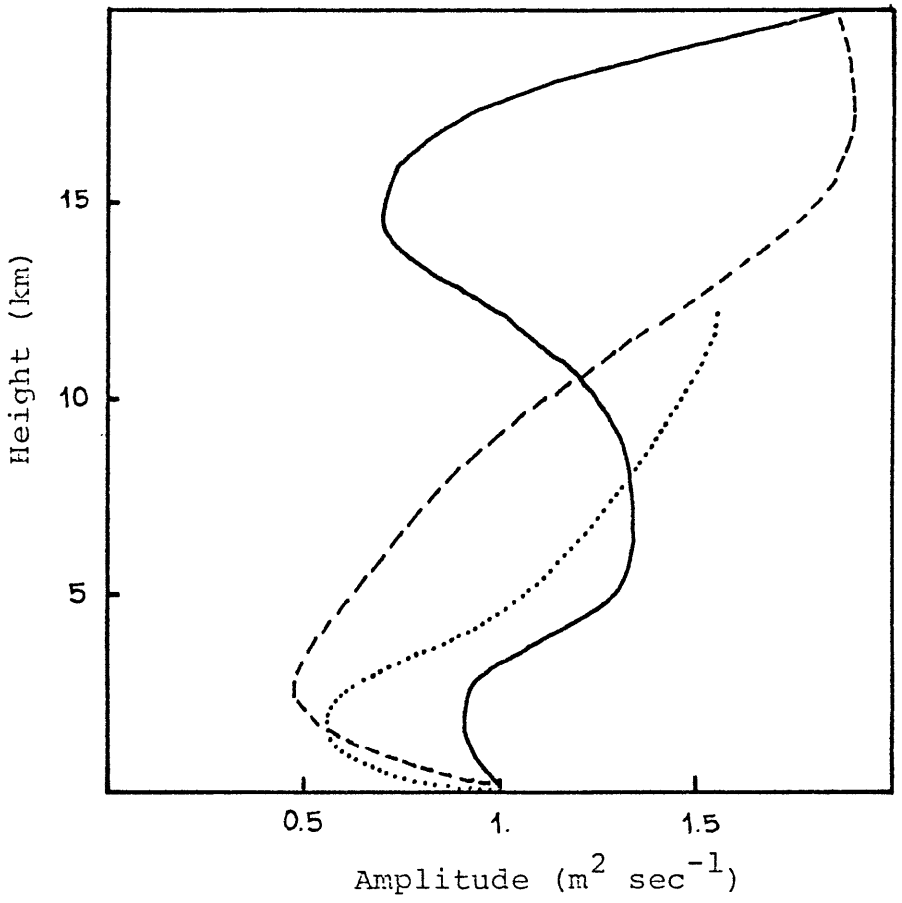

Figure 4.24 Winter Simulations of the Scale Amplitude Using the Reference Model (Solid Line), the ZG Model (N=50) with a Rigid Top at 20 km (Dashed Line), and the ZG Model (N=50) with a Rigid Top at 12 km (Dotted Line).

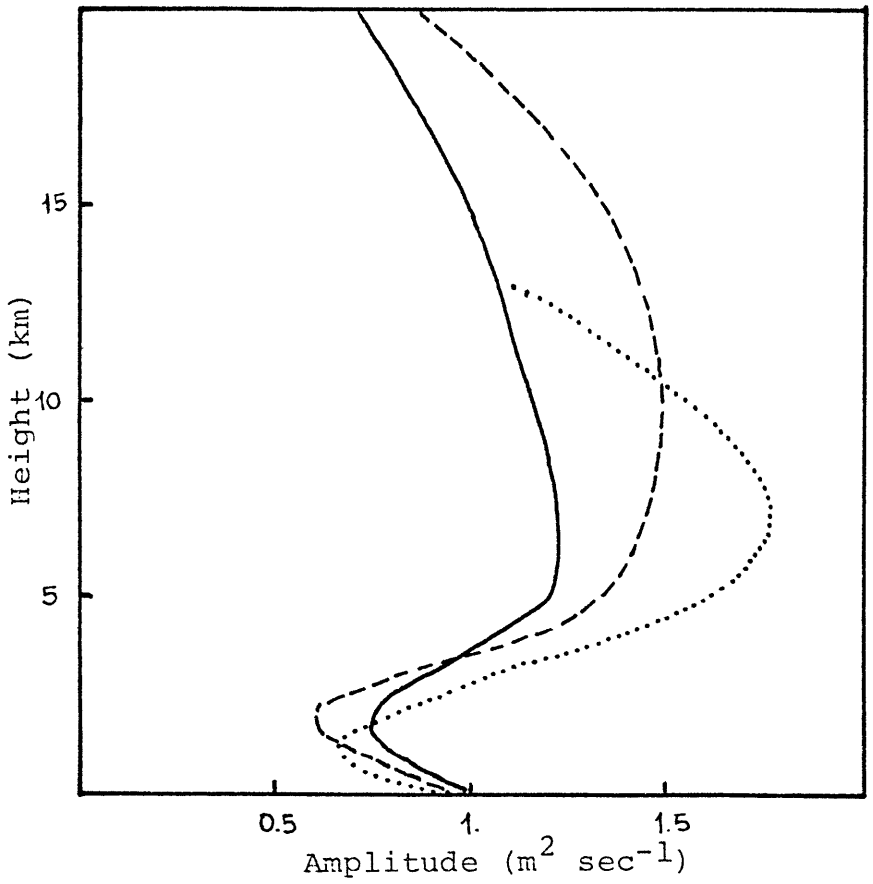

Figure 4.26 Summer Simulations of the Scale Amplitude Using the Reference Model (Solid Line), the ZG Model (N=50) with a Rigid Top at 20 km (Dashed Line), and the ZG Model (N=50) with a Rigid Top at 12 km (Dotted Line).

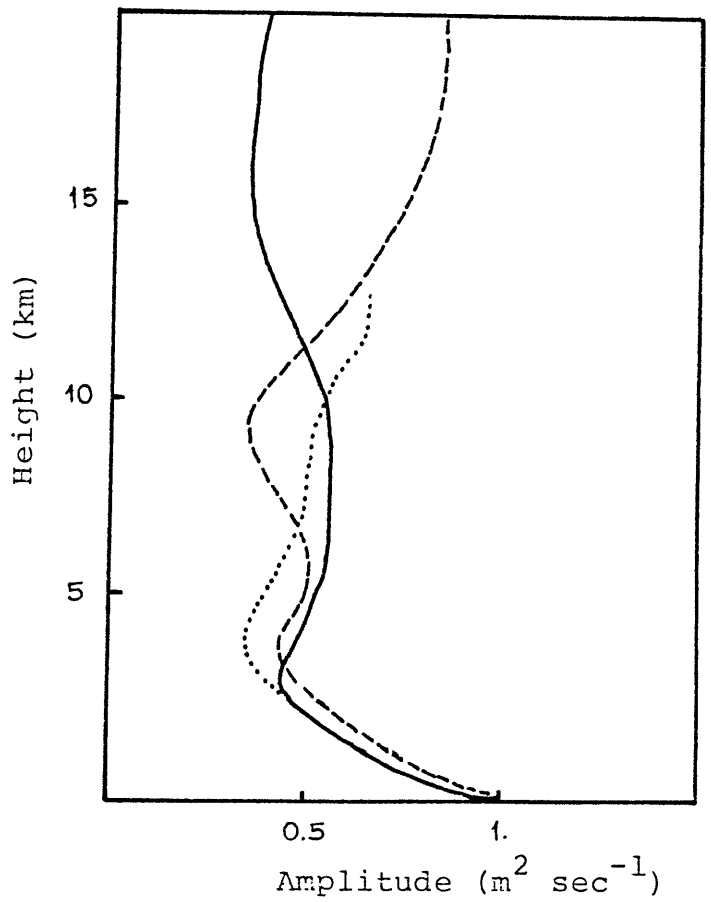

Figure 4.25 Fall Simulations of the Scale Amplitude Using the Reference Model (Solid Line), the ZG Model (N=50) with a Rigid Top at 20 km (Dashed Line), and the ZG Model (N=50) with a Rigid Top at 12 km (Dotted Line).

4.3.7 Simulations with the N = 10 Models

One of the purposes of this study is to increase our understanding of the effect of the top boundary condition on current general circulation model simulations. Therefore, we made extensive comparisons of the numerical results obtained using N = 10 levels (typical of current general circulation models) but varying the position of the top and the distribution of vertical levels.

We chose the 10 level models with the position of the top at six different heights: 1, 5, 10, 50, 100, and 200 mb. As reference, we are going to specify each model by the position of the top in mb. (i.e., T10 means that the top is situated at 10 mb.)

To help in the interpretation of the results, the distribution of the computational levels are given in the following tables:

Top in mb.	1.0	5.0	10.0	50.0	100.0	200.0
Top in km.	53.5	36.7	30.5	18.9	14.5	10.3
	50.2	34.0	28.6	17.9	13.7	9.8
	41.1	19.3	25.0	15.9	12.3	8.9
	34.7	25.2	21.5	13.9	10.8	7.9
Computational	28.6	21.2	18.3	12.0	9.4	7.1
Levels	23.2	17.5	15.2	10.1	8.1	6.1
Model ZG	18.3	14.0	12.2	8.3	6.8	5.0
	13.7	10.6	9.4	6.6	5.3	3.9
	9.4	7.5	6.8	4.7	3.7	2.8
	5.3	4.2	3.7	2.5	1.9	1.4

Top in mb.	1.0	5.0	10.0	50.0	100.0	200.0
Top in km.	47.1	35.3	30.7	20.4	16.1	11.7
	19.9	19.5	18.9	16.0	13.6	10.5
	13.1	12.9	12.8	11.6	10.5	8.5
	9.8	9.8	9.7	9.0	8.2	6.9
Computational	7.6	7.6	7.5	7.0	6.5	5.6
Levels	5.8	5.8	5.8	5.5	5.1	4.4
Model PG	4.3	4.3	4.3	4.1	3.8	3.3
	3.1	3.0	3.0	2.9	2.7	2.4
	1.9	1.9	1.9	1.8	1.7	1.5
	0.9	0.9	0.9	0.9	0.8	0.7

As illustration, we present the levels distribution of some of the general circulation models currently in operation.

Models:	GFDL(18)	GISS(9)	BMO(12)	NCAR(12)	GFDL(9)
Height (km):	∞		44		
			35	36	
				33	
			30	30	31.60
	27.90		27	27	
			24	24	
	21.47	20.2	21	21	
	18.33		18	18	18.00
	15.29		15	15	
	12.89	13.0	12	12	12.00
	10.50	9.7	9	9	
	8.68	7.4			8.30
	6.86		6	6	
	5.43	5.5			5.50
	4.01	4.0			
	2.11	2.7	3	3	3.30
	1.49	1.6			1.70
	0.86		1		
	0.52	0.6			0.64
	0.17				
	0.08				0.07

Simulations were performed using models ZG (constant Δz with H variable) and PG (constant Δp) for four different situations: constant, Winter, Fall, and Summer conditions.

Figure 4.27 shows the results obtained with the PG model under constant zonal winds and temperature conditions. The models T1, T5, and T10 are completely in error. As the top is lowered from T50 to T200, the solution approaches the reference solution. This surprising behavior is explained by the fact that the lower boundary condition strongly influences the solution in the troposphere. As the top is lowered, the tropospheric resolution increases. For T200, the ten levels are in the troposphere. Using equations (33) and (34) the analytic solution

$$\Omega(z) = \cos\gamma z - \cot\gamma z_t \sin\gamma z$$

is obtained. For values of $\gamma^2 t$ near $\frac{\pi}{2}$, $\cos\gamma^2$ is dominant and is near unity in the vicinity of the ground.

Essentially the same results are obtained with the ZG model, as shown in Figure 4.28.

Figure 4.29 shows the PG Winter simulations. To interpret these results two facts have to be taken into consideration: the effective position of the top, and the effect of the lower boundary condition. Models T1, T5, and T10 have a poor representation of the troposphere, while as the top is lowered, the representation of the troposphere

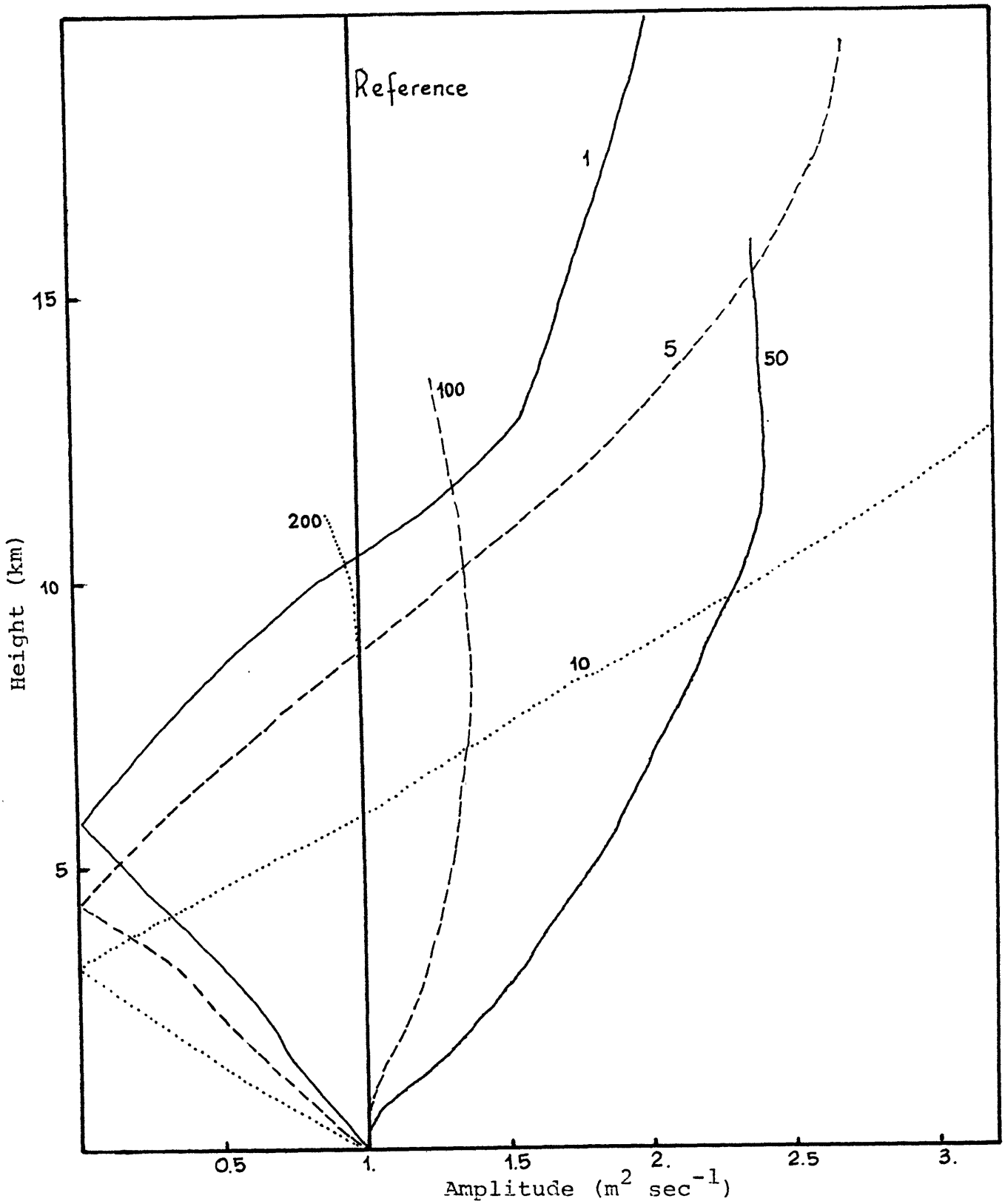

Figure 4.27 Scaled Amplitudes Computed Using the Reference Model and the PG Model with a Rigid Top at 1, 5, 10, 50, 100, and 200 mb. U = 20 m sec^{-1}, α=0, and T_o = 239° K.

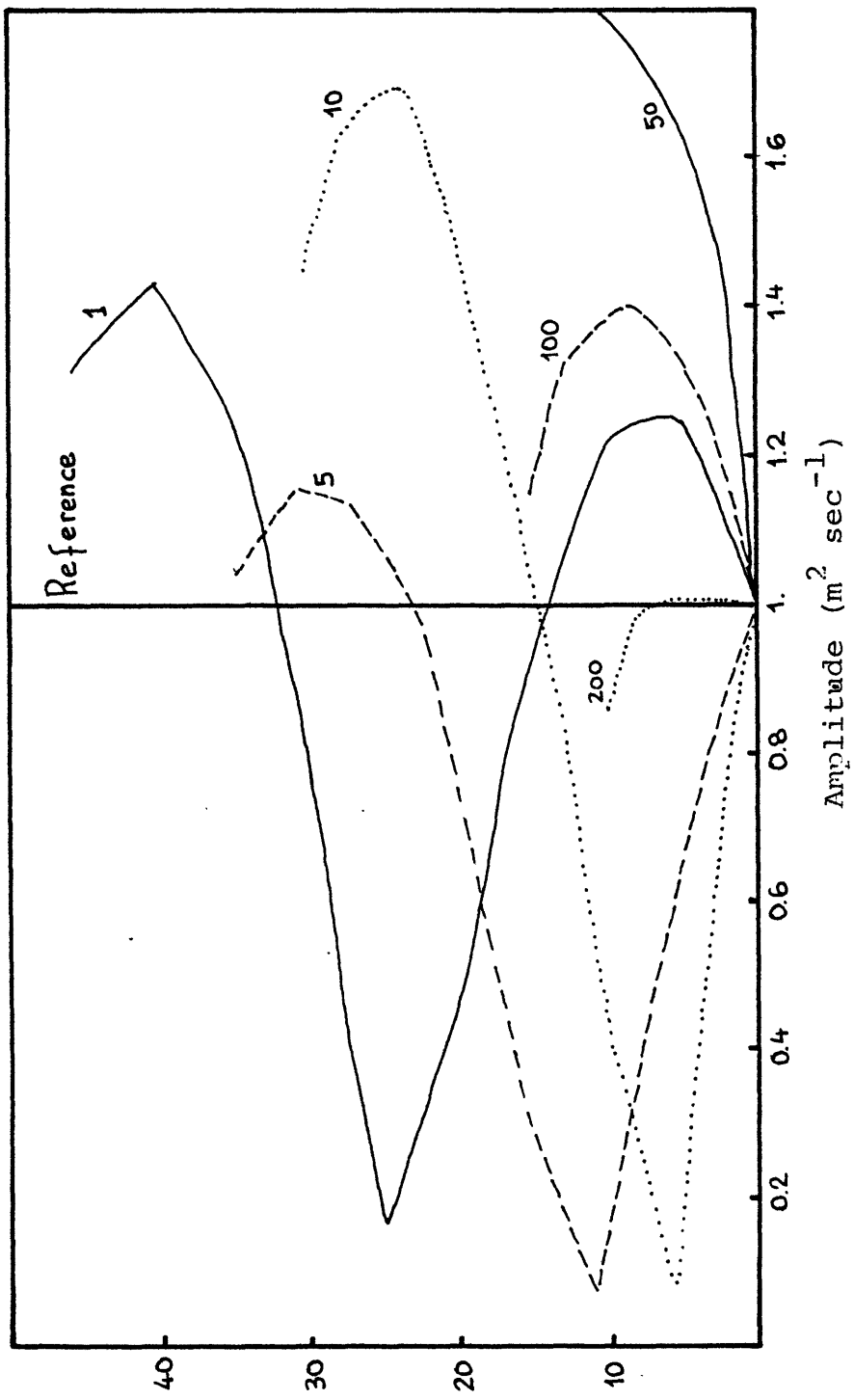

Figure 4.28 Scaled Amplitudes Computed Using the Reference Model and the ZG Model with a Rigid Top at 1, 5, 10, 50, 100, and 200 mb. U = 20 m sec^{-1}, α=0, and H = 7 km.

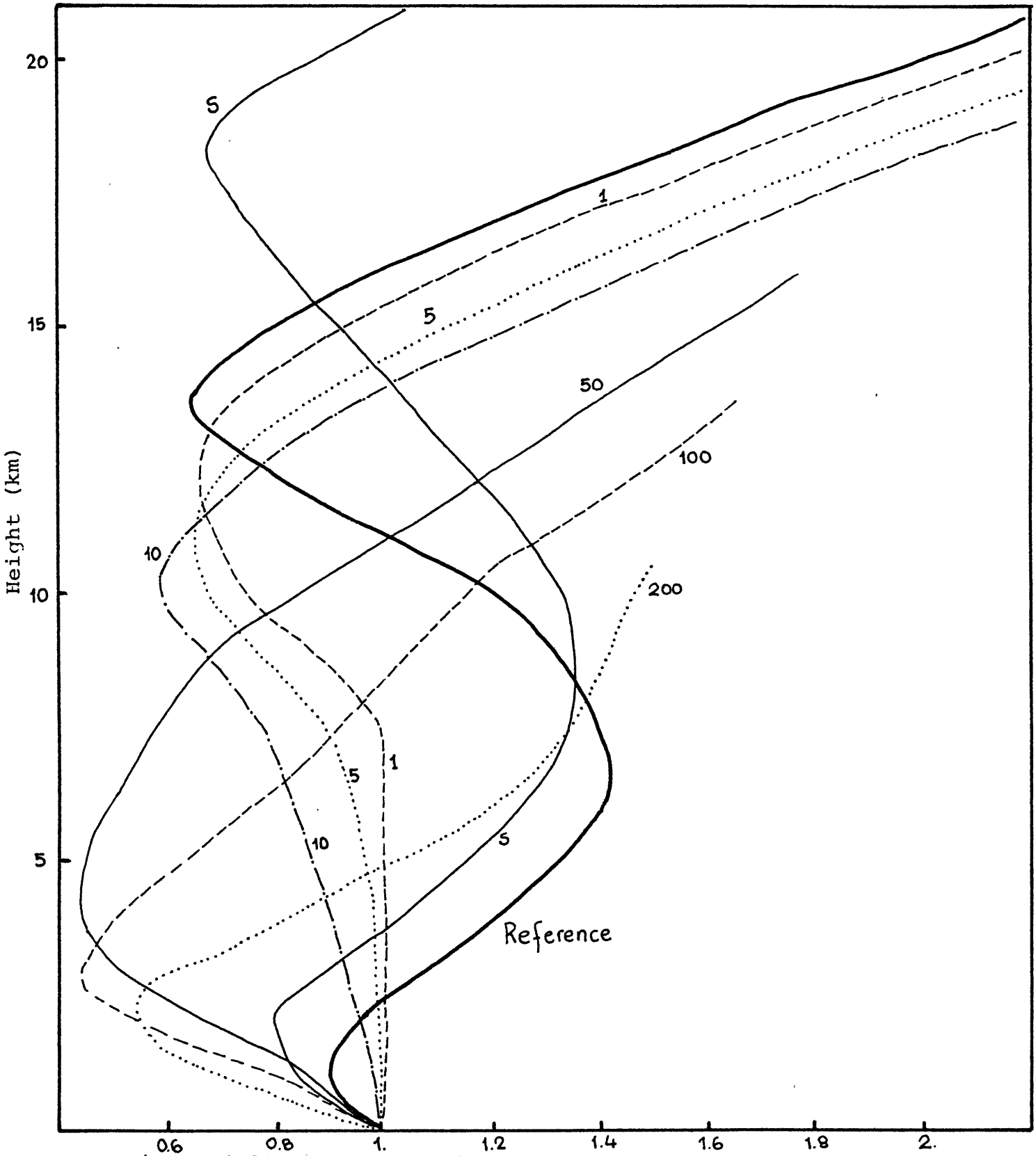

Figure 4.29 Scaled Amplitude for Winter, Computed Using the Reference Model and PG Model with a Rigid Top at 1, 5, 10, 50, 100, and 200 mb. Model S Used GFDL Vertical Structure (Smagorinsky et al., 1965).

improves. For Winter (see Section 3.3.3) there is a reflective layer around 40 km. None of the PG models can detect the strong stratospheric winds that produce the reflective layer. The inclusion of an artificial top can help to simulate that reflective layer, but the effective position of that top becomes crucial.

In order to investigate this interpretation, the simulation of wavenumber 2 for Winter was performed (Case III in Section 3.2). In this case, the position of the reflective layer is situated at a lower height, aroung 20 km. The results shown in Figure 4.30 are in reasonable agreement with the reference solution. Model T100 produced the best results as it seems to obtain a good combination of tropospheric resolution and position of the top. More evidence is obtained in another experiment in which the vertical resolution is varied as in the GFDL model (Smagorinsky et al., 1965). The levels are arranged to give maximum resolution in pressure at the extremes of the atmosphere, namely near the ground and in the stratosphere. The Winter simulation using this vertical structure (S10 for reference) is shown in Figure 4.29 and is by far the best tropospheric simulation.

The Winter simulations using model ZG are shown in Figure 4.31. The T1 model is in very good agreement. The top has no influence in the solution since it is situated inside the reflective layer. However, the troposphere with only two levels is not well represented. As the top

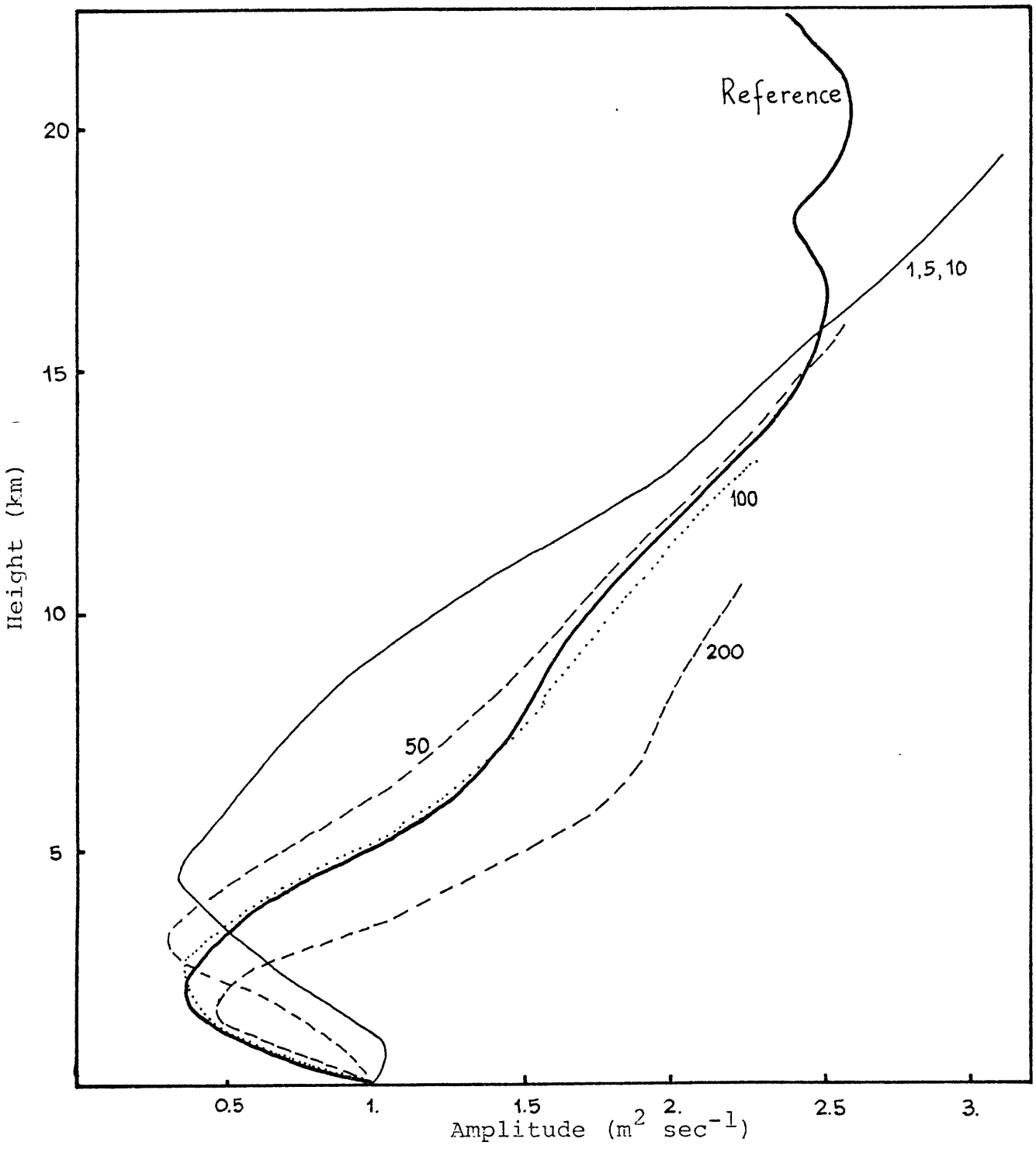

Figure 4.30 Winter Simulations of Scaled Amplitude Computed Using the Reference Model and PG Model with a Rigid Top and 1, 5, 10, 50, 100, and 200 mb., for Case III of Section 4.3.2.

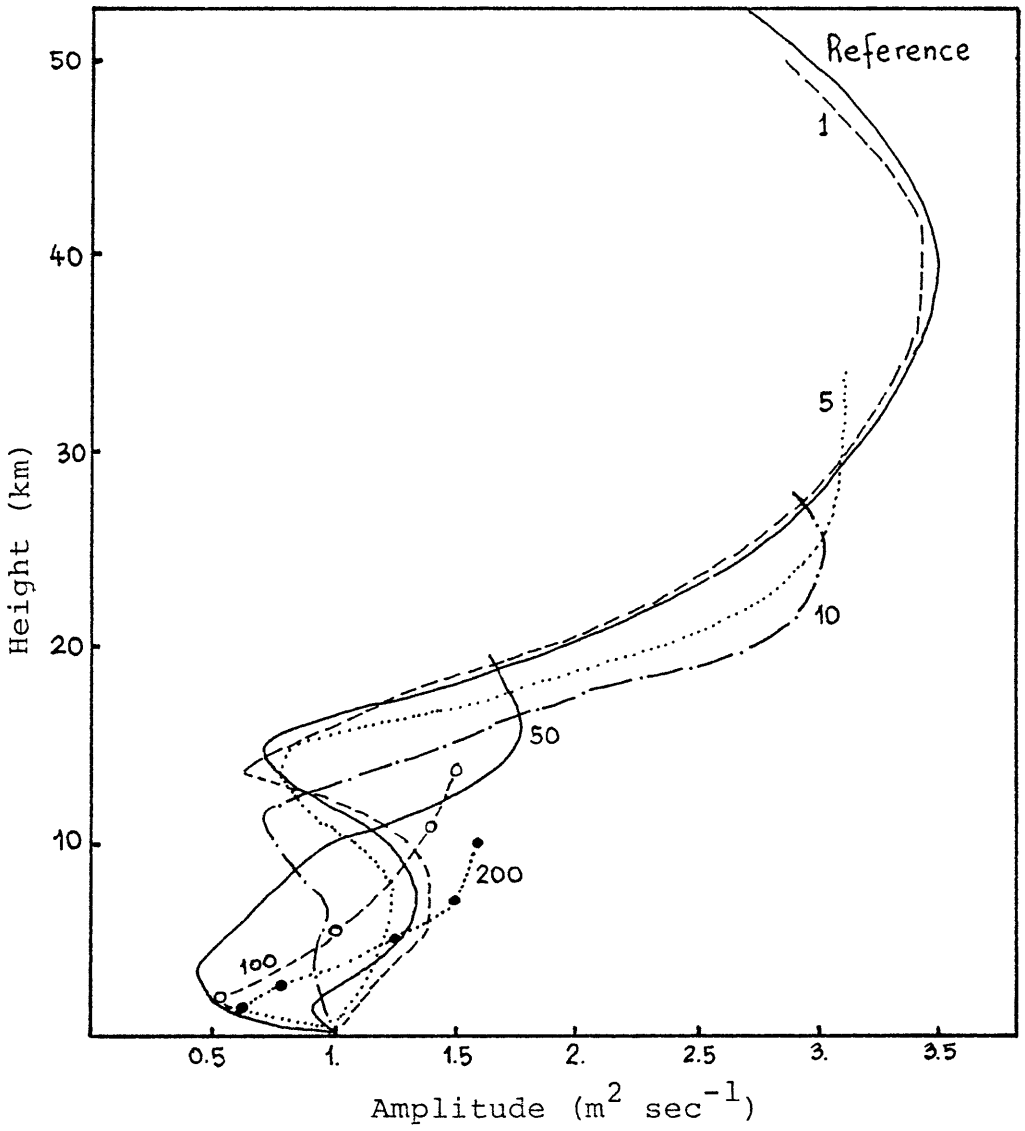

Figure 4.31 Winter Simulations of Scaled Amplitude Computed Using the Reference Model and ZG Model with a Rigid Top at 1,5,10,50,100, and 200 mb.

decreases, the tropospheric representation improves but the effect of the rigid top is more evident and clearly modifies the vertical structure.

Figure 4.32 shows the PG Fall simulations. Here the picture is quite different from the Winter case. The models T1, T5, T10 are in good agreement with the reference solution. It seems that with weak westerly winds the damping effect of Newtonian cooling removes the upward energy in such a way that the position of the top is not important. However, as the top is lowered, in models T50 and T100 the effect of the rigid top becomes evident. For model T200 this effect is partially canceled by the effect of the lower boundary.

These results strongly suggest that the optimal position of the top for a N = 10 model is seasonal dependent. As expected, model S10 produces good tropospheric results (Figure 4.33).

With model ZG (Figure 4.34), model T1 produces a good simulation in the stratosphere. Models T5 and T10 with more tropospheric resolution produce a reasonable simulation throughout the atmosphere. Model T50, in spite of having a better tropospheric resolution, it does not produce a good simulation. On the other hand, models T100 and T200 produce good tropospheric simulation.

Figure 4.35 shows the results obtained with the PG model under summer conditions. Models T1, T5, and T10 are in very good agreement with the reference simulation. The effective

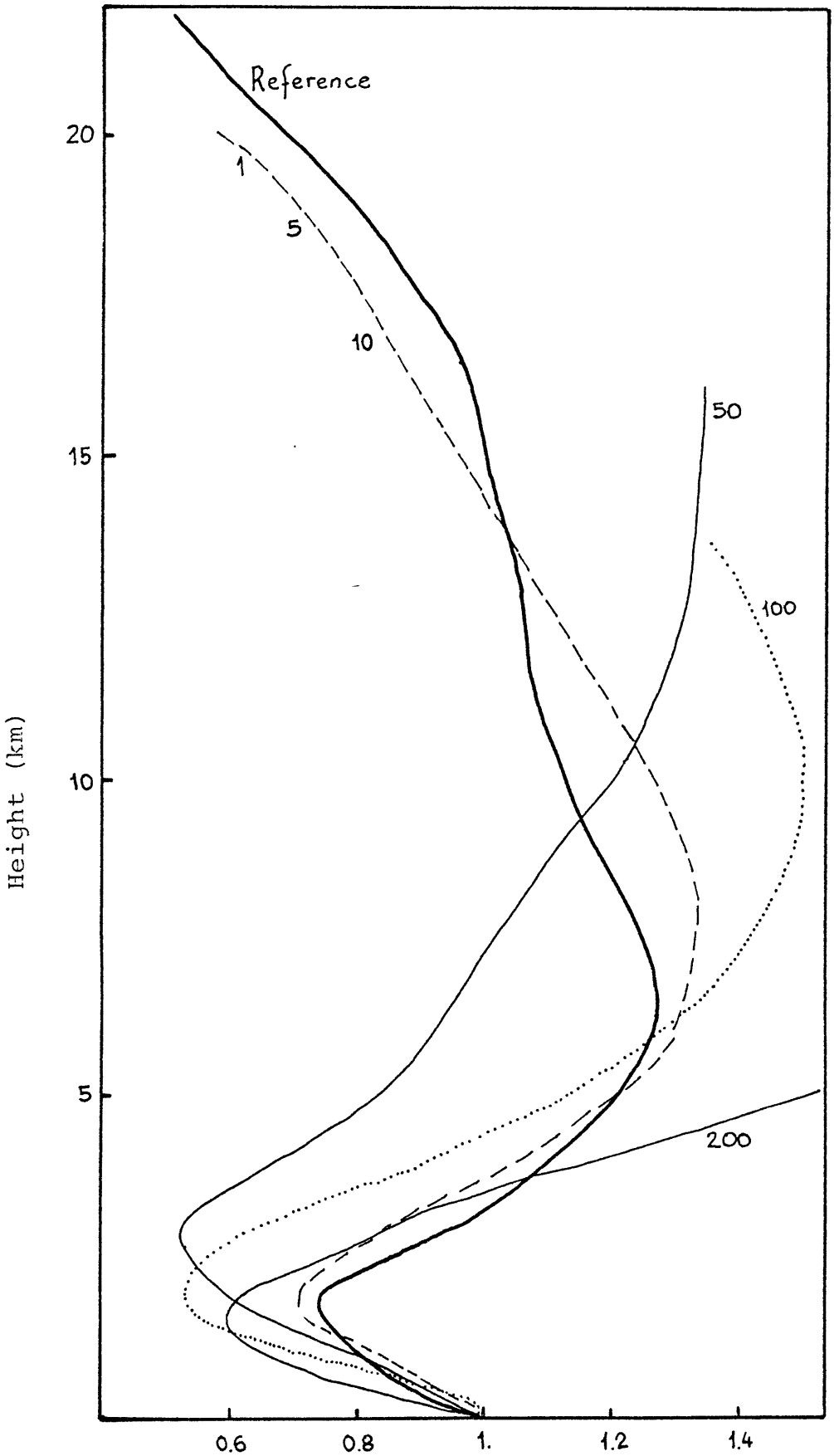

Figure 4.32 Fall Simulations of Scaled Amplitude Computed Using the Reference Model and PC Model with a Rigid Top at 1, 5, 10, 50, 100, and 200 mb.

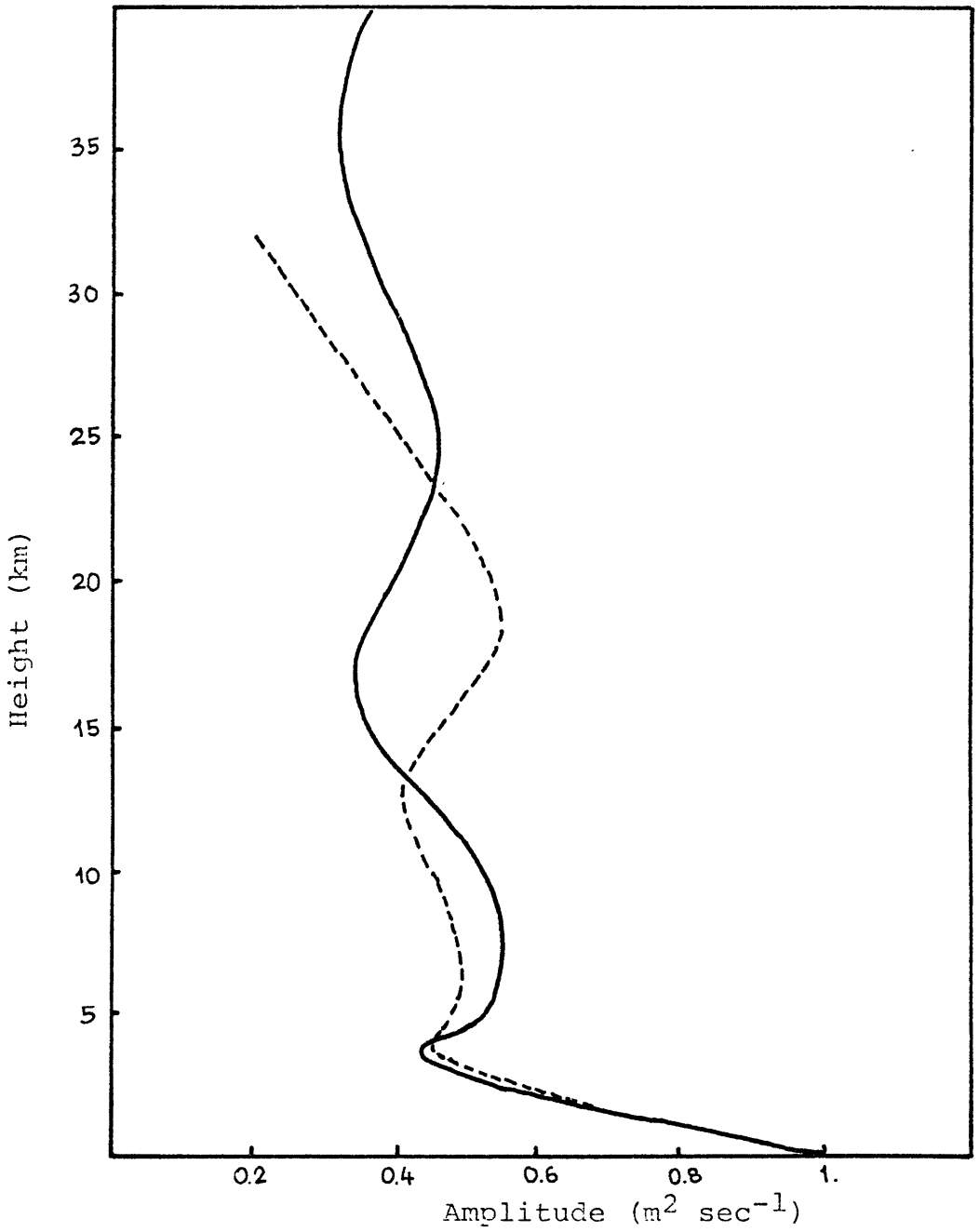

Figure 4.33 Fall Simulations of the Scale Amplitude Computed Using the Reference Model (Solid Line) and the PG Model with the GFDL Vertical Structure (Smagorinsky et al., 1965) (Dashed Line).

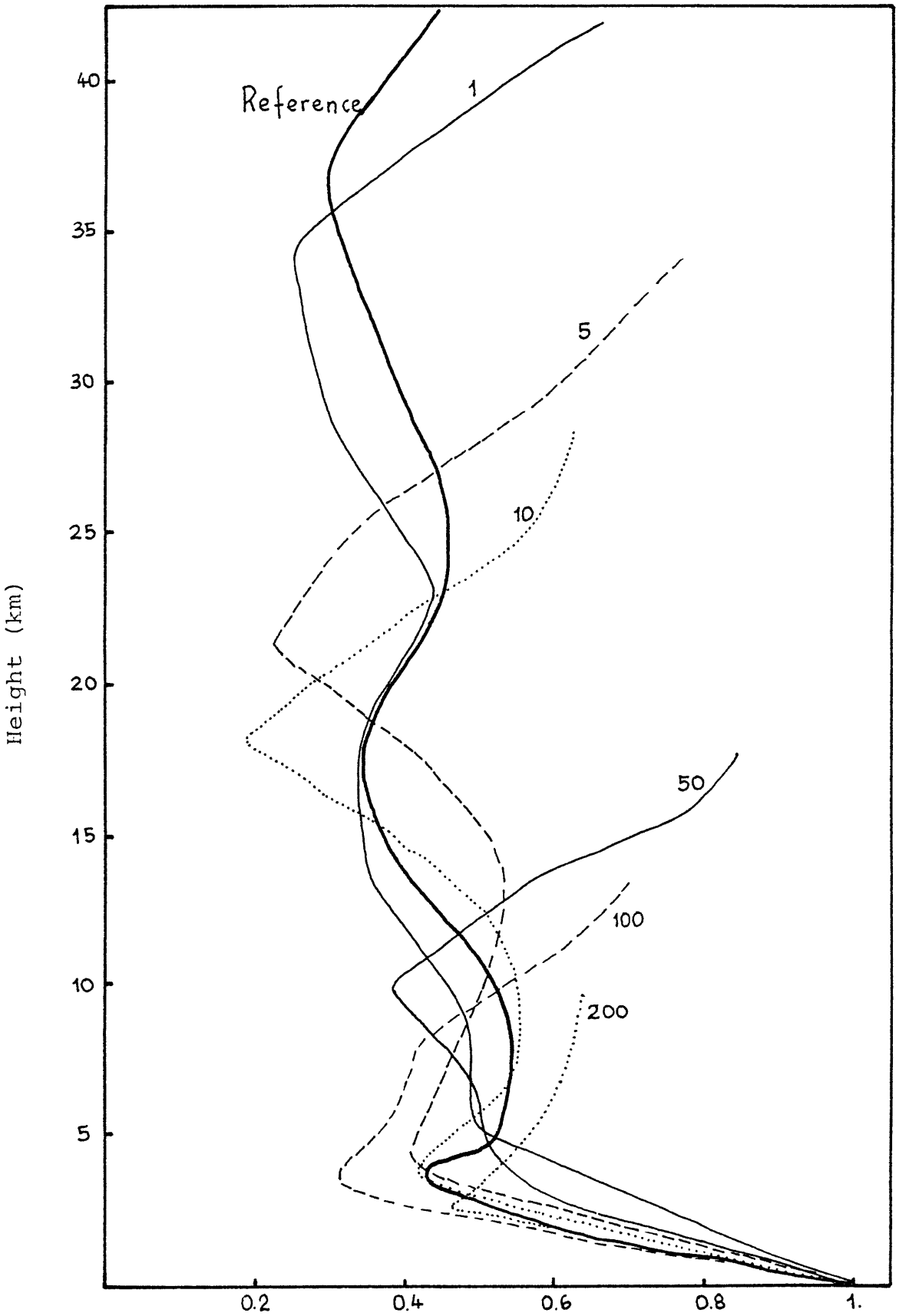

Figure 4.34 Fall Simulations of Scaled Amplitude Computed Using the Reference Model and ZG Model with a Rigid Top at 1, 5, 10, 50, 100, and 200 mb.

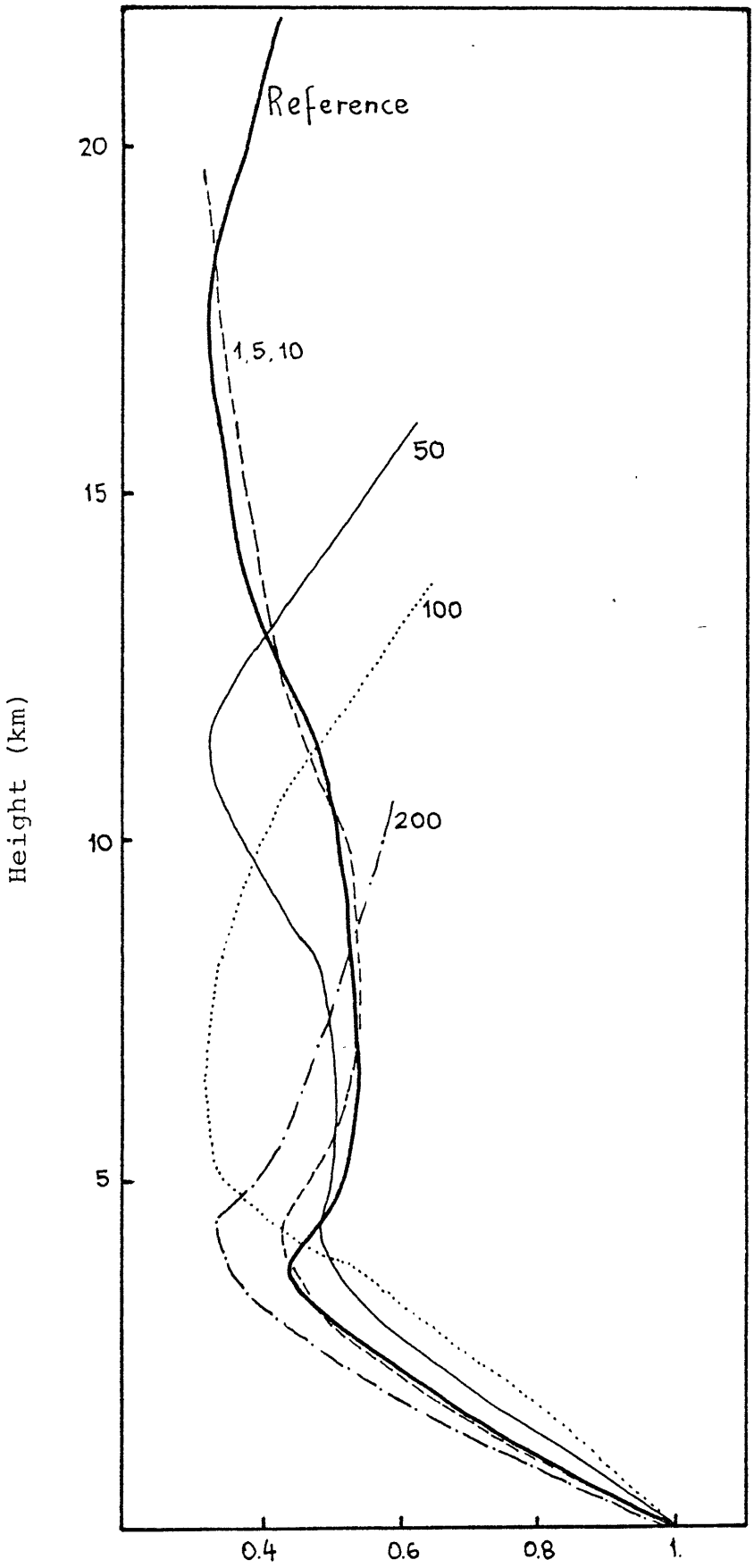

Figure 4.35 Summer Simulations of Scaled Amplitude Computed Using the Reference Model and PG Model with a Rigid Top at 1, 5, 10, 50, 100, and 200 mb.

rigid top has little influence in the wave structure since it is situated in the vicinity of the reflective layer produced by the easterly winds. When the top decreases (models T50, T100, and T200), the rigid top is no longer able to simulate the reflective layer, and the wave structure presents the effects of the reflected waves.

The S10 model produces very good results since it has good resolution in the troposphere and low stratosphere (Figure 4.36).

The Summer simulations obtained with the ZG model are presented in Figure 4.36. Models T1, T5, and T10 present good agreement with the reference solution in the stratosphere. For the troposphere, the sparcity of levels does not allow for a good simulation in this region. Models T50, T100, and T200, as in the PG simulations, misrepresent completely the wave structure. The position of the top in these models is too low to represent the effects of the reflective layer.

5. ALTERNATIVE APPROACHES TO THE UPPER BOUNDARY CONDITION

In the previous sections we showed that the upper boundary condition can fundamentally affect the entire solution by the reflections produced at the rigid top. In this section we will be concerned with developing a mechanism to reduce or to avoid the reflections at the upper top.

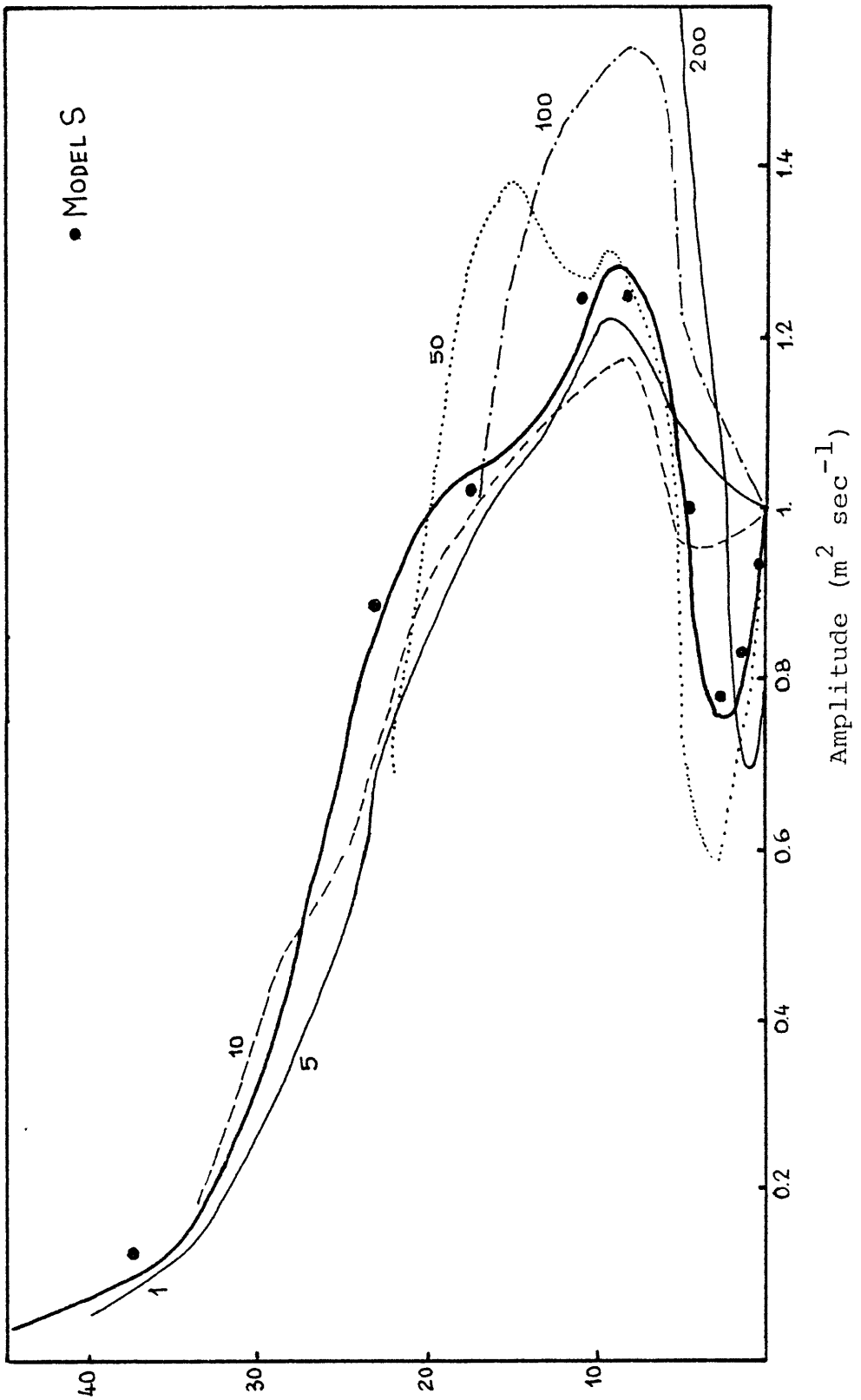

Figure 4.36 Summer Simulations of Scaled Amplitude Computed Using the Reference Model and ZG Model with a Rigid Top at 1,5,10,50,100, and 200 mb. Model S Used GFDL Vertical Structure (Smagorinsky et al., 1965).

5.1 Sponge Layer

One possible mechanism is to have a complex index of refraction in a layer below the upper boundary, so the waves can be damped before they reach the upper boundary. The index of refraction of this sponge layer can be modified by the introduction of viscosity in the horizontal equations of motion,

$$\frac{\partial \xi}{\partial t} + U \frac{\partial \xi}{\partial x} = -\beta v_g + f_o \left(\frac{\partial w}{\partial z} - \frac{w}{H} \right) + \mu \nabla^2 \xi$$

or by the Newtonian cooling coefficient, or the thermal conductivity coefficient in the thermodynamic equation,

$$\frac{\partial T}{\partial t} + U \frac{\partial T}{\partial x} + v_g \frac{\partial T_o}{\partial y} + S w = -\alpha T + \eta \nabla^2 T$$

With these modifications, the ZG model becomes:

$$\frac{dW}{dz} = \frac{1}{f_o^2} \left(-\mu m^4 + i \left(\beta K - \omega m^2 - K m^2 U \right) \right) F + \frac{W}{H} \qquad (36)$$

$$\frac{dF}{dz} = \frac{i R S}{(\omega + UK - i(\alpha+\eta)) H} W + \frac{K}{(\omega + UK - i(\alpha+\eta)) H} \frac{dU}{dz} F \qquad (37)$$

in which μ the viscosity coefficient, and η the thermal conductivity coefficient are in general, functions of z.

Assuming constant conditions, system (36)-(37) can be written as:

$$\frac{d^2\Omega}{dz^2} + \gamma^2 \Omega = 0 \tag{38}$$

in which $$\Omega(z) = F(z)\, e^{z/2H}$$

and $$\gamma^2 = \frac{(\beta K - \omega m^2 - K m^2 U) RS + i \mu m^4 RS}{f_0^2 H (\omega + UK - i(\alpha+\eta))} - \frac{1}{4H^2} \tag{39}$$

The expression for γ^2 shows that the presence of at least one of the coefficients μ, α or η are necessary to obtain the complex index of refraction. It also shows that both methods (dynamic or thermodynamic effects) have inverse behavior with respect to the horizontal wavenumber k. However, they are essentially equivalent methods if the appropriate coefficients for the desired range of horizontal wavelengths are used.

The inclusion of this sponge layer has the purpose to damp the upward propagating wave energy before it can be reflected from the upper boundary. Because of the influence of this damping layer on the wave structure, it is necessary to evaluate its reflection characteristics. An analysis

based on linear wave theory is presented below.

Beneath the sponge layer, the solution of (38) is:

$$\Omega_1(z) = A e^{inz} + B e^{-inz} \tag{40}$$

in which n is the appropriate index of refraction for the atmosphere. In the sponge layer, the solution will be:

$$\Omega_2(z) = C e^{imz} + D e^{-imz} \tag{41}$$

providing that μ, α or η are constant coefficients.

For a horizontal wavenumber $k > 0$, the A term corresponds to upward propagation of energy, while the B term represents the downward propating mode (see Section 3). By assuming $|A| = 1$ for convenience, the value of $|B|$ will be a measure of the reflectivity produced by the upper region. By matching solutions at $z = z_o$ (bottom of the sponge layer), and by imposing $\Omega = 0$ at the top $z = z_{top}$, the expression for B becomes:

$$|B| = \left| \frac{n-m - (m+n)\, e^{2im(z_t - z_o)}}{n+m + (m-n)\, e^{2im(z_t - z_o)}} \right| \tag{42}$$

At the interface between the two media, there is a discontinuity in viscosity that will also produce reflections. In order to minimize this effect caused by a rapid increase

in viscosity, we will gradually increase the coefficient μ (or α) from zero at $z = z_o$ to a constant value μ_k at the top $z = z_{top}$, according to:

$$\mu = \mu_K \left[\exp\left(0.7 \frac{z - z_o}{z_t - z_o}\right) - 1 \right]$$

or some other suitable expression. Under these conditions, expression (42) is no more valid. To obtain a new expression for B, we have to solve the equation:

$$\frac{d^2\Omega}{dz^2} + m^2(z)\,\Omega = 0 \qquad \text{in the domain } z_o \le z \le z_{top} \qquad (43)$$

Assuming $z_o = 0$ for simplicity, the matching condition $\Omega_1 = \Omega_2$ at $z = 0$ produces:

$$1 + B = \Omega_2(0)$$

and condition $\frac{d\Omega_1}{dz} = \frac{d\Omega_2}{dz}$ produces:

$$in - in\,B = \frac{d\Omega_2(0)}{dz}$$

By eliminating B, we obtain the condition:

$$\frac{d\Omega}{dz} + in\Omega - 2in = 0 \qquad (44)$$

at $z = 0$. Then, we solve (43), subject to (44) and $\Omega = 0$ at $z = z_{top}$. We obtain the solution numerically by using second order differencing and inverting the resulting tri-diagonal matrix. Then, we calculate B by:

$$|B| = |\Omega - 1.| \qquad \text{at} \quad z = 0.$$

The depth of the atmosphere, below the sponge layer, does not influence B. B only depends on the depth of the sponge layer, the vertical wavenumber n, and in the characteristics of the coefficients (μ, α or η) used. The reflectivity B is plotted in Figure 5.1 as a function of α_k using for α the expression:

$$\alpha = \alpha_k \left[\exp\left(0.7 \, \frac{z - z_o}{z_t - z_o}\right) - 1 \right] \qquad (45)$$

for several thicknesses of the sponge layer. In order to make comparisons, we utilize as conditions for the atmosphere those defined in Section 4.2. The results show that for a given d (d is defined as the ratio of the depth of the sponge layer $z_{top} - z_o$ to the vertical wavelength $\frac{2\pi}{n}$),

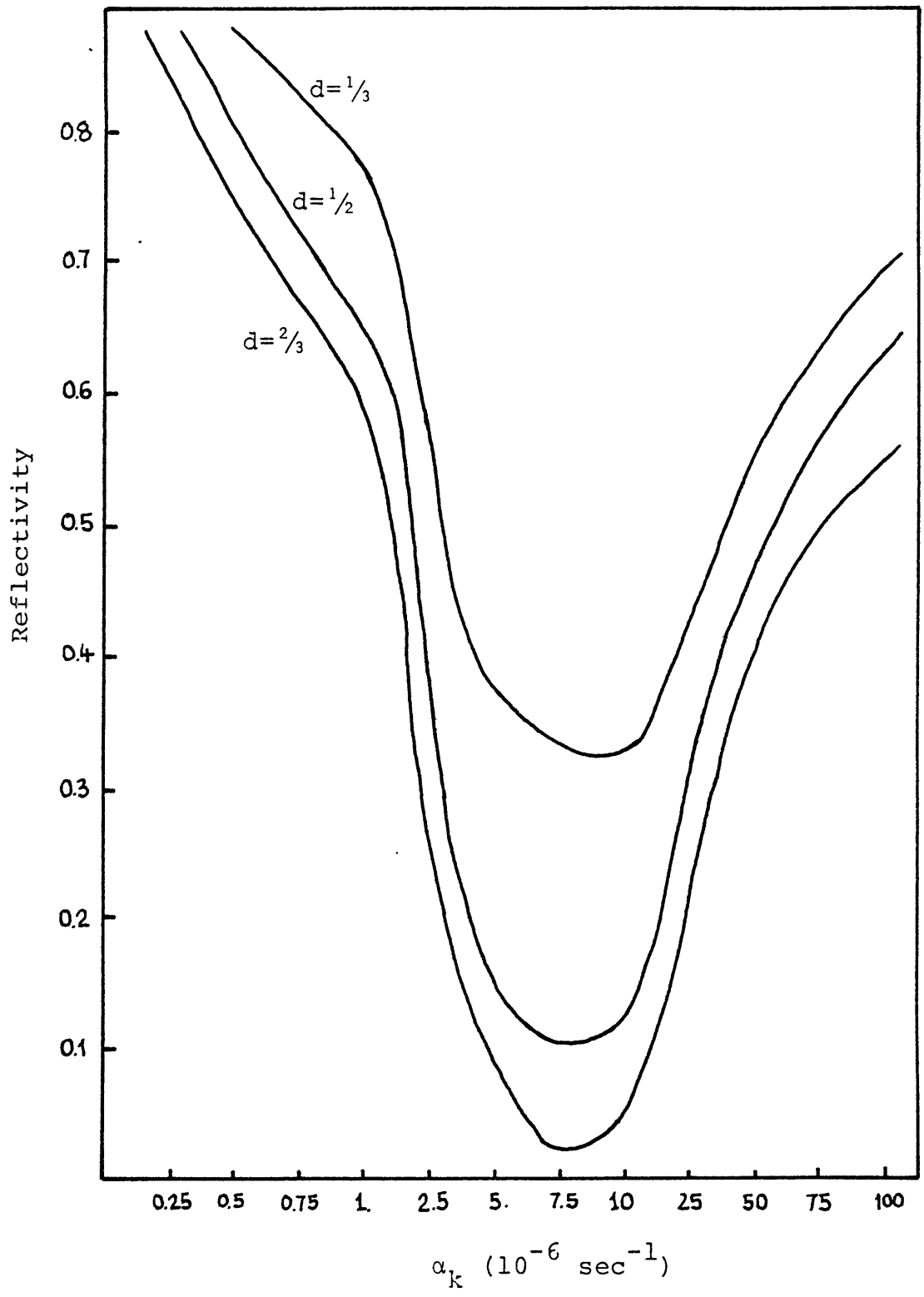

Figure 5.1 Reflectivity as a Function of the Newtonian Cooling Coefficient for Various Sponge Layer Depths Using the Exponential Profile.

B first decreases rapidly with increasing α_k and then begins to increase. The large reflectivity at low values of α_k results from the reflections at the upper boundary due to insufficient damping. The damping is not enough to eliminate the amplitude of the wave before it reaches the top of the layer. On the other hand, when the value of α_k becomes larger, its vertical gradient is responsible for internal reflections. As the sponge layer increases in depth there is a general decrease in reflectivity. Nevertheless, we must say that the effects upon the reflectivity are rather complicated. Reflections occur from the upper boundary as well as throughout the sponge layer. The effect of these partial reflections on the atmosphere below, depends upon the phase of the reflected mode when it reenters the atmosphere.

We tested these results using the ZG model under constant conditions and with a rigid top (see Section 4.2). The exponential function (45) was applied at the levels below the top of the model. From Figure 5.1 we selected the best value for each d: $\alpha_k = 7.5 \times 10^{-6}$ for $d = \frac{1}{2}$ and $d = \frac{2}{3}$, and $\alpha_k = 1.0 \times 10^{-5}$ for $d = \frac{1}{3}$. The results appear in Figure 5.2. As expected, as d increases, the numerical solutions approach the reference solution.

For comparison, other profiels were evaluated. For three of these,

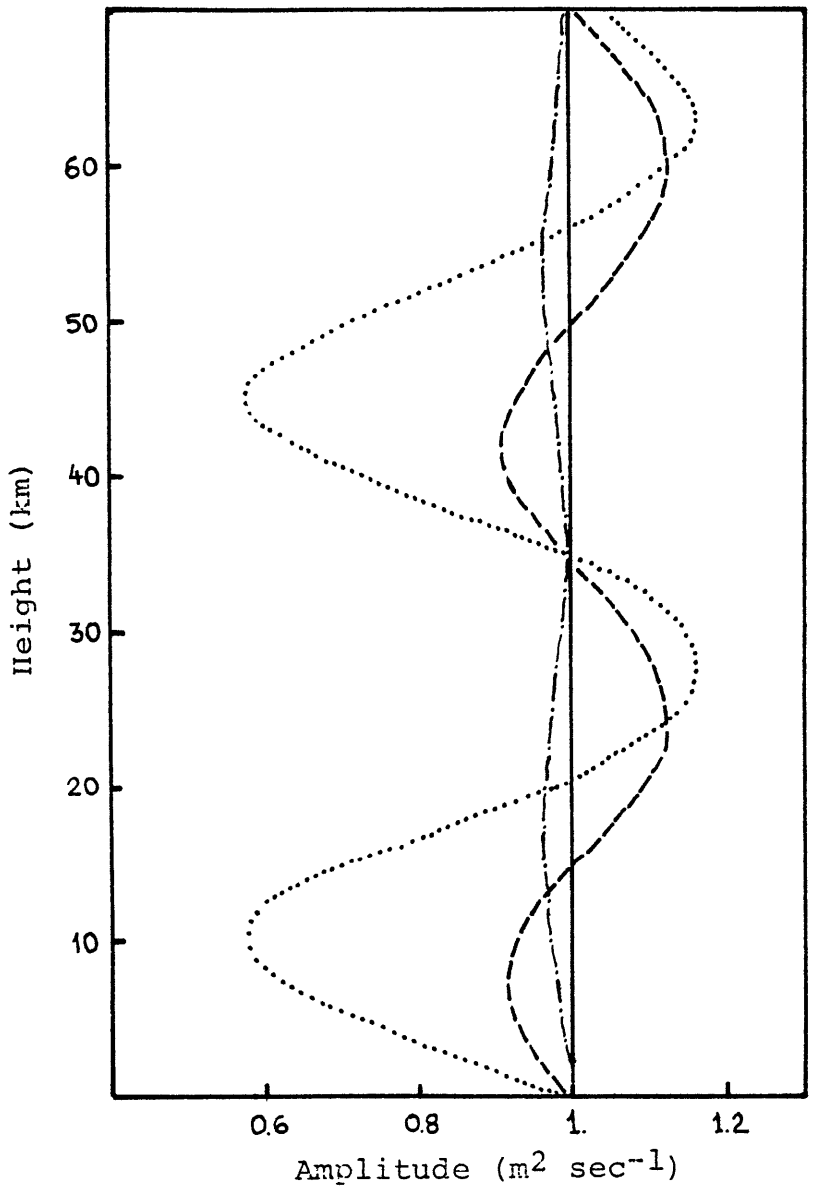

Figure 5.2 Scaled Amplitude Computed Using the Reference Model (Solid Line) and the Sponge Layer Formulation for Various Sponge Layer Depths: d=1/3 (Dotted Line), d=1/2 (Dashed Line), and d=2/3 (Dashed-Dotted Line). The Exponential Profile was Used with $\alpha_k=7.5\times10^{-6}$ for d=1/2 and d=2/3, and $\alpha_k=1.0\times10^{-5}$ for d=1/3.

$$\alpha = \alpha_k \frac{z - z_o}{z_t - z_o}$$

$$\alpha = \alpha_k \qquad \text{only for} \quad z_o \leq z \leq z_{top}$$

$$\alpha = \alpha_k \sin\left(\frac{\pi}{2} \frac{z - z_o}{z_t - z_o}\right)$$

the reflectivity B is shown in Figure 5.3. We choose the case $d = 2/3$, but other values of d produce similar results. Reflection from the constant profile is high for all α_k, due to the discontinuity of $z = z_o$. The other profiles, all of which increase α_k gradually from zero at $z = z_o$ to α_k at $z = z_{top}$ produce comparable results.

If only waves with a single wavenumber were present, it should be possible to use a relatively thin sponge layer with the α_k chosen to achieve the minimum possible reflection for that thickness. In general, we must be concerned with a range of frequencies, all of which will have a specific pair of vales d , α_k that minimize the reflectivity. The desired damping for one frequency will not be, in general, adequate for other frequencies. The results, also show that relatively big values of the coefficients does not guarantee a proper damping.

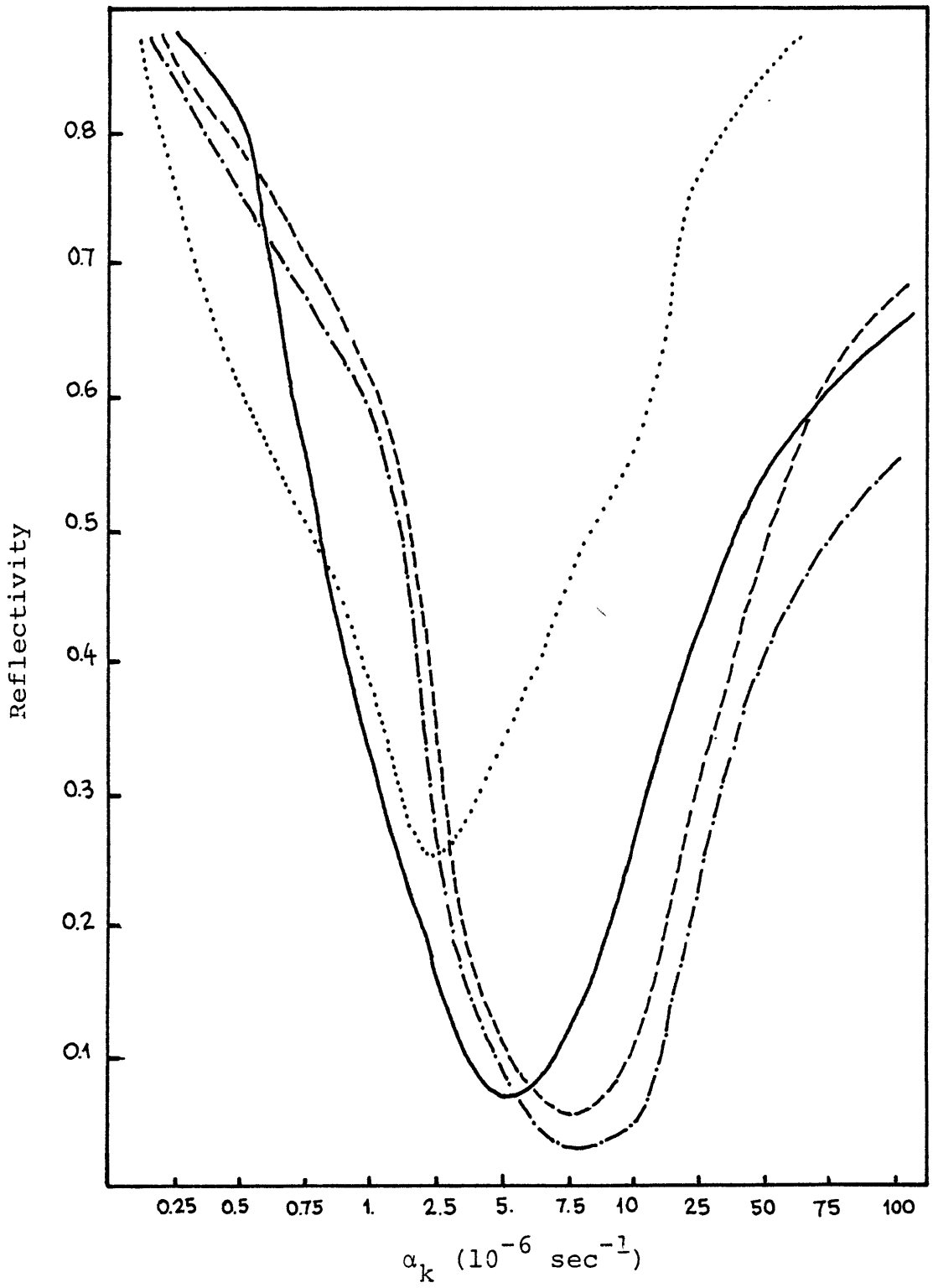

Figure 5.3 Reflectivity as a Function of the Newtonian Cooling Coefficient for Various Newtonian Cooling Profiles: Constant Profile (Dotted Line), Linear Profile (Solid Line), Sine Profile (Dashed Line), and Exponential Profile (Dashed-Dotted Line).

5.2 Destructive Interference

The sponge-layer method showed the importance of the waves produced at the interface between the atmosphere and the viscous layer above. To deal with this problem we are going to use this uppermost layer to eliminate the unwanted waves by producing a destructive interference between the waves reflected at the interface and the waves internally reflected in the sponge layer. We are going to show that, if only waves with a single frequency are present, a simple layer is enough to eliminate them. Unfortunately, we must be dealing with a range of frequencies. For this situation, say N frequencies, a layer with N sub-layers, each of them with a characteristic index of refraction, is needed. The following discussion is based in a linear wave analysis.

Let us express the general form of a linear steady-state wave in the atmosphere as:

$$\Omega(z) = A_0 e^{ik_0 n z} + B_0 e^{-ik_0 n z}$$

in which k_0 is the wavelength of the wave in an arbitrary medium n_0, and

$$\Omega(z) = A_1 e^{ik_0 m z} + B_1 e^{-ik_0 m z}$$

for the sponge layer. As we mentioned before, the A terms correspond to the mode that propagates energy upward while the B terms represent the mode propagating energy downward. Graphically, we have

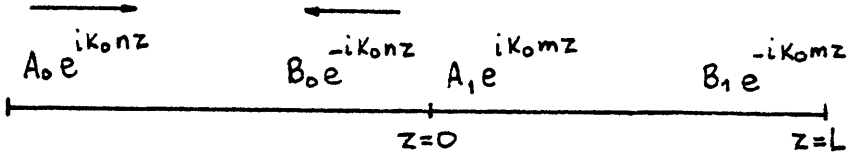

Because we want to avoid the downward mode, suitable values of L and m must be chosen, to obtain $B_o = 0$. By imposing the conditions $B_o = 0$, continuity of Ω and $\frac{d\Omega}{dz}$ at $z = 0$, and $\Omega = 0$ at $z = L$, we obtain the system:

$$1 = A_1 + B_1 \tag{46}$$

$$n = m A_1 - m B_1 \tag{47}$$

$$A_1 e^{iK_o mL} + B_1 e^{-iK_o mL} = 0 \tag{48}$$

Solving for A_o and B_o in (46) and (47), and substituing in (48), we obtain:

$$(m+n) e^{2iK_o mL} + (m-n) = 0 \tag{49}$$

The reflected waves produced at $z = 0$ are cancelled by interference with the waves reflected at $z = L$. However, the mathematics mask this physical interpretation, which is shown in an appendix. Equation (49) solves the problem for waves with a single frequency, because the values of the distance L and the index of refraction m that satisfy (49) make the amplitude B of the reflected wave vanish.

The idea behind the general procedure can be shown with the two frequency case. Let us consider two waves with wavelength k_o and k_1 respectively. Under linear conditions, these two waves can be treated separately. Graphically we have

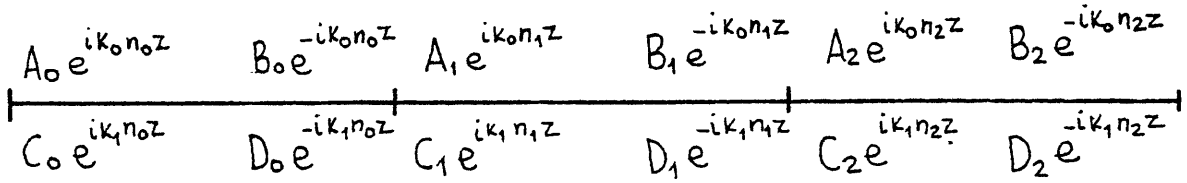

The procedure to eliminate the reflection in the atmosphere, $B_o = D_o = 0$, is as follows. Firstly, we impose $A_2 = B_2 = 0$, so that the waves of wavelength k_o are not transmitted into the medium n_2. This is formally equivalent to the case $N = 1$. Consequently,

$$(n_1 + n_o)\, e^{2ik_o n_1 L_1} + (n_1 - n_o) = 0$$

is obtained, and L_1 and n_1 evaluated. Secondly, the waves of wavelength k_1 are transmitted into the media n_1 and n_2. At each interface, reflected waves are generated. We select n_2 and L_2 (note that L_1 and n_1 are already determined) so that $D_o = 0$. This means that the reflection in the atmosphere of these particular waves is avoided. By a procedure similar to that of the previous case, we obtain:

$$1 = C_1 + D_1 \tag{50}$$

$$n_o = n_1 C_1 - n_1 D_1 \tag{51}$$

$$C_1 e^{iK_1 n_1 L_1} + D_1 e^{-iK_1 n_1 L_1} = C_2 e^{iK_1 n_2 L_1} + D_2 e^{-iK_1 n_2 L_1} \tag{52}$$

$$n_1 C_1 e^{iK_1 n_1 L_1} - n_1 D_1 e^{-iK_1 n_1 L_1} = n_2 C_2 e^{iK_1 n_2 L_1} - n_2 D_2 e^{-iK_1 n_2 L_1} \tag{53}$$

$$C_2 e^{iK_1 n_2 L_2} + D_2 e^{-iK_1 n_2 L_2} = 0 \tag{54}$$

Solving for C and D in (50) to (53), and substituing in (54), we obtain:

$$\left(\left(n_2+n_1\right)\left(n_1+n_0\right) e^{2ik_1 n_1 L_1} + \left(n_2-n_1\right)\left(n_1-n_0\right)\right) e^{2ik_1 n_2 \left(L_2-L_1\right)}$$

$$+ \left(n_2-n_1\right)\left(n_1+n_0\right) e^{2ik_1 n_1 L_1} + \left(n_2+n_1\right)\left(n_1-n_0\right) = 0$$

In this equation, L_1 and n_1 are known, and we solve for L_2 and n_2.

For the general case of N wavelengths, k_i (i = 1, 2, ..., N), the following recursive formulas are obtained:

$$A_0 = \frac{n_1 + n_0}{2n_1} \qquad B_0 = \frac{n_1 - n_0}{2n_1}$$

$$A_{j+1} = \frac{n_{j+1}+n_j}{2n_{j+1}} A_j e^{ik_m \left(n_j - n_{j+1}\right) L_j} + \frac{n_{j+1}-n_j}{2n_{j+1}} B_j e^{-ik_m \left(n_j + n_{j+1}\right) L_j}$$

$$B_{j+1} = \frac{n_{j+1}-n_j}{2n_{j+1}} A_j e^{ik_m \left(n_j + n_{j+1}\right) L_j} + \frac{n_{j+1}+n_j}{2n_{j+1}} B_j e^{-ik_m \left(n_j - n_{j+1}\right) L_j}$$

$$A_m e^{ik_m n_m L_m} + B_m e^{-ik_m n_m L_m} = 0$$

For each m varying between 1 and N, j varies between 0 and m-1. Therefore, to obtain the values of L_j and n_j, N equations must be solved. For m = M, the values

of L_M and n_M are evaluated using the known values of L_j and n_j (j = 1, 2, ..., M-1) previously calculated.

This method was tested by solving numerically a simple case. For constant conditions, and Case I of Section 4.2, a value for n of 1.25664 km^{-1} was obtained. By solving equation (49) with an arbitrary depth of the sponge layer of L = 10 km, a complex number 1.73572 + i 0.09074 for m was obtained. Then, we solved equation

$$\frac{d^2\Omega}{dz^2} + n^2\Omega = 0 \tag{55}$$

in the atmosphere with $\Omega(0) = 1$, and equation

$$\frac{d^2\Omega}{dz^2} + m^2\Omega = 0 \tag{56}$$

in the sponge layer, subject to $\Omega(\text{top}) = 0$.

The solution was obtained numerically by using second order differencing and inverting the tridiagonal matrix that results. Figure 5.4 shows the results for the atmosphere. For comparison, computations made with a radiation condition, and with $\Omega(\text{top}) = 0$ without the sponge layer are included. The results confirmed the viability of the method. However, the computations were made using several levels in the sponge layer, an impractical procedure from the point of view of

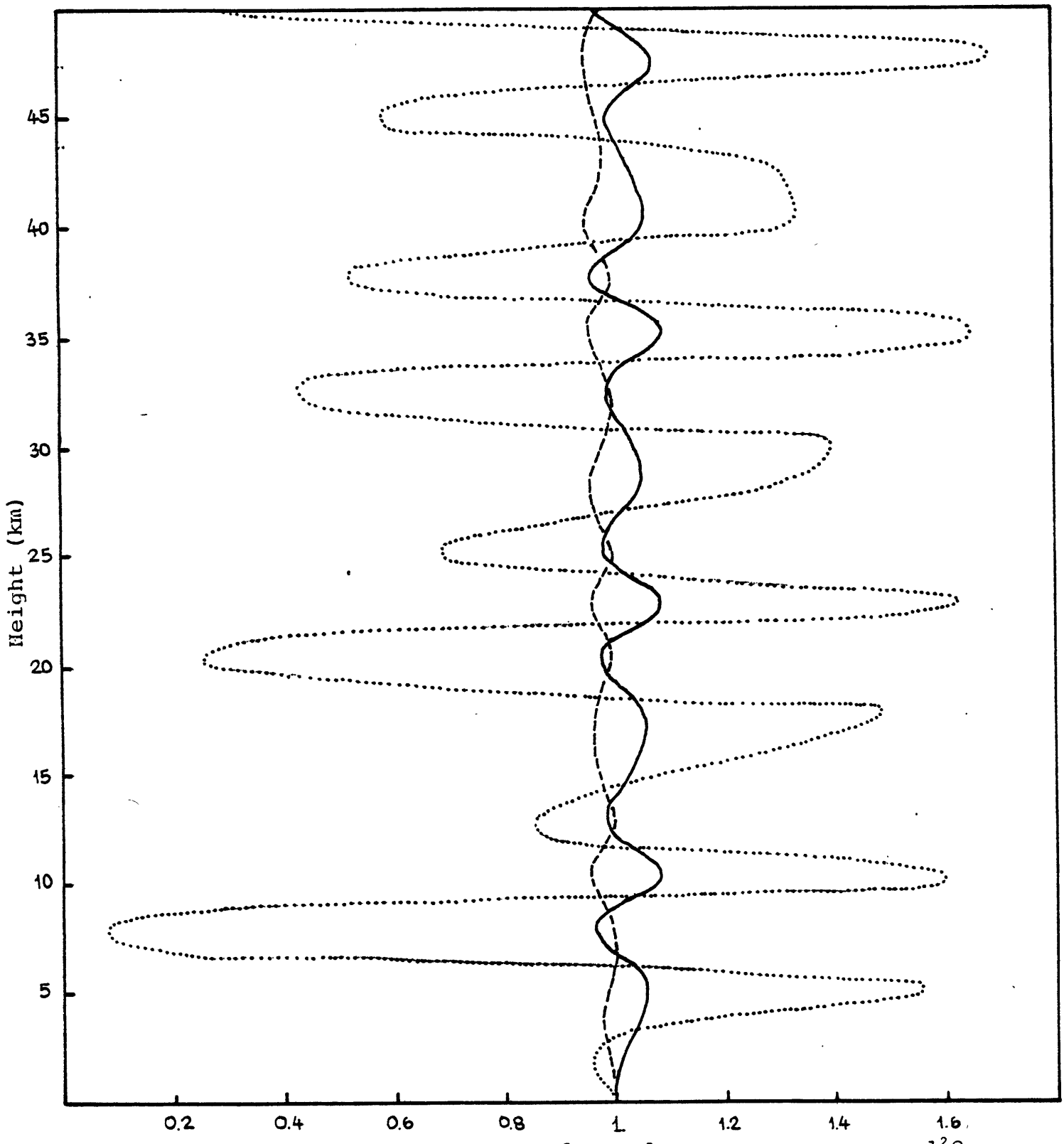

Figure 5.4 Scaled Amplitude (m^2 sec^{-1}) Computed Solving $\frac{d^2\Omega}{dz^2}+n^2\Omega=0$ with a Radiation Condition (Dashed Line), a Rigid Top (Dotted Line), and the Destructive Interference Mechanism (Solid Line).

a general circulation model. Reducing the number of levels in the sponge layer caused trouble, because system (46) to (48) corresponds to a continuous cases (infinite number of levels, $\Delta z \to 0$) and instead a discrete solution was obtained that was highly dependent on the value of Δz (by decreasing the number of levels, Δz increases). The outline of the correct procedure to be applied on the discrete case is presented below.

In finite difference form, equation (55) becomes

$$\phi_{K+1} + (n^2 \Delta^2 z - 2)\, \phi_K + \phi_{K-1} = 0 \qquad (57)$$

and equation (56), becomes equation (57) where n is replaced by m. The solution of these equations are

$$\phi_K = A\, b_o^K + B\, b_1^K \qquad \text{and} \qquad \phi_K = C\, b_2^K + D\, b_3^K$$

respectively, where A, B, C, D are constant coefficients,

$$(b_o, b_1) = \frac{2 - n^2 \Delta^2 z \pm n \Delta z \left(n^2 \Delta^2 z - 4\right)^{1/2}}{2} \qquad (58)$$

and (b_2, b_3) is obtained by replacing n by m in (58).

By specifying for convenience $A = 1$, the discrete

structure as

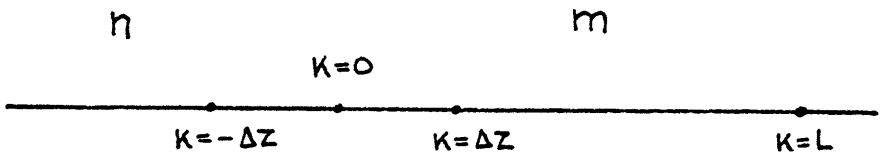

and $B = 0$ to avoid reflections, the analog in finite difference of system (46) to (48) becomes:

$$1 = C + D$$

$$C b_2^L + D b_3^L = 0$$

$$\eta^{-2} b_0^{-\Delta z} + \left(\Delta_z^2 - m^{-2} - n^{-2} \right) + m^{-2} \left(C b_2^{\Delta z} + D b_3^{\Delta z} \right) = 0$$

By eliminating C and D, the analog equation of (49) can be obtained. Then, by specifying the depth of the sponge layer L, it is possible to solve for m. Unfortunately, to solve this system is quite more complicate than to solve system (46) to (48), since b_2 and b_3 have a functional dependence with m.

6. SUMMARY AND CONCLUDING REMARKS

In the present work, linear mid-latitude models on a beta-plane, were formulated to study the consequences of using a rigid top as an upper boundary condition, to examine the effect of vertical resolution and the position of the top on the simulation of forced planetary waves, and to test alternative approaches for the upper boundary condition. Two of the models are based on the primitive equations (with pressure and log-pressure vertical coordinates respectively), while two other are based on the quasi-geostrophic equations, with the same two vertical coordinates. The simulations using a rigid top boundary condition, $\frac{dp}{dt} = 0$ (or $\frac{dz}{dt} = 0$) were compared with a reference model using a radiation condition. Forced small perturbations subject to Newtonian cooling were superimposed upon a mean thermal basic state having realistic vertical mean zonal wind profiles for Winter, Fall, and Summer.

The use of a constant coefficient beta-plane approximation in the primitive equation models produced a complex index of refraction, introducing artificial damping of the solutions when the meridional wavelength was finite. Therefore, most of the computations were performed with the quasi-geostrophic models.

Simulations were performed first using constant values of the zonal velocity and temperature. This allowed us to make

comparisons with analytic solutions. In agreement with previous investigations we found that the introduction of a rigid top at some finite height produces spurious reflections which are dependent on the vertical resolution of the model. The pressure and log-pressure coordinate models were incapable of representing a vertically propagating wave, although external modes, with no energy propagation, were well represented by the models.

We later performed computations of the planetary wave structure with the pressure and log-pressure coordinate models using realistic mean zonal wind profile for Winter, Fall, and Summer, and Newtonian cooling. We found that for Winter and Summer the planetary waves can be successfully simulated in spite of the presence of a rigid top, if there is enough vertical resolution. With low resolution models, the wave structure was in error throughout the entire atmosphere. For the pressure model, insufficient stratospheric resolution produced an inadequate definition of the zonal wind structure, and, in consequence, the models were unable to detect the stratospheric reflective layer. The spurious reflections produced at the upper boundary were responsible for the misrepresentation of the wave. For the log-pressure simulations, the models could not resolve the wave structure properly due to the sparcity of levels in the lower atmosphere. Under Fall conditions, Newtonian cooling was found to be an important factor, in agreement with Dickinson's results (1969). The simulation

with high resolution pressure models produced a wave structure in good agreement with the reference model. The cooling prevented some of the wave energy from reaching the upper reflecting boundary. Also good agreement was obtained with the high resolution log-pressure models, except in the mesosphere where the values of Newtonian cooling are small, and consequently the damping was not effective. The low resolution models present a different behavior depending on the vertical coordinate. The log-pressure simulations were completely erroneous due to the poor resolution in the lower atmosphere. On the other hand, the pressure models produced reasonable simulations suggesting that with a properly resolved lower boundary condition, good tropospheric resolution will produce adequate tropospheric results regardless the conditions of the upper atmosphere.

From the results obtained for Winter, Fall, and Summer, with different resolutions, it may be concluded that the absolute minimum number of levels necessary to obtain a relatively good wave structure simulation is ten.

The influence of lowering the upper boundary in a model with high resolution was not critical to the structure of the waves for Winter and Summer, if the upper boundary was placed at the middle stratosphere. However, the Fall simulation was in error because the model was not affected by the damping effect of Newtonian cooling at the upper stratosphere. If the upper boundary was placed below 35 km, distorsions in the

wave structure due to energy reflection at the upper boundary became evident, regardless the wind profile used. When the top was set at the lower stratosphere, the wave structure was substantially modified.

The pressure and log-pressure models with ten levels were used to study the behavior of the vertical propagating waves when the height of the rigid top was varied. For Summer and Winter, the use of an artificial top can help to simulate the reflective stratospheric layer, but the effective position of that top becomes crucial. The results show that the optimal position of the top is seasonally dependent. The conclusion obtained for a model with ten levels is that in order to obtain good results, a compromise between the low atmosphere resolution and the position of the top has to be made. For the log-pressure models this compromise is more difficult to obtain because if the top is placed at the appropriate height, the tropospheric resolution becomes very poor. The best simulations were obtained with a nonuniform vertical resolution similar to the one used by Smagorinsky et al. (1965), in which levels are chosen to give maximum resolution at the extremes of the atmosphere. For the Fall, with weak westerly winds that does not inhibit energy propagation, the radiative damping compensates the effects of the rigid top. However, for the log-pressure models is more evident that poor tropospheric resolution produces a misrepresentation of the wave structure in this region.

In view of the modifications in the wave structure that a rigid top can produce, two "sponge layer" mechanisms to reduce the reflection of wave energy were tested. In one of them, a complex index of refraction was set in a layer below the upper boundary, in such a way that the waves could be damped before they reached the upper boundary. To obtain the desired index of refraction, adequate coefficients of viscosity or of Newtonian cooling were used. A complex index of refraction that increases smoothly with height was found to produce better results that a constant one. It was found that there is an optimum value of the viscosity (or of the Newtonian cooling) coefficient, which is a function of the frequency of the waves and the depth of the sponge layer. Lower values produce insufficient damping, and higher values produce internal reflections due to the strong vertical gradient of viscosity. The second approach uses a single layer at the top to eliminate the reflected wave by producing destructive interference between the wave reflected at the top and the wave at the bottom of the sponge layer. With this approach the thickness of the sponge layer can be chosen in accordance with the requirements of the model used. A generalization of this method when several frequencies are present is proposed.

The problem of the proper choice and effect of the top boundary condition on general circulation models is very complex. The results obtained in this study with simple models can provide a guidance in the analysis of the effect of the rigid top boundary condition in a realistic general circulation

model, in the choice of an optimum distribution of vertical levels for a minimization of the negative effect of the rigid top, and in further studies of the possible improvement of the treatment of the top boundary condition.

APPENDIX

The principle of operation of the destructive interference can be seen with the help of Figure A.1, where a layer with its two interfaces is shown. A wave of unit amplitude is incident at the first interface. A fraction R_{12} of the amplitude is reflected. The transmitted wave of amplitude T_{12} proceeds on to the second interface, where it is reflected again and partially transmitted (or as in our case, only reflected). The reflected wave proceeds back to the first interface, where part of it is transmitted out to the first medium and is added to R_{12}, and part is reflected back to medium 2, and so on.

The total reflected wave is the vector sum of the amplitudes produced by all the multiple reflections. The change in amplitude and the phase retardation caused by the traveling of the layer has to be included.

Firstly, by a procedure similar to that of page 102, we calculated that $1 + R_{12} = T_{12}$, $R_{12} = \frac{(n-m)}{(n+m)}$, and $T_{12} = \frac{(2n)}{(n+m)}$, where n and m are the indices of refraction of the media 1 and 2 respectively.

Secondly, we calculated the first reflections:

First R_{12}

Second $T_{12}R_{23}T_{21}\, e^{2iKL} = (1-R_{12}^2)R_{23}\, e^{2iKL}$

Third $T_{12}R_{23}R_{21}R_{23}T_{21}\, e^{4iKL} = (1-R_{12}^2)R_{23}^2R_{21}\, e^{4iKL}$

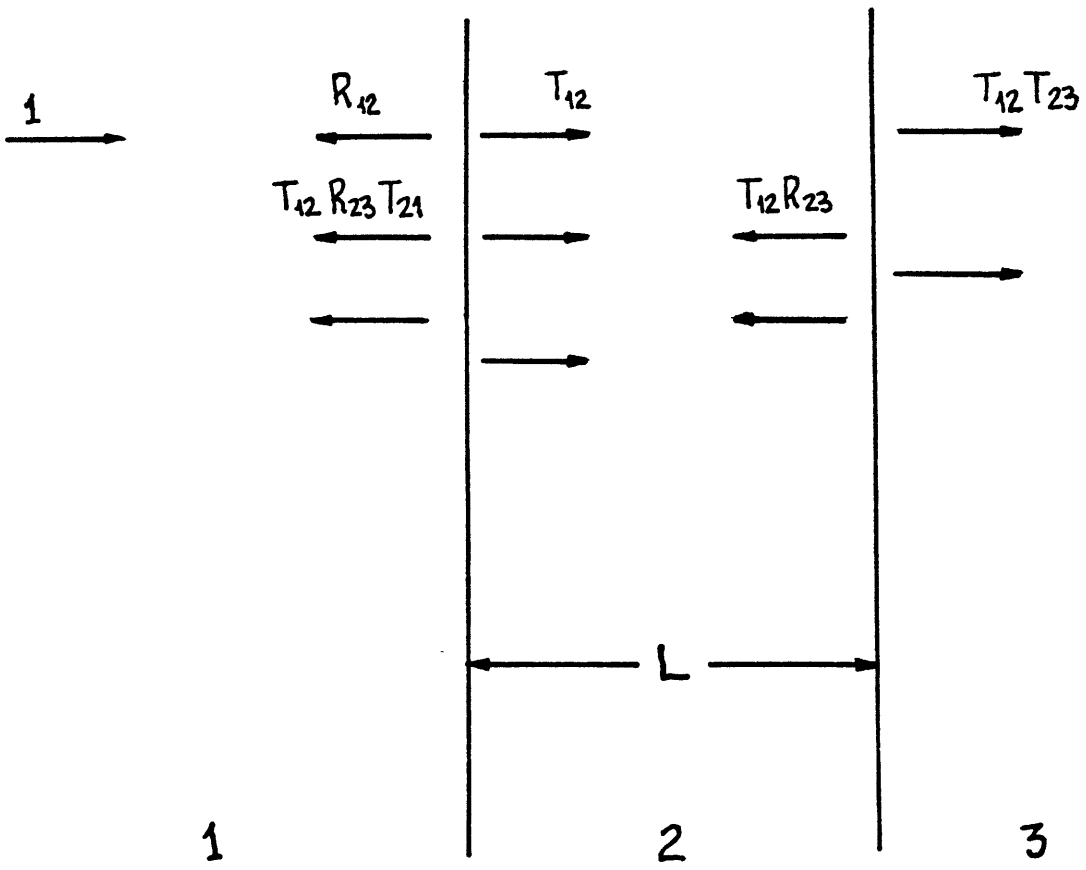

Figure A.1 Destructive Interference.

and by induction, the N reflection will have an amplitude equal to $(1-R_{23}^2)\ R_{21}^{N-1}\ e^{2i(N-1)KL}$. Then,

$R_{total}=R_{12} + (1-R_{12}^2)R_{23}e^{2iKL}(1+R_{21}R_{23}e^{2iKL}+R_{21}^2R_{23}^2e^{4iKL}+ \ldots)$,

and because $|R_{21}R_{23}\ e^{2iKL}| < 1$,

$$R_{total} = R_{12} + \frac{(1-R_{12}^2)\ R_{23}\ e^{2iKL}}{1 - R_{21}R_{23}\ e^{2iKL}}$$

For the case considered in Section 5, $R_{23} = -1$ and $k = m$. Then

$$R_{total} = \frac{R_{12} - e^{2imL}}{1-R_{12}e^{2imL}} \qquad (59)$$

We have no reflection if the numerator in (59) is zero, or when $(n-m) - (m+n)\ e^{2imL} = 0$, equation (49).

REFERENCES

Arakawa, A., and Tokioka, T., 1974
The UCLA Atmospheric Model, UCLA

Charney, J. G., and Drazin, P. G., 1961
Propagation of Planetary Scale Disturbances from the Lower into the Upper Atmosphere. J. Geophys. Res., 66, 83-109

Dickinson, R. E., 1969
Vertical Propagation of Planetary Rossby Waves Through an Atmosphere with Newtonian Cooling.
J. Geophys. Res., 74, 929-938

Dickinson, R. E., 1973
Method of Parameterization for Infrared Cooling Between Altitudes of 30 and 70 Kilometers.
J. Geophys. Res., 78, 4451-4457

Eliassen, A., and Palm, E., 1961
On the Transfer of Energy in Stationary Mountain Waves
Geofys. PubliKsjoner, 22, 1-23

Holton, J. R., 1975
The Dynamic Meteorology of the Stratosphere and Mesosphere
American Meteorology Society, 216 pp.

Houghton, J. T., 1977
The Physics of Atmospheres. Cambridge University Press, 203 pp.

Kasahara, A., Sasamori, T., and Washington, W. M., 1973
Simulation Experiments with a 12-Layer Stratospheric Global Circulation Model. J. Atmos. Sci., 30, 1229-1251

Kirkwood, E., and Derome, J., 1977
Some Effects of the Upper Boundary Condition and Vertical Resolution of Modeling Forced Stationary Planetary Waves
Mon. Wea. Rev., 105, 1239-1251

Lindzen, R. S., Batten, E. S., and Kim, J. W., 1968
Oscillations in Atmospheres with Tops.
Mon. Wea. Rev., 96, 133-140

Manabe, S., and Terpstra, T. B., 1974
The Effects of Mountains on the General Circulation of the Atmosphere as Identified by Numerical Experiments
J. Atmos. Sci., 31, 3-42

Matsuno, T., 1970
Vertical Propagation of Stationary Planetary Waves in the Winter Northern Hemisphere. J. Atmos. Sci, 27, 871-883

Nakamura, H., 1976
Some Problems in Reproducing Planetary Waves by Numerical Models of the Atmosphere. J. Meteor. Soc. Japan, 54, 129-146

Simmons, A. J., 1974
Planetary-Scale Disturbances in the Polar Winter Stratosphere. Quart. J. Roy. Meteor. Soc., 100, 76-108

Smagorinsky, J., Manabe, S., and Holloway, J. L., 1965
Numerical Results from a Nine-Level General Circulation Model of the Atmosphere.
Mon. Weather Rev. 93, 727-768

ACKNOWLEDGEMENTS

I am deeply grateful to Professors Jule Charney and Eugenia Kalnay-Rivas who gave me the excellent opportunity to study at M.I.T. Also, I want to express my gratitude to Professors Manuel Sadosky and Alberto Rivas for their confidence and help when I applied to M.I.T.

I want to express my immense gratitude to my advisor and friend Professor Kalnay-Rivas. Without her invaluable assistance this work would not have been possible. She helped and encouraged me in every moment of my three years at M.I.T. I highly appreciate her scientific achievements, but even more her human kindness.

Dr. Fred Alyea made it possible for me to work with large computational systems and obtain an invaluable experience; but most of all I want to thank him for his friendship. He gave me constant encouragement, and when things were not as good as desired, he always had a nice word to say.

Discussions with fellow students, Stephen Brenner, Ron Errico, and Affonso Mascarenhas were very useful. My comprehension of physical concepts was immensely enriched by discussions with Dr. Fernando Garcia Golding.

This work was supported in part by NASA Grant NSG-2010. The computer time was provided by NASA at the Goddard Institute for Space Studies. Thanks are due to Dr. Milton Halem for making this facility available and to Dr. James Hansen for his partial support through NASA Grant NGR 22-009-727.

Carlos Cardelino
September, 1978.